博士論文

論文題目　Decadal Shifts and their Impact on Climate of East and Southern Africa

（数十年周期変動と東アフリカ・南アフリカ気候への影響）

氏　　名　デスモンド　マナツサ / Desmond Manatsa

論文内容の要旨

論文題目：
Decadal Shifts and their Impact on Climate of East and Southern Africa
数十年周期変動と東アフリカ・南アフリカ気候への影響

氏名：デスモンド　マナツサ

10月から12月の東アフリカの降水量とアフリカ南部の地上気温に見られる経年変動の長期変調について、統計的に調べた。本研究では、19世紀後半から20世紀初頭までの観測データと再解析データを用いた。その結果、1917年、1961年、1997年にインド洋で統計的に有意なシフトが起こっており、インド洋ダイポール(IOD)の時系列の特徴に現れているだけではなく、マスカリン高気圧の北端と東端がそれぞれ赤道側と東側に変位していることも確認された。東アフリカとアフリカ南部の気候変動が主にインド洋における循環に支配されているため、この現象は東アフリカとアフリカ南部の気候における急激な変化として解釈される。

注目すべきことは、これら3つのシフトにおいて、シフトの発達の仕方が非常に類似していたことである。シフトが発生する時期には、まず弱い負のIODが発達し、翌年に強い負のIODとなり、さらに翌年（シフトの年）に正の強いIODに変化していた。この2つの強いIODは、シフト発生時において1900年以来記録的に大きな振幅を伴っていた。このことは、20世紀の終わりに向かってシフトが起こるにつれ、シフトの過程が時代ごとに強くなっていくことを意味している。使用した海面水温データに関係なく、この3年に渡るシフトの過程が1870年以降のIODの時系列に見られたことは、将来、類似した現象を見つけることで新たに海盆規模のシフトの存在を示すことにつながる。インド洋で統計的に有意なシフトと認められるほど十分にデータが蓄積される前であっても、十分な信頼度をもってシフトと結論づけることができる。

また、興味深いことに、マスカリン高気圧も、シフトの過程に関わっているようである。シフトが発生する前年には、マスカリン高気圧は極側と西側に異常に変

位し、負のIODが同時に発生していた。一方で、シフトの年には、マスカリン高気圧は強化して赤道側に変位し、IODの東側の極で湧昇を強めることにより、正のIODが同時に発生していた。このように、シフトが起こる年の前後で、マスカリン高気圧の位置が急激に変化し、それゆえ強度も変化していた。また、シフトが発生する度に、マスカリン高気圧は赤道側とオーストラリ西岸への変位が増加するため、3つの連続したシフトにおいて、このシフトの過程が強くなってきていた。それゆえ、マスカリン高気圧の赤道側と東側への変位に伴う風の南北成分が平均場に加わることで、近年IODが強い振幅をもって正の符号をとるようになった原因となるであろう。同時に、この現象が時代ごとに強化していたことが、1917年、1961年、1997年にかつてないほどの振幅を示していた理由となるであろう。

しかし、IODと東アフリカの降水の関係は、1961年に突然強くなり、1997年から急激に強くなっているように見える。規格化された降水量の指数で定義された東アフリカの降水量の時間分布によると、東アフリカの降水量変動は20世紀初めから大きくなり、過去数十年で洪水と干ばつがより頻繁に発生していた。より極端な降水現象の増加は穏やかに続いており、IODのシフトで定義される時代に強く特徴づけられる。このIODの長期変調はまた、1887年から1917年にかけて、負のIODが支配的であったように、各年代で3つのシフトを明確に特徴づけている。それ以降の年代では、負のイベント数が徐々に減少し、正のイベントが発生しやすくなり、1998年から2010年にかけて正のイベントが支配的になっていた。この正と負のIODの周期が規則正しく急激に変化したことは、IODの時系列における分散や歪度が各シフトにおいて変化したためである。

さらに、東アフリカの降水量変動は、マスカリン高気圧の変位、特に高気圧の東端の東西変位と強く関係していることが分かった。マスカリン高気圧の東端が通常の位置より西側（東側）に変位すると、南インド洋において南東貿易風が強化（弱化）される。高気圧の東端が西側に変位すると、比較的冷たく乾いた風が東アフリカに移流し、地域の対流や地形性降雨を抑える。このため、マスカリン高気圧の東端の東西変位は東アフリカの極端な降水量の指標となり、過剰な降水に比べ干ばつをより良く決めるものとなる。東アフリカの降水におけるIODの影響は非対称的であり、正のIODは洪水と強く関係すると報告されている。それゆえ、この発見は東アフリカの地域社会において広く応用される。東アフリカでは、極端な降水現象がより多くなってきたものの、伝統的な指標としてENSOやIODが主に深刻な干ばつの予測に用いられている。

1997年のシフト後、アフリカ南部で地上気温が急激に変化したことについて、マスカリン高気圧やセントヘレナ高気圧がアフリカ南部から離れ、アンゴラ低気圧が強化していたことは注目すべきである。その結果、暖かい空気が低緯度から大

陸の低気圧に向かって移流し、それによってアフリカ南部が暖まっていた。この過程と同時に、南半球環状モードが正の符号に変化しており、1990年代半ばに成層圏のオゾンホールが発達したことによる影響が考えられる。この比較的大きな成層圏のオゾンホールが発達する前は、平均的な風の南北循環は南風であったが、環状モードが正の符号に変化したことと同時に、北風に変化していた。

このIODと東アフリカの降水、オゾンホールと地上気温との関係における長期変動は、近年の研究者の間であまり考えられてこなかった。しかし、この時代ごとのシフトは、現在認識されていなくとも、過去のデータで定常的に見られる関係に基づいた現業の統計的予測手法を悪化させるであろう。それゆえ、今後、人類によるストレス、特に成層圏のオゾンホールのもとで、地域の気候の長期変調を評価していく場合、地球の気候システムの研究社会において、この非線形なパラダイムを受け入れていく必要がある。

Doctoral Dissertation

Decadal Shifts and their Impact on Climate of East and Southern Africa.

数十年周期変動と東アフリカ・南アフリカ気候への影響

By

Desmond Manatsa

Department of Ocean Technology, Policy and Environment, Graduate School of Frontier Sciences

UNIVERSITY OF TOKYO

February 2014

Abstract

The low frequency modulation of the interannual variability of East African rainfall and the surface air temperature (SAT) of southern Africa for the October to December period is statistically explored. Observations and reanalysis data dating from the late 19th to the early 20th century are used in this study. It is revealed that there exist three statistically significant shifts in the years 1917, 1961 and 1997 in the Indian Ocean basin manifesting not only in the Indian Ocean Dipole (IOD)ôs temporal characteristics but also the Mascarene High (MH)ôs equatorward and eastward epochal displacement of the northern and eastern ridges respectively. Hence by virtue of the dominant portion of the climate variability of East and southern Africa being controlled by circulation patterns originating from the Indian Ocean basin, this phenomenon is seen to be translated as abrupt changes in the climate of East and southern Africa.

It is intriguing to note the close similarities in the shift development during each of these three shifts. The occurrence of the shift appears to be initiated when a moderate negative IOD event intensifies to an extreme negative IOD event in the succeeding year but reverses to a positive extreme IOD event in the subsequent year (the shift year). The last two extreme IOD events reach record breaking magnitudes during their respective occurrence since 1900. This implies epochal intensification of the shift process as the occurrences progress towards the end of the 20th century. The observation that this three-year shift process is unique within the entire IOD time series used from 1870, irrespective of the sea surface temperature dataset used, entails that the identification of a similar

phenomenon in the future may imply a new existence of a basinwide shift. The fortunate aspect is that this conclusion can be reached with some reasonable degree of confidence even before data will have accumulated long enough to confirm the occurrence as a statistically significant shift in the Indian Ocean basin.

Interestingly, the MH seems to also participate in the shift process. During the year before the shift, the MH is anomalously displaced poleward and westward but coinciding with the negative IOD event. On the other hand, the subtropical high intensifies and moves equatorward during the shift year thereby possibly amplifying the coinciding positive IOD event through enhancing upwelling over the eastern pole of the mode. It then follows that the abrupt change in the position and hence the intensity of the MH, from one year to the other is achieved during the shift years. The intensity of this process has also been escalating during each of the three successive shifts because there has been an epochal shift of the MH both equatorward and towards the western coast of Australia after every shift. Hence adding the meridional wind component associated with the equatorward and eastward displacement to the mean state could be responsible for the epochal phase alterations towards the positive polarity with maximum positive IOD intensity in the last epoch. At the same time, the epochal intensification of this phenomenon could explain why the shift years of 1917, 1961 and 1997 acquired unprecedented magnitudes.

However the coupling between the IOD and the of East African rainfall (EAR) seem to have become suddenly robust in 1961 with a further abrupt increase from 1997. It is noted through the temporal distribution of the EAR event classes determined by the standardized precipitation index technique, that the EAR variability intensified significantly from the turn of the twentieth century with more floods and droughts occurring in the recent decades. This increase towards more extreme rainfall events has not been gradual but is strongly characterized by epochs which were dictated by shifts in the IOD mode. These IOD modifications also characterize the three shifts manifesting through phase modulation such that during the 1887ï 1917 epoch, negative IOD events dominate. In the subsequent epochs, the negative events gradually diminish in number at the expense the positive events at each succeeding epoch until eventually the frequency of the positive events dominate in the last epoch from 1998 to 2010. This systematic but abrupt change in the mean frequency of the positive and negative IOD events has been established through sudden change in the variance and skewness of the IOD time series at each shift point.

It is also revealed that the EAR variability is strongly linked to the MH displacements, in particular the zonal movement of the MH eastern ridge. When the MH eastern ridge is anomalously displaced to the west (east) of its normal position, the southeast trade winds over the south Indian Ocean anomalously strengthen (weaken). The westward migration of the eastern ridge helps advect relatively cooler and less moist low level airflow over East Africa which in turn suppresses both regional convection and orographic rainfall.

Thus the zonal migration of the MH eastern ridge provides a novel indication for the EAR extremes which can resolve better the droughts than the surplus rainfall. The IOD impact on EAR has been documented as being asymmetrical whereby it is the positive phase of the IOD which is strongly related to floods rather than the reverse. Therefore this revelation has immense social application in East Africa. Here rainfall extreme events have become more prevalent against the background of deteriorating drought forecasts which are predominantly generated from traditional indicators like ENSO and the IOD.

With regard to the abrupt change in SAT over southern Africa during the last epoch after the 1997 shift, we also note that the displacement of the MH and the St Helena High away from the mainland simultaneously led to the deepening of the Angola Low. As a result warm air was advected from the lower latitudes towards the continental low, thereby warming southern Africa. This process coincided with the change to positive polarity in the Southern Annular Mode (SAM) which is believed to have been influenced by the development of the stratospheric ozone hole in the mid-1990s. The mean meridional circulation before the development of the relatively large stratospheric ozone hole was southerly but reversed to northerly in sympathy with the alteration in polarity of the SAM to become positive.

This epochal variations in the IOD ï EAR and ozone hole- SAT relationship are novel and have rarely been considered by recent researchers. Yet epochal shifts if not

recognized timely, can undermine the current operational statistical prediction schemes that are based on stationarity relationships in historical data. Hence given the promising nature of our results, it is imperative that the earthôs climate system research community embraces this nonlinear paradigm if we are to move forward in the assessment of regional climate modulations under the anthropogenic stress, especially the stratospheric ozone hole.

ACKNOWLEDGMENTS

I really appreciate the wise guidance and instructions which I got from Prof Behera. I also thank Prof Yamagata and Dr. Morioka for the advice and commitment that they showed to makes sure that I accomplish this thesis. I am also indebted to the teamwork I got whilst in Zimbabwe from Prof Matarira and Dr Mukwada which culminated into the several papers which I was able to publish during are the tenure of this PhD thesis. I also do not forget the moral support I got from my wife Faith and children Kelly, Tina and Tariro when during the occasions things were becoming unbearable. Lastly I acknowledge the research facilities which I got from JAMSTEC and Bindura University including the JSPS RONPAKU Fellowship financial support which enabled me to undergo these PhD studies. But above all, bow down to our Lord Jesus Christ for his mercy which enabled me to sail through the turbulent times and enabled me to successfully complete all the necessary PhD program requirements.

TABLE OF CONTENTS

CHAPTER I

GENERAL INTRODUCTION

The east and southern African region is intrinsically and inextricably tied to rain fed agriculture. The rainfall pattern is highly variable both spatially and temporarily, and is characterized by relatively amplified frequencies of droughts and floods (e.g. Jury and Mwafulirwa 2002). Of late climate change, mostly attributed to anthropogenic causes is believed to be increasing the summer surface temperatures (Shongwe et al 2009) thereby complicating the already dire economic situation of the African community. Accurate seasonal to interannual climate monitoring and forecasting could significantly contribute to a reduction in extreme climate vulnerabilities. Hence continuous improvement in the knowledge of the regional temperature and rainfall triggering mechanisms and teleconnections is not an option. Currently, the climate forecast of East and southern Africa assumes stationary relationships in the climate modes used as predictors for regional climate forecasts. Yet the climate system is well known for being characterized by shifts (Tsonis et al., 2007). Identification of these discontinuities in the predictors and their impacts on the regional climate is a prerequisite for more accurate climate forecasts in the long term. Thus improved forecasts can only be achieved with the identification of a mode that is reasonably coupled to the climate of the two regions whilst at the same time is principally responsible for the low frequency modulation of the climate. In this way, shifts in the climate regimes that are related to the modes may not come as a surprise but can become predictable.

Both observational and modeling studies seem to suggest that the Indian Ocean Dipole (IOD) is consistently influencing the rainfall variability over East Africa (Clark et al. 2003; Black et al.

2003; Yamagata et al. 2003; Behera et al. 2005) in recent decades. However, these studies have not considered the decadal shifts in the behaviors of the IOD and the ôshort rainsô of East Africa. In fact, shifts in temporal relations between major coupled climate modes, for example El Niño Southern Oscillation (ENSO) and the associated rainfall have also been largely ignored in other regions. This is despite the fact that the earthôs climate system is known to be highly nonlinear and the low-frequency evolutions of climate modes are often episodic and abrupt, rather than slow and gradual, with multiple equilibria being the norm (Rial et al. 2004). It is therefore not surprising that theoretical models developed to better understand the temporal nature of most major coupled climatic modes are still primarily guided by a linear dynamic framework (e.g. Wang and Chang 2008). This could explain why the nonlinear evolution of not only the IOD, but the Southern Annular Mode (SAM) and the accompanying ramifications on the rainfall of East Africa and surface air temperature (SAT) of southern Africa, has eluded previous researches. Therefore, understanding of these nonlinearities, their origins and impacts on the regional climate system can greatly enhance climate forecasts on both seasonal and longer time scales.

Climate shifts are amongst the main sources of uncertainties for the predictabilities of the future climate variations. The nonlinearity in the climate system results in highly diverse, usually unanticipated and often counterintuitive observations (Kaplan and Glass 1995). This is a pattern that having frequently interspersed previous climates, like the Pleistocene, the Holocene and the relatively recent great Sahel drought that abruptly started in the 1960s (Biasutti and Giannini, 2006) and the 1976/77 Pacific climate shift (Huang et al., 2005), will likely dominate in the future also. Thus the climate record for the past 100,000 years clearly indicates that the climate system has undergone periodic--and often extreme--shifts. The causes of abrupt climate changes

have not been clearly established, but such a change could be triggered instantly by natural processes or by human-caused global warming (Stott, 2003) hence with little warning. This creates compelling evidence for the urgent need to improve our understanding of the physical processes involved. Enormous strides have been made in improving the Indian Ocean and the Antarctic observation systems especially with the advent of the satellite data. This effort substantially reduced the large errors which formerly existed in the model initial conditions for IOD and SAM forecasts. Despite this positive development, most current ocean-atmosphere coupled models for IOD and SAM forecasts still suffer from deficiencies in correctly simulating their temporal nature in the long term (e.g. Cai et al. 2009 & Marshal et al., 2010). Consequently, theoretical explanations of the temporal nature of both the IOD and SAM including their related impacts on southern Africa and the surrounding Indian Ocean rim countries in a shifting environment remain outstanding. It appears the difficulty in accommodating shifts in the dynamic analysis hinges on the fact that the climate system is known to be complex, occasionally chaotic, dominated by abrupt changes and driven by competing feedbacks of largely unknown thresholds (e.g. Alley et al. 1999; Rahmstorf 2000).

In the current work, I investigate the nonlinear nature of the IOD and SAM and their influence on rainfall and SAT of East and southern Africa respectively. Considering the limitations that are inherent in observational studies in this thesis which cannot simulate an experiment and the related statistical methods of analysis, a definitive causal relationships remains to be shown and mechanisms elucidated through modeling studies. However these modeling studies are beyond the scope of this thesis. Consequently, the focus of this study is to unravel the climate shift processes, hidden in the IOD and SAM time series, and project their impacts on East African

rainfall and SAT of southern Africa respectively. We investigate abrupt shifts and trends of climatic time series that occurred at decadal time scales over the equatorial parts of East Africa and the Indian Ocean including the recent shift in SAM. Excluding the role of these shifts in the climate system of East and southern Africa could be limiting the efficiency of the existing regional climate prediction schemes.

The thesis is organized in the following manner: After the introductory chapter, the existence of three shifts (1917, 1961 and 1997) in the Indian Ocean basin are established which are then related to the Mascarene High (MH) displacements. In chapter two, the impacts of these shifts by taking East African rainfall (EAR) variability as a case study are demonstrated before relating the rainfall variability of this region to the MHôs displacements in chapter four. In chapter five, the most recent shift of 1997 is selected and also linked the displacement of the MH. This occurred simultaneously with the recent abrupt warming of the SAT over southern Africa that is linked to the development of the ozone hole which coincided with the SAMôs shift to positive polarity. I then concluded the thesis with chapter six by summarizing the results using schematic diagrams so as to add on clarity in the summary of the thesis. I also provided explanations to the possible causes and linkages to the identified shifts. The work presented in chapter two to five is almost entirely lifted from four published papers though all in all twelve papers were published in refereed journals in preparation of this thesis from the year 2011. As such intense citation of results from these other papers is found in my thesis.

CHAPTER TWO

Establishing the major shifts in the Indian Ocean basin

2.0 Brief Chapter Synopsis

This chapter is based on the paper which was published as:

Manatsa D and SK Behera (2013). On the major shifts in the IOD during the last Century, the role of the Mascarene High displacements (2013). *International Journal of Climatology,* DOI: 10.1002/joc.3820.

The chapter establishes the existence and nature of three major shifts in the IO basin through the phase shifts of the dominant tropical mode of the basin, the IOD and demonstrated the shifts are strongly coupled to epochal alterations in the Mascarene High (MH) variability.

2.1 Introduction

Significant rainfall and temperature anomalies of not only the Indian Ocean rim countries but the globe at large, are associated with the development of the Indian Ocean Dipole (IOD, Behera et al., 2005; Saji and Yamagata 2003; Yamagata et al., 2003). The recently discovered skewness of the IOD that occurs in defined periods (Hong et al., 2008; Tozuka et al., 2007), has proved to be one of the fundamental characteristics of the coupled modeôs cycles. The multi-decadal extent of the related IOD epochs makes this phenomenon induce prolonged impacts on the population and oceanic ecosystems within its sphere of influence (Abram et al., 2003). A better understanding of the mechanisms related to the epochal skewness and the associated shifts is a prerequisite for the

IOD systemôs more realistic simulation, while holding the key to its long term predictability. Yet surprisingly details of the shifts remain entirely speculation, leaving this research component unresolved and hence outstanding. No wonder why sufficiently forecasting IOD events and their implications to rainfall variability and other climatic parameters still persist as a major regional challenge (Annamalai et al., 2010).

The availability of more reliable and increased ocean data from the late 1950s has made it possible to study the IOD events. 1961 and 1997 years have always been projected as being more anomalous than the other positive IOD events. In east Africa which is within the zone of the influence of the western pole of the IOD, it is during these two years that the highest rainfall anomalies of the century which exceeded 3 standards deviations over most stations (Conway et al., 2005, Manatsa et al., 2012) were recorded. Initial inspection of the two years indicated that the wind stress field was highly unusual during September to December with strong easterlies along the whole equatorial belt of the basin, replacing the climatological westerlies (Murtugudde et al., 2000). Upwelling into the mixed layer was observed everywhere along the equatorial stretch with chlorophyll anomalies originating from the subsurface of the equatorial western coast being observed west of 90º E. These observations are a clear indication that in the 1961 and 1997 events, the whole basinôs ocean and atmospheric parameters co-varied in a manner that is consistent with a basin wide adjustment of the mean state. Thus we can draw parallel to the Pacific Ocean event which occurred in the year 1976/77 that was related to ENSO (Miller et al., 1994). That year ushered an extended period in which the tropical Pacific Ocean was warmer than normal, with stronger ENSO events occurring after that period, contrasting the weaker ENSO variability in the decades before (Hoerling et al., 2004). Hence similar to ENSO these

Indian Ocean shifts also ushered new characteristics to the IOD events with distinct properties which are at variance with those of the preceding epochs.

In this study we demonstrate that the years 1918, 1961 and 1997 were not only record breaking positive IOD events but were part of a three year process leading to the respective climate shifts. It is known that ENSO is the dominant mode of variability in the tropics (Miller et al., 1994), but given the absence of substantial trends in ENSO indices over the twentieth century (Manatsa et al., 2012), it is unclear whether changes in El Nino activity could have forced the observed IOD shifts. We therefore downplayed the involvement of ENSO in the IOD decadal variability. In this way we reveal a novel process that describes the major IO climate shift mechanisms with improved insights which have not yet been reported on in previous literature. The work is organized as follows; section two describes the data and methods used in the analysis; section three relates to the existence of a three year process culminating into the major shifts in the IOD including an accompanying systematic displacement of the MH during the shifts. Section four concludes the work.

2.2 Data and methods of investigation

The interest of this study is particularly in the multidecadal variability of the IOD. In this regard we found the 20th Century Reanalysis data to provide the necessary atmospheric variables both in the spatial and temporal domains for the present analysis. The data is extracted from http://www.esrl.noaa.gov/psd/. Though it is the best freely available data for spatial-temporal analysis (from the late 19th to the early 21st century) within the tropics and sub-tropics, its accuracy is still questionable, especially during the pre-satellite era. As such a number of recent

studies have highlighted problems with the reanalysis products prior to the 1970s, meaning that the changes as represented in these data may be significantly in error. However, some indication of the general processes that took place in the IO can still be better inferred since the equatorial Indian Ocean displays rich data coverage from the late 19th century compared to the equatorial eastern Pacific (e.g. Ihara et al., 2008). The study notes the constraints of using Indian Ocean SST data prior to the satellite era of 1979 as addressed by Ihara et al. (2008). Thus we use caution in the interpretation of the results based on these data-sparse periods and compensate for the limitations of the data quality during these periods by using other different SST reconstructions for verification purposes.

The climatology in this study for the time series is defined as the mean SST during the period between 1970 and 2010 to address the state of the Indian Ocean SST, including the trend component. Since the years 1918, 1961 and 1997 were identified as the climate shift years in the IO (Manatsa et al., 2012) the climatic trend of the Indian Ocean from 1870 to 2010 may not be monotonic. Thus we try to take into account the four different regimes of the warming trend in our analysis and hence all data are analyzed separately in the four periods: 1871 to 1917, 1918 to 1960, 1961 to 1996 and 1997 to 2010. In this way our work becomes significantly different from previous work (e.g. Ashok et al., 2003; Kripalani and Kumar, 2004; Ihara et al., 2008). The epoch approach also assists in separating the analysis according to regimes and as such it will be possible to isolate and scrutinize individually, earlier periods where data is usually treated with less confidence.

To describe secular changes in the mean states of the south IO from 1870, we focus on variables that control IOD dynamics which includes sea surface temperature (SST) and sea level pressure (SLP). For the construction of the time series for the respective climate modes, HadSST is the major dataset used since it proved satisfactory in providing the general trends of SST events. On the other hand reference is made to other datasets like ERSST and Kaplan SSTs for verification purposes. The HadSST, ERSST and the Kaplan datasets were extracted from http://climexp.knmi.nl/data/ihadisst1_dmi.dat. An east west SST difference in the Indian Ocean for the period September to November that is standardized by its respective standard deviation is an often-used IOD index (e.g., Saji et al. 1999; Ashok et al. 2004; Song et al. 2007). However, here we used a slightly different approach to define the index. Though we constructed the SST time series of the east-west SST gradient from averages using the standard locations, i.e. over the eastern (0 ï 10 °S, 90 ï 100 °E) and the western (15N ï 15S, 40 ï 80 °E), the SST time series are not normalized. The Dipole Mode Index (DMI) is derived by simply calculating the SST cumulative gradient for the individual months of the OND season. DMI values that are greater (less) than ±0.7 ºC are considered extreme positive (negative) IOD events. We opted for October to December (OND) averaging period because it is the seasonally stratified period of the transition of the strength of the Mascarene High (MH) and also coincides with the seasonal shifts of the climatological winds (Roxy et al., 2010). The MH is related to the variability of the IOD through its northeastern part of the averaged region of (90 ºE-100 ºE, 28 ºS-18 ºS). This region was deliberately chosen to coincide with the eastern pole of the Indian Ocean Subtropical Dipole (Behera and Yamagata, 2001).

Shifts were detected using the cumulative sum technique, the shift detection technique by Rodionov (2004) and the skewness method. The first technique represents the running total of the deviations of the first observations from a mean based on the same interval (Ibanez et al., 1993). In this case, the cumulative IOD value corresponding to a particular IOD value is the sum of all the DMI values up to and including that value. It can be represented by the following formula:

$\square_{\square} = \sum_{\square\square\square}^{\square} \square_{\square}$ *where* $\square_{\square}$ *is the cumulative DMI for the* $\square$*th IOD event* $\square_{\square}$.

These are plotted over time (years) to allow one to determine the year when an abrupt change occurred through identifying inhomogeneity within the data series. However, despite its simplicity in implementing, this approach is considered robust in detecting change points (e.g. Breaker, 2007). The second method provides a probability level for the identified year of regime shift in the mean and/or variance. In the algorithm, the procedure for detecting regime shifts in the variance is similar to the one for the mean, except that it is based on the F-test instead of the Studentôs t-test. This technique involves sequential data processing in which the testing is done in sequence. The current work uses a large cutï off length (31 years) and a probability level of to 0.01 to confirm significance. The method has been widely used in physical (Figura et al. 2011), biological (Overland et al. 2008) and economic context (Dionne et al. 2009). The software for the detection of a regime shift is available on the website http://www.beringclimate.noaa.gov/regimes.

The last method determines the shifts in the IOD time series by assisting to identify abrupt changes in the skewness of the SST data using the following formula:

$\gamma_k = \frac{n}{(n-1)(n-2)} \sum_{i=1}^{n} \left[\frac{x_i - \bar{x}}{\sigma_k} \right]^3$ where $\bar{x} = \frac{\sum_{i=1}^{n} x_i}{n}$, x_i is the *i*th observation (monthly mean) γ_k and σ_k are the skewness and standard deviation respectively for n (n = 31) data series for the *k*th year beginning from (1870 + n)th year. γ_k is the skewness values at the end of the kth 31 year segment. This returns the 31 year segment skewness distribution for the IOD time series. The skewness characterizes the degree of asymmetry of the IOD distribution around its mean. Positive skewness indicates a distribution with an asymmetric tail toward more positive values and the negative skewness indicates a distribution with an asymmetric tail toward more negative values. Running variances, regression and correlation techniques are employed to determine the temporal manifestation of these parameters for a conservative sample-size estimate of 31. For this sample-size, a correlation coefficient of 0.36 is the 95% significance level based on a 2 tailed Student's *t* test.

2.3 Results

2.3.1 Shifts in the IOD System

Much has already been studied with regard the IOD and its temporal variability but these previous studies are based on the positive minus negative IOD composites which may not address the shift issue. Here we reexamine the DMI but in search of unique properties and systematic patterns of the coupled mode from 1870 especially related to shifts in the system. An inspection of the temporal time series of this long term IOD index reveals both strong interannual and low frequency background variability (Figure 2.1). This figure gives an impression that the IOD phase and amplitude generation is chaotic in the sense that the mode seem to be flipping in an unsystematic way (randomly) from one phase to another of its three preferred quasi-stable states (normal, negative and positive). Deterministic models have also

been able to exhibit this chaotic behavior qualitatively and reproduce the irregular oscillations of the IOD for strong coupling between ocean and atmosphere (e.g., Luo et al., 2007). Closer scrutiny of the IOD SST anomalies depicted in Figure 2.1 reveals that discontinuities could be highly characterizing the IOD climate system.

The IOD time series shows some degree of asymmetry between the positive and negative phases. For example, we note a wide difference between standard deviation magnitudes of the two opposite phases. The positive events have a standard deviation of 0.74 °C that is almost twice as much as the negative events whose value is 0.38 °C. The highest magnitude of the positive events during the study period is 3.95°C (1997) which is more than twice as much as its negative counterpart that has a value of 1.55°C (1874). We also see that the asymmetric nature of the events can be differentiated by three locations shown by arrows in Figure 2.1 (i.e. 1918, 1961 and 1997, shown as positive red bars). It has to be noted that in Figure 2.1 the red bars are preceded by two negative (brown and green) bars in succession.

While the amplitude of the extreme negative events does not show any significant trend during the study period, the intensification to higher amplitudes after 1917 is quite obvious in Figure 2.1. It is also intriguing to note that despite indicating significant decadal modulation of the 31year moving IOD variance-envelop, Figure 2.1 also depicts the year of change to occur just after a period of relatively low variance. But in general a four step-like increase in the variance trend can be noted during the entire period. To confirm such an interesting pattern of IOD decadal variability, we examined other datasets from the National Climatic Data Center Extended Reconstructed SST dataset version v3b (NCDC ERSST v3b) and Kaplan SST dataset

over the same period. They also revealed similar decadal phase and variance variations of the IOD index (diagram not shown) that can be easily approximated to four regimes. Thus from the seeming chaotic nature of the IOD four systematic nonrandom epochs that display some high degrees of homogeneity can be identified (i.e. from 1871 to 1917, 1918 to 1960, 1961 to 1996 and 1997 to 2009) irrespective of the SST dataset used. We also note that the decadal fluctuations of the opposing IOD phases feature prominently within the temporal records. This behavior should be a very important property of the long-term IOD index. Accordingly, such decadal phase and amplitude variations should also be given due attention and prioritized as yet another important characteristic of the IOD mode.

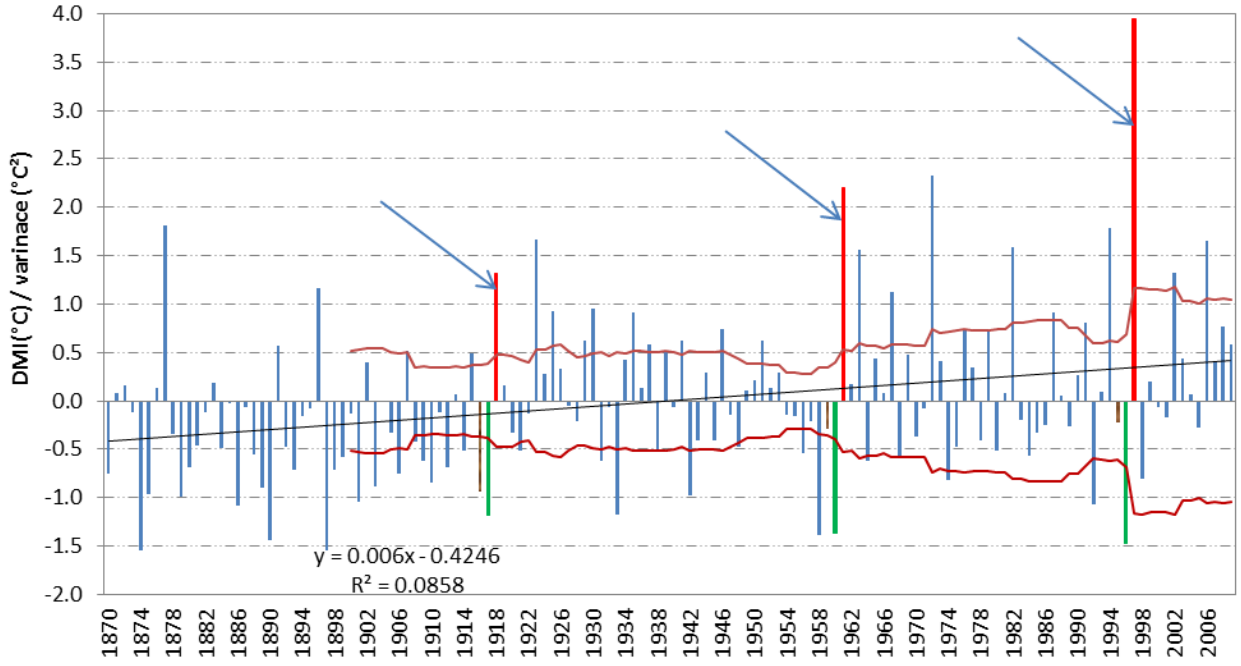

Figure 2.1: Temporal manifestation of OND IOD index (bars) with its linear trend (solid straight line) and the 31 year moving variance envelop. Both the bars and the solid curve use the y-axis on the left. Note, two successive negative bars (brown followed by green) always precede the positive (red) bars.

More evidence for the epoch demarcation is provided through the examination of the IOD index using the cumulative method. This method is capable of identifying inhomogeneity within time

series. In figure 2.2 this technique confirms that some systematic and predictable patterns are inherent in the SST anomaly data series. The major three (1918, 1961 and 1997) turning points delineating the earlier identified four epochs are quite conspicuous in the figure. Since the latter two shifts occurred during a more recent period when the data quality had improved, it is easier to confirm their existence through other various data sources. However, confidence in accepting the first shift as real is boosted by the fact that other studies (e.g. Abram et al. 2003; Nakamura et al., 2009a,b), on reporting on the recent intensification of the IOD based on a completely different data source, the coral records for the past 150 years, noted a shift to stronger IOD events since 1920. This implies that the first shift of 1918 is correctly approximated and could be responsible for the noted abrupt change in the coral records. Having established the epochal nature of the IOD, from now on, all the data are analyzed separately in the four regimes: 1871 to 1917, 1918 to 1960, 1961 to 1996 and 1997 to 2010, as we now consider the years 1918, 1961 and 1997 as the shift years for the IOD. For ease of reference, the epochs will be correspondingly referred to as 1^{st} epoch to 4^{th} epoch. It has to noted however, in the interpretation of the results that the last epoch is still of indeterminate period.

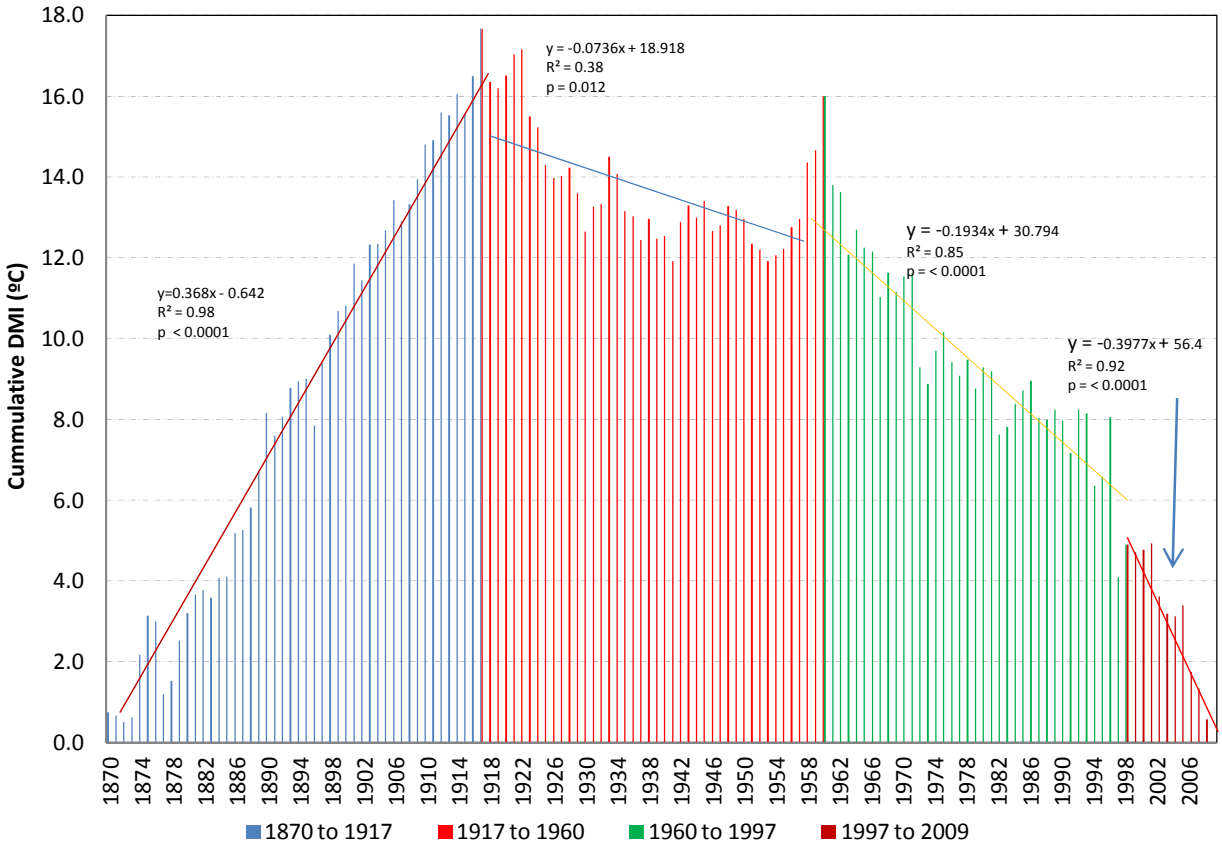

Figure 2.2: Temporal structure of the IOD index from 1870 to 2010 using the cumulative method. The value represents the sum of the preceding DMI values including that of that year The graph has been reversed to ease visual impression

To further confirm the homogeneity within each epoch regression lines inserted in figure 2.2 indicate that they fit quite well to the data points by producing very high R^2 values that have p values close to zero. In addition, the significant abrupt change in the gradient on each of the three turning points reveal notable sudden óswitch onô of the gradient from one epoch to the next. This denotes the breakdown of a prolonged regime and the emergence of a new regime. Since the graph has been reversed to ease visual appreciation, the related regression equations have to be multiplied by -1. Thus we note that in the first epoch (1901 to 1917), there is a predominant cumulative contribution of negative DMI values, indicating a period dominated by negative IOD events. The corresponding regression line shows a relatively steep negative gradient. The second

epoch, (1918 to 1960) is characterised by a transitional period but with majority of contributing positive IOD events and a relatively moderate positive gradient. The third epoch (1961 to 1996) has increased and stronger positive events, with incremental values that translate into a steeper positive gradient. Finally the last epoch has the steepest positive gradient that indicates the highest contribution of predominantly positive events with increased frequency but relatively reduced amplitudes compared to its immediate predecessor.

This observation is consistent with Tozuka et al. (2007) who, using a high-resolution coupled model, interpreted the decadal IOD variability as decadal modulation of interannual IOD events through asymmetric occurrence of positive and negative events. Similar epochs were derived by other recent studies (Kripalani and Kumar 2004; Yuan et al., 2008) that noticed that the IOD was in a negative phase in the period between 1880 and 1920 and was in a positive phase in the period between 1960 and 2000. However their period of analysis could not allow them to identify the 4^{th} epoch and the work also did not provide enough detail on the nature and cause of the asymmetry.

Since there appear to be a strong bias in the development of the different phases of the IOD relative to the epochs, in figure 2.3 we indicate the epochal frequency of the pIOD and nIOD events including the sum of events for each phase during the whole period. We note that the 1^{st} epoch is dominated by relatively strong negative events. Of the twenty extreme events eighteen are negative. The 2^{nd} epoch has a substantially reduced number of extreme negative events making it appear to be a transitional period with four negative and six positive extreme events. Thus after this transitional period, the 3^{rd} epoch is dominated by positive events with ten positive

and only three negative events. Finally the last epoch has the least number of events, most probably because the epoch is still immature. However, it is comprised of one negative and three positive events but the latter events are of suppressed amplitudes relative to the preceding epoch. This is the epoch that has been noted to have broken the 20th century record by having three consecutive positive events from 2006 to 2008 (e.g. Cai et al., 2009). It should be noted that in the current work, 2007 failed the set criteria for a pIOD event unless the September to November averaging period is used.

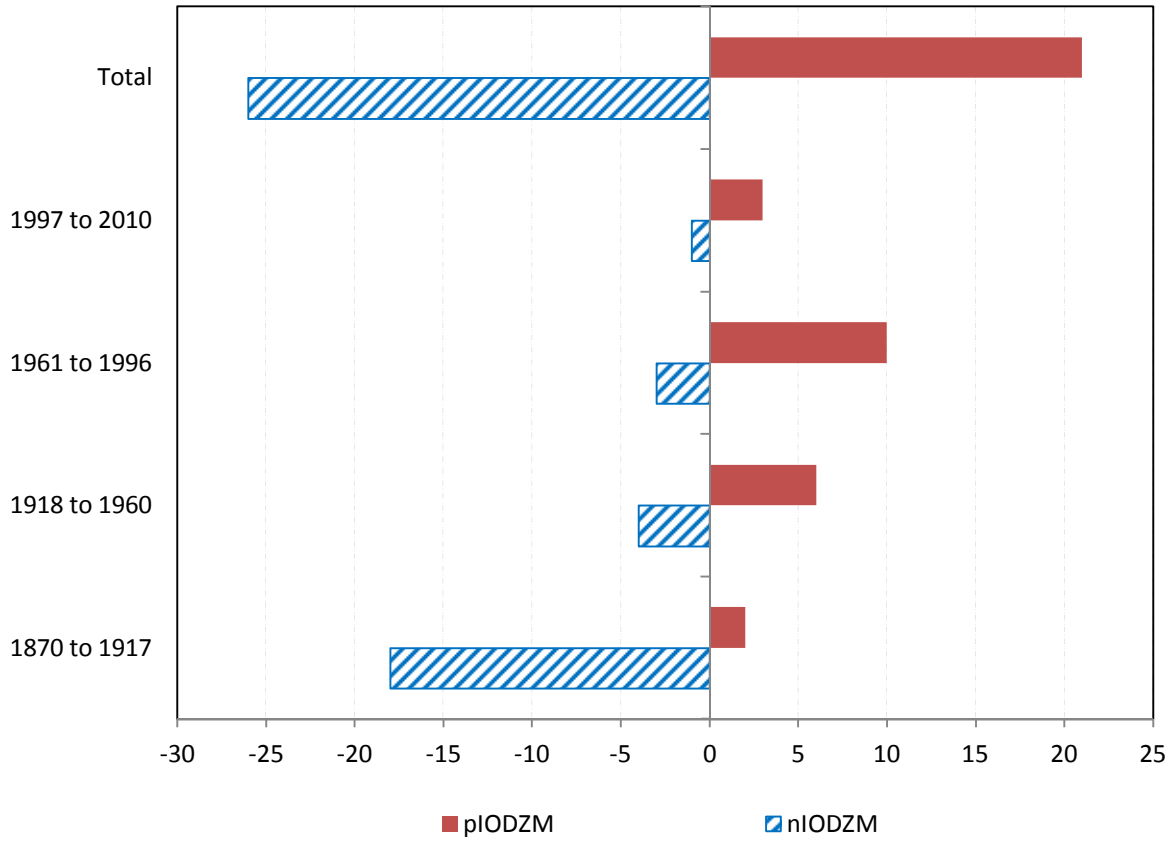

Figure 2.3: Epochal frequency of the nIOD and pIOD events for the period 1870 to 2010. The negative sign in the x-axis is for emphasis of the phase difference only.

We then investigate this asymmetry in the light of the background SSTs as conditioned by the 4 epochs. In the light of global warming we suppose that the associated warming trends are

homogeneous in space, and hence it is expected that the anomalous SST gradient over the equatorial Indian Ocean should remain the same. But if not, these differing trends could affect the strength of both positive and negative dipole events, and may be related to the multidecadal variability of the IOD events. Thus, it is vital that we delineate the relationship between the SST anomalies in the western and eastern poles of the dipole mode over the long term in consideration of the warming trend over these regions. In figure 2.4 we present the epochal SSTA not only for the DMI and the corresponding standard deviations but for its decomposed components of the eastern and western poles. In this figure, we note that the DMI SST anomalies had moderately strong negative gradient in the 1st epoch, weakened to become positive in the 2nd epoch but with little alterations in the corresponding DMI standard deviations, before reaching their highest gradient values and almost doubled their initial standard deviation magnitudes in the last epoch. On the other hand the poles warmed differently with the western pole warming considerably faster than its eastern counterpart. In the last epoch the western pole warmed by 2.4 ^{o}C whilst the eastern pole warmed by 1.3 ^{o}C, giving a significant difference of more than 1 ^{o}C. The lowest SST anomalies for both poles were found in the 2nd epoch with the highest anomalies accompanied by a sharp rise of the DMI variability in the last epoch.

From this important observation, we can conclude that the responsible process does not affect the poles randomly but systematically and inversely. We note that it is only in the first epoch that the western pole is anomalously cooler than the eastern pole. The SST anomalies are both negative in the second epoch but with the east being cooler by a relatively smaller margin. The eastern pole remains cooler in the remaining epochs with the biggest difference in the last epoch. Theoretically, a situation in the tropical IO with a cooler western pole background is conducive

for the formation of negative IOD events whilst the reverse favors the development of positive IOD phases. This could explain why in figure 2.3 we see that the first epoch is dominated by negative IOD events, with the second epoch being a transitional period to the last two eras which have increasingly predominant positive IOD events. Therefore we can deduce that there could be a process in the background that is imposing tendencies of the occurrences that are initially dominantly negative and eventually changes through three gradual regimes to one that is dominated by positive dipole events in the first decade of the 21st century.

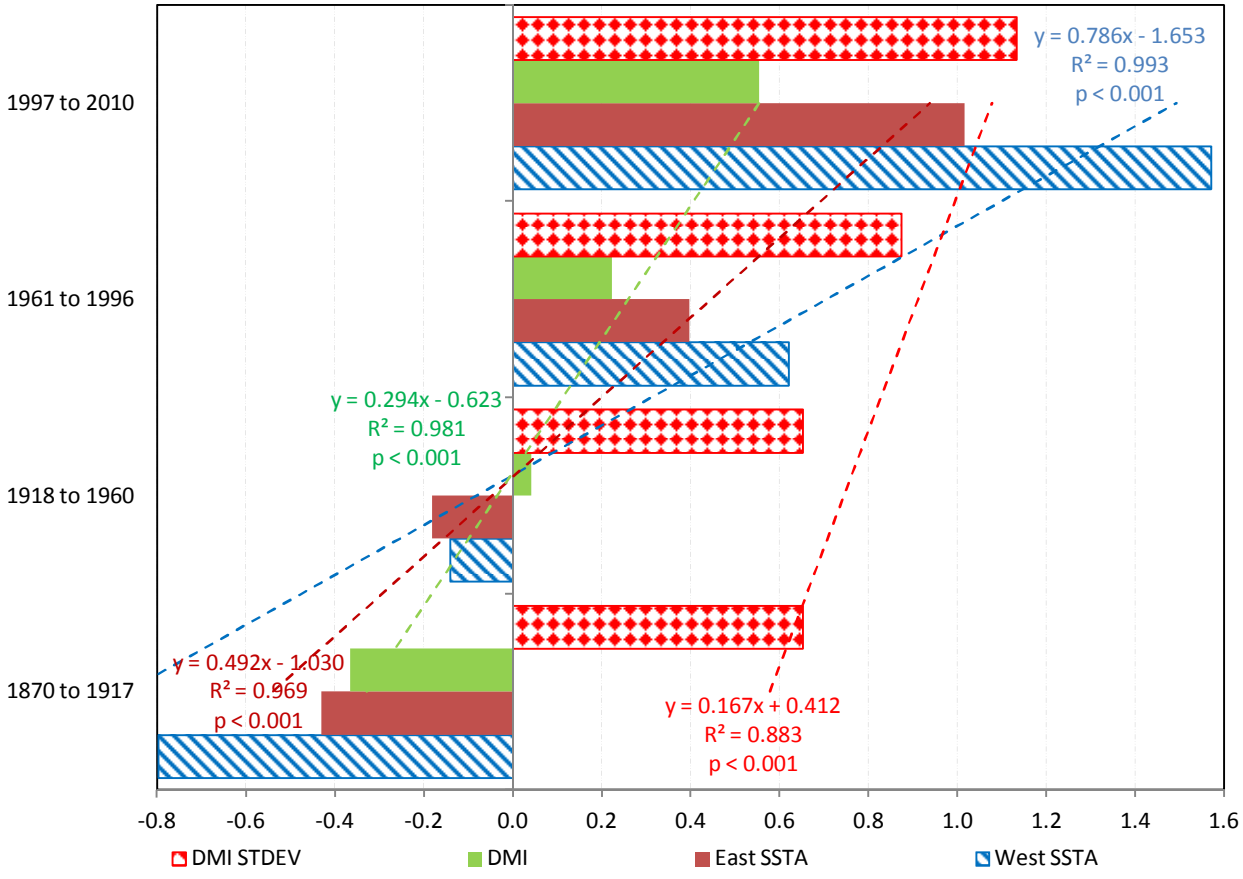

Figure 2.4: Epochal SST anomalies for the East and West poles, the DMI and the corresponding standard deviations of the IOD for the period 1870 to 2010. Colors for regression equations and their lines correspond.

At this moment we found it logical to demonstrate evidence of these epochal changes by employing a more objective regime shift detector method by Rodionov (2004). This may reduce the possibility that the noted shifts in the tropical Indian Ocean SST mean state could be discernible from residuals in the statistics. The software is designed to automatically detect shifts in both the mean level of fluctuations and the variance. Hence a regime shift is confirmed when a statistically significant difference exists between the mean value of the variable before and after a certain point based on the Studentôs t-test/F-test. We were motivated to use this method as it proved to be a simple detection technique capable of detecting regime shifts, not only in the mean but also in the second-order statistics such as the variance. The technique of simultaneous detection of the significant shifts in both the mean and variance is more ideal for confirming the proposed shifts as major alterations in the mean may not necessarily translate to significant swings in the variance. Therefore for a shift to have occurred in the IOD system, it is suffice to have it confirmed by at least either of the two test methods.

It is essential to note in this regard that the algorithm is designed to detect abrupt shifts for certain parameters and may not work if a transition from one epoch to another is more gradual for other parameters. Thus the change in sign of the DMI while not significantly altering the variance from 1918 may have resulted in the detection of a statistically significant abrupt change only in the mean. The change in variance detected for the later years of 1958 and 1994 were revealed as significant but were not associated with corresponding DMI epochal means with sufficient differences to be detected as statistically significant. Thus the transition in 1918 proved to be too gradual for significant variance changes while for the same reasons 1958 and 1994 failed to pass the requisite test during their respective epochal mean alterations. The reason is

that while variance yields squared values it does not detect changes in the sign if this is not accompanied by significant change in the DMI amplitudes. On the other hand the change in the sign accompanied by little variance transitions may result in larger corresponding mean differences. Thus we note that changes in variance (mean) do not necessarily tally with the timing of the shifts in the mean (variance). However, the last two alterations in variance were established as significant climate shifts in the Indian Ocean but with a time lag of three years in both cases (1958 and 1994, Table 2.1) as compared to previous detected shift periods. As such 1918 is considered a shift on account of significant differences in the mean but not in the variance. On the other hand 1961 and 1997 are acknowledged as shifts due to significant alterations in the variance but not in the mean.

Table 2.1: Shift detection technic in the DMI using the software designed by Rodionov (2004) for (a) the mean when the cutoff period length (L) = 31yrs, the Huber weight parameter (H_W) = 4 and target significance level = 0.1 (b) the variance when the cutoff length (L) = 31yrs and the target significance level = 0.1

(a)

Shift Year	Duration before shift	Mean after (before) shift (ºC)	RSI	P-Value
1918	48 yrs.	0.041 (-0.366)	0.412	0.004

(b)

Shift Year	Duration before shift	Var after (before) shift (ºC²)	RSI	P-Value
1958	88 yrs.	0.774 (0.454)	0.002	0.047
1994	36 yrs.	1.501 (0.774)	0.122	0.100

Where: Shift year is the period when the shift was detected, RSI is the Regime Shift Index, Var is the variance of the regimes, Duration is length of the regime to shift, P-Value is the significance level of the difference between the means (variances) of the neighboring regimes based on the Student's two tailed t-test and (Fisher's F-test).

We also measured the asymmetry in the DMI where the strength of the asymmetry is measured by the concept of skewness (Hong et al., 2008). Four regimes of distinct skewness can be extracted from figure 2. 5. The regimes have a tendency towards more positive values especially in the last two. Since skewness can also be used to measure discontinuity within time series, here

we note that 1918, 1961 and 1997 come out also as significant shift years. In figure 2.5 we note that the skewness of the SST anomalies of the eastern (broken line) reflect more of the IOD event asymmetry. The skewness of the eastern pole was highly positive up to the early decades of the 20th century. The values diminished but remained positive from the late 1920s before reversing sign to negative in the early 1960s. This negative trend was moderate up to the late 1900s when the negative values shifted to unprecedented levels which reached maximum values from 1997. It has to be noted that 1997 clearly distinguishes itself as the period beyond which the eastern pole started to dominantly participate in the overall skewness of the IOD events. On the other hand the skewness of the western poleôs SST anomalies (solid line) lacks a more coherently defined trend. As such it can be assumed that the western pole may be playing a less significant role in the asymmetric nature of the IOD events. This gives us a clue that the processes responsible for driving this skewness impact more on the eastern pole than on the western side. Thus, we are poised to concur with Hong et al. (2008) who conceded that the DMI amplitude asymmetry is primarily driven from the eastern pole of the IOD.

Analysis of the DMI amplitudes reveals that the three identified turning points display a unique but strong biennial tendency, meaning that the SST gradients (hence the zonal wind anomalies) in each event reverses sign from one year to the next, i.e. 1916-1917, 1960-1961 and 1996-1997. In fact it is only these three occasions related to the major shifts which can be identified with an extreme negative IOD event occurring back to back with an extreme positive IOD event within the whole DMI time series. However, this is not the first time that this particular unique sequence in pairing of successive mature IOD events of different phases has been noted. Using a different DMI time series constructed by Rao et al. (2002) but for the period 1958 to 2000, we also note

that this exceptional combination of a strong negative IOD event that is followed by a positive IOD event could only be identified in 1960-1961 and 1996-1997 periods. This is the first time that such type of phase reversal in its extreme sense that is also linked to the shift process, has been mentioned in the IOD related literature though the IOD has generally been known for its biennial tendency (Saji., 1999).

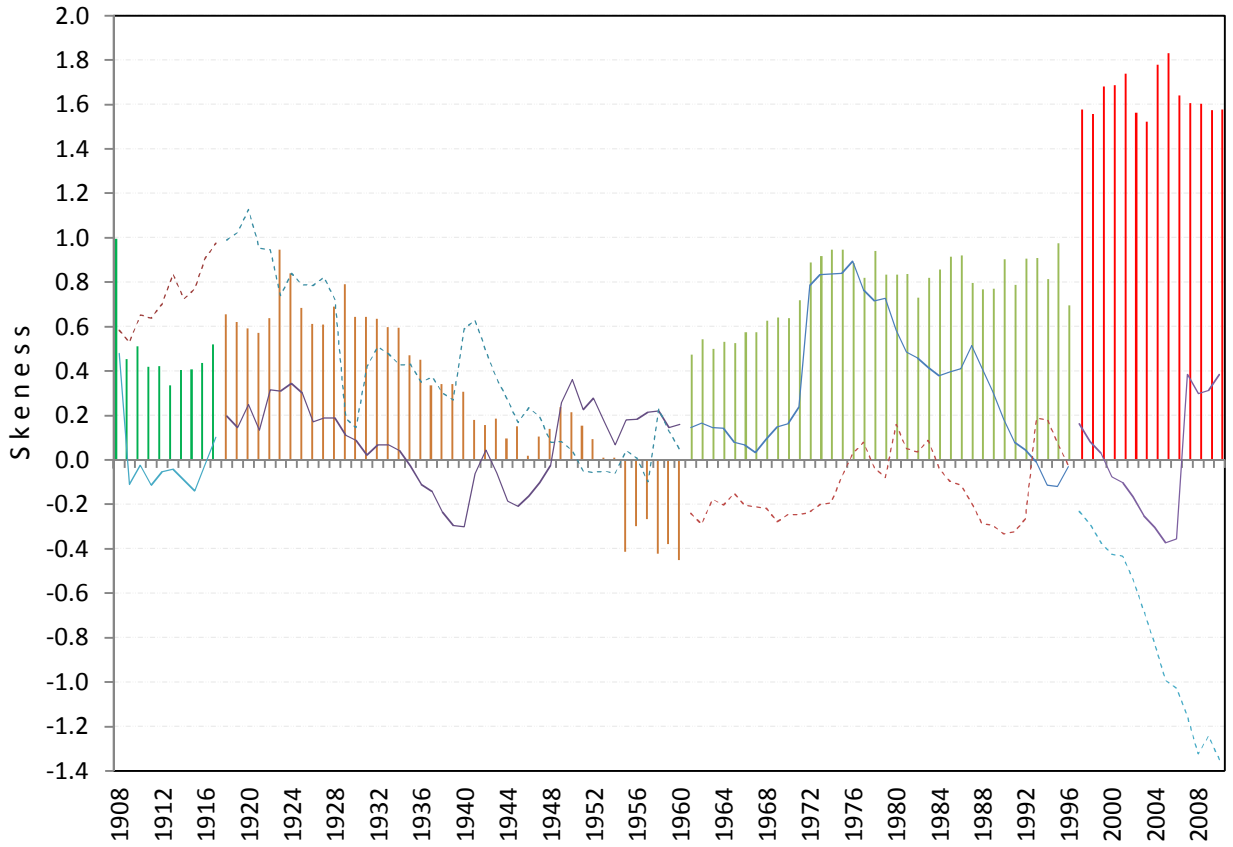

Figure 2.5: Temporal manifestation of OND DMI 31 year moving skewness (bars) with that of the SSTA of the western (solid line) and eastern (broken line) poles. Values are at the end of the 31 year segments.

2.3.2 Biennial tendency in the IOD shifts

A closer scrutiny at the period close to the shift points further brings out a stunning revelation of a process that extends beyond the biennial tendency. An interesting unique three year event sequential pattern manifests itself before each of the major shift episodes. Here (using the

HaDSST 1 dataset in figure 2.6), a negative SST gradient steepens to a very strong extreme negative IOD event the following year which then reverses to an extreme positive IOD event during the shift year. This is a novel development in IOD literature which requires confirmation from alternative SST data sources. The idea is to provide additional evidence to the likelihood that the peculiar IOD phase sequence that has been derived from the HadSST1 dataset is indeed real and not an artifact of data source. Thus we present in figure 6, the three year sequence from other independent SST datasets of the ERSST and Kaplan. By analyzing the three year sequence using all the three datasets, the coincidence in both amplitude and direction of IOD events reveals that it is highly unlikely for all these three datasets to have synchronous IOD phase errors. As a result we are more inclined to believe that the robustness of the three year sequence of events does represent a nonrandom physical process leading to a major shift in the IOD system.

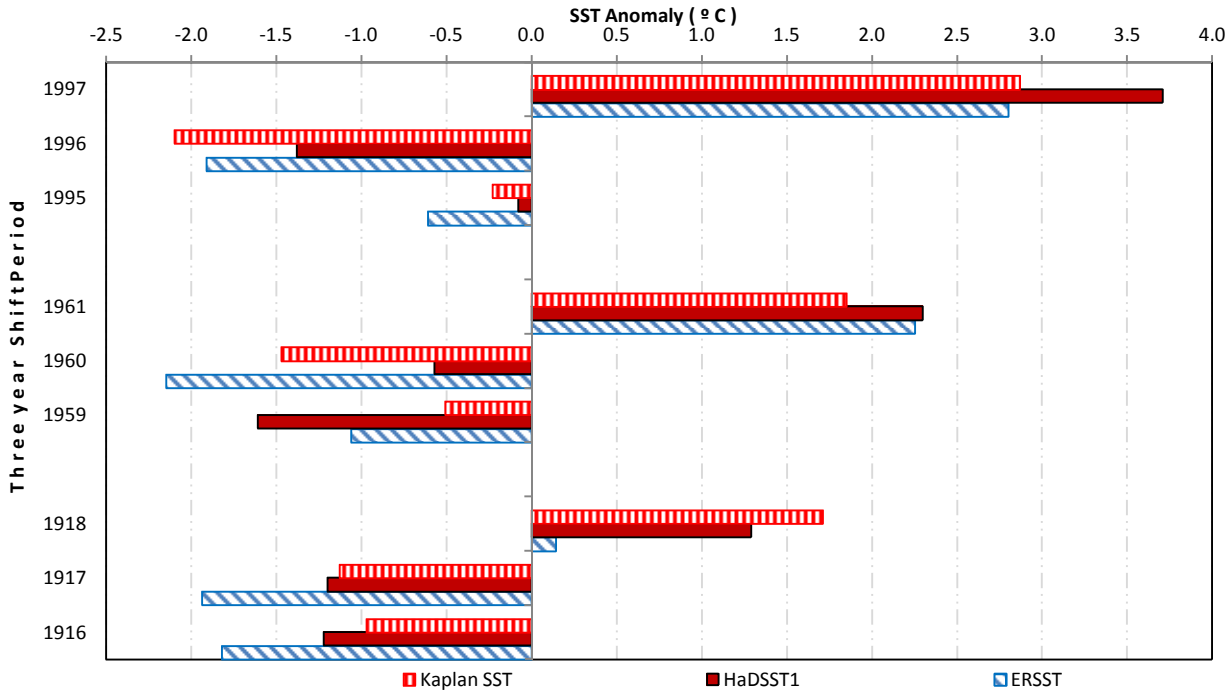

Figure 2.6: The shift year sequence of IOD from ERSST, HadSST, Kaplan SST datasets and their mean for (a) 1918 shift sequence (b) 1961 shift sequence and (c) 1997 shift sequence. The unique sequence is extracted from the common period from 1870 to 2007.

Furthermore we show in Figure 2.7 that the peculiar progression of the IOD phase events prior to the shift is not only confined to seasonal scales but can be traced to monthly SST gradient measurements as well. This is especially true for the period from the months of June to December, which coincides with the IOD event progression from the developmental phases to mature stages (Saji et al., 1999; Webster et al., 1999). It has to be noted that in this work year (-2) refers to the two years before the shift, similarly year (-1) denotes the year prior to the shift and year (0) is the actual shift year. It is further revealed that for each occasion, a negative DMI event grows to a negative IOD event of unprecedented intensity the following season before a phase reversal to a positive IOD of unparalleled strength during the shift year. Thus each positive and negative IOD event occurring prior to the shift appears to be shifting to its highest value relative to the previous regime. This means that for the epochs 1871 to 1918, 1919 to 1961 and 1996 to 2010 the average in the three datasets reveals that year(-1) and (0) have the highest magnitudes in their respective epochs. A negative IOD can be considered as an intensification of the normal Indian Ocean climate state whereas a positive IOD represents conditions nearly opposite to the normal. Therefore the noted shift sequence can be considered as a rapid enhancement of the normal state of the tropical IO towards the last two years of an epoch. This culminates into a major shift through its reversal in the third year and in so doing terminates the existing epoch. This observation indicates that these shifts are not random events but constitute a defined process which has been intensifying on each shift (Figure 2.7).

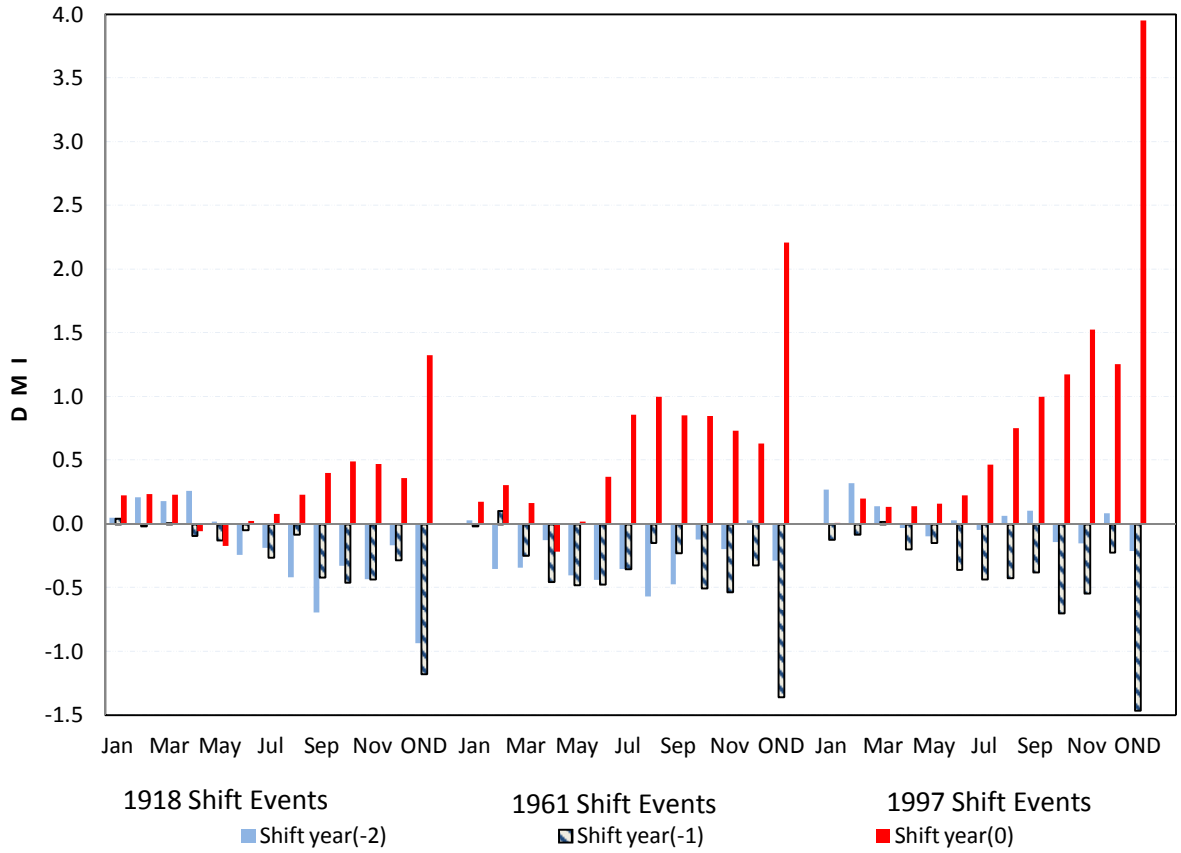

Figure 2.7: Averaged monthly IOD SST gradients for year (-2), year (-1) and year (0) of (a) 1918 (b) 1961 and (c) 1997.

Better visual appreciation can be achieved through presenting the shift process in the cumulative sense. In this procedure, we model the three year shift process by taking the monthly averaged gradient values that are calculated cumulatively. This means that the gradient values at each point is the total gradient anomaly since the beginning of the three year process. For example, the SST cumulative anomaly gradient value for December 1997 is the overall value of all the preceding anomaly gradients since the beginning of the three year shift process (Figure 2.8). The use of cumulative variables in the analysis of climate problems is not new. It derives from the idea that certain climate driven quantities respond not only to the instantaneous climate, but to the accumulated effects of the climate variables over the period of time. Thus this method

enables the shift process to be considered holistically, being composed of sequenced and linked events rather than seasonal events that are independent. In figure 2.8 we present the cumulative manifestation of the monthly SST gradients beginning with year (-2), year (-1) and eventually year (-0) for all the three shift processes. It has to be noted that this pattern cannot be compared with any other set of arrangement of IOD events within the time series because the shift year sequence is unique within the whole IOD time series. However we have combined the cumulative mean of pIOD events and the mean values of the nIOD. This enables the temporal depiction for comparison between the cumulative nature of the monthly SST anomaly gradients of the positive and negative IOD events occurring within the shift and those developing outside the shift.

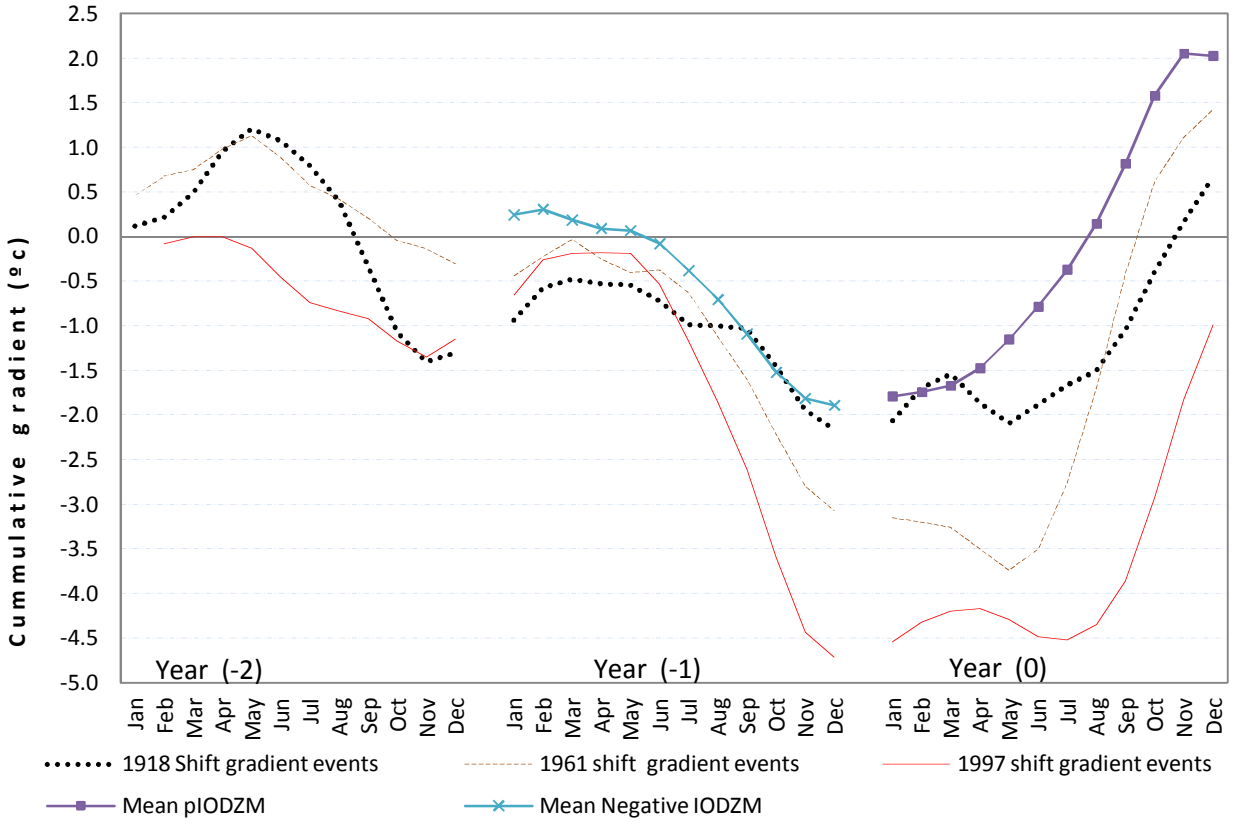

Figure 2.8: The progression of the IOD averaged OND events leading to the major 1918, 1961 and 1997 IO climate shift. The cumulative mean gradients of those that occur outside the shifts are shown with solid lines which have markers.

Here we see that on average, the cumulative SSTA gradients of the IOD events that took part in the shifts process are steeper than those which occur outside the shift. However, there are some differences within those which took part in the shift process. For example, the 1996 event appears to have started to steepen monotonously in July, whilst that of 1960 started to develop in August and that of 1918 started evolving late in September. As for the pIOD events, the 1997 event seem to have started late in July whilst those of 1918 and 1961 both started early in May. On the overall, figure 2.8 confirms that the strength of the nIOD event prior to the shift is related to the intensity of the pIOD taking part in the shift. However, it appears such a pattern of cumulative SST anomaly gradients is unsustainable in the Indian Ocean basin. It is unique and confined only to IOD shift periods. Whenever this peculiar pattern develops, the resulting processes trigger threshold crossing mechanisms which culminate into the attainment of a new equilibrium state in the tropical IO manifesting as a separate IOD regime. Thus we are bound to conclude that nonlinearity is a necessary condition for switching behavior of the averaged IOD characteristics in the basin.

2.3.3 Linking the HM displacements to the IOD shifts

We have noted that the IODôs prominent temporal characteristic cannot be explained by the linear theory. As such we consider that the decadal variation in IOD may arise from a nonlinear source(s) which can be either external or internal. Consideration of more systematic inþuences in the proximity of the tropical IO, in particular the inter-decadal variability of the Subtropical High pressure system also known as the Mascarene High (MH, Figure 2.9a) becomes relevant to understand the cause of the recent methodical decadal variation in the IOD skewness. The MH is forced by the subsiding branch of the Southern Hemisphere (SH) Hadley cell owing to the

Equator-to-Antarctica temperature gradient. In figure 2.9 we note that the regional circulation is dominated by the MH with southeasterly trade winds in its northern flank and a westerly belt to the south. It is this meridional gradient which drives the south easterly trade winds towards the equator hence affecting both the eastern and western poles of the IOD system as shown in figure 2.9b. Thus it is easy to appreciate that not only the strength but also the relative distances of this high pressure system to the two poles of the IOD have profound impacts on the IOD characteristics. It is therefore conceivable that the structural change including either meridional or zonal shift through weakening(strengthening) of the eastern(western) ridge from the mean in the MH may affect IOD characteristics like oscillation amplitude and period. This occurs through the anomalous meridional winds adding or subtracting to the mean meridional wind through variations in the pressure anomalies in the eastern pole of the IOD.

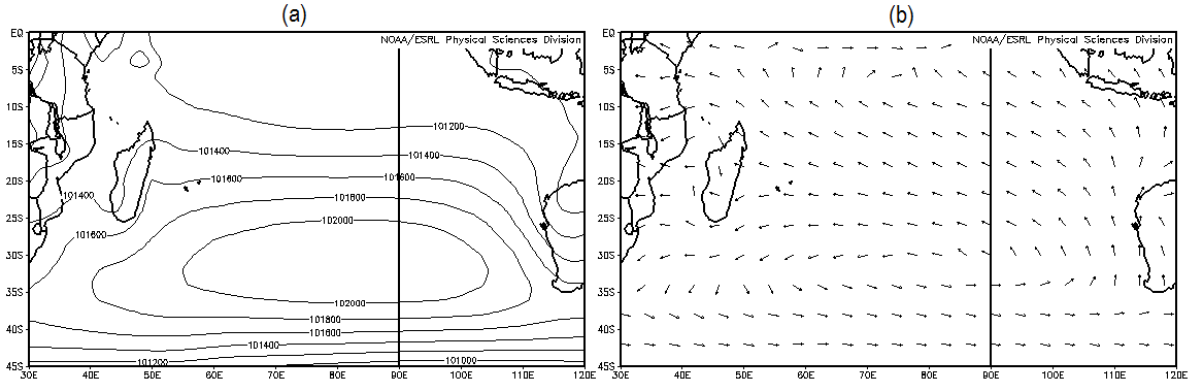

Figure 2.9: Climatology (1970 to 2012) of (a) SLP (pressure in mb) and (b) winds (vectors in m/s),over the south Indian Ocean.

Recent literature has it that the MH has been building up in tandem with SAMôs migration to its positive polarity (Xue et al., 2004) and is displacing eastwards (Manatsa et al., 2012) but the details of this build up is still lacking. In order to appreciate the nature of the buildup of the MH with regard to the eastern part, we first made an assumption that the IOD development is

predominantly determined by its eastern pole. Thus in figure 2.10 we show the 31 year variance of the eastern part of the MH (EMH) alongside with its annual variability. Here we observe a significant multidecadal signal consistent with a weakened atmospheric EMH from 1870 to 1918 and eventually a step like strengthening from 1920-61, 1961- 1997 and finally 1998 to 2010. In this way comparable epochal variability of the EMH and that of the IOD becomes quite distinct in both the variance and the interannual variability itself. In fact the mean SLP of the EMH has been increasing as already been observed but in correspondence to the IOD established epochs.

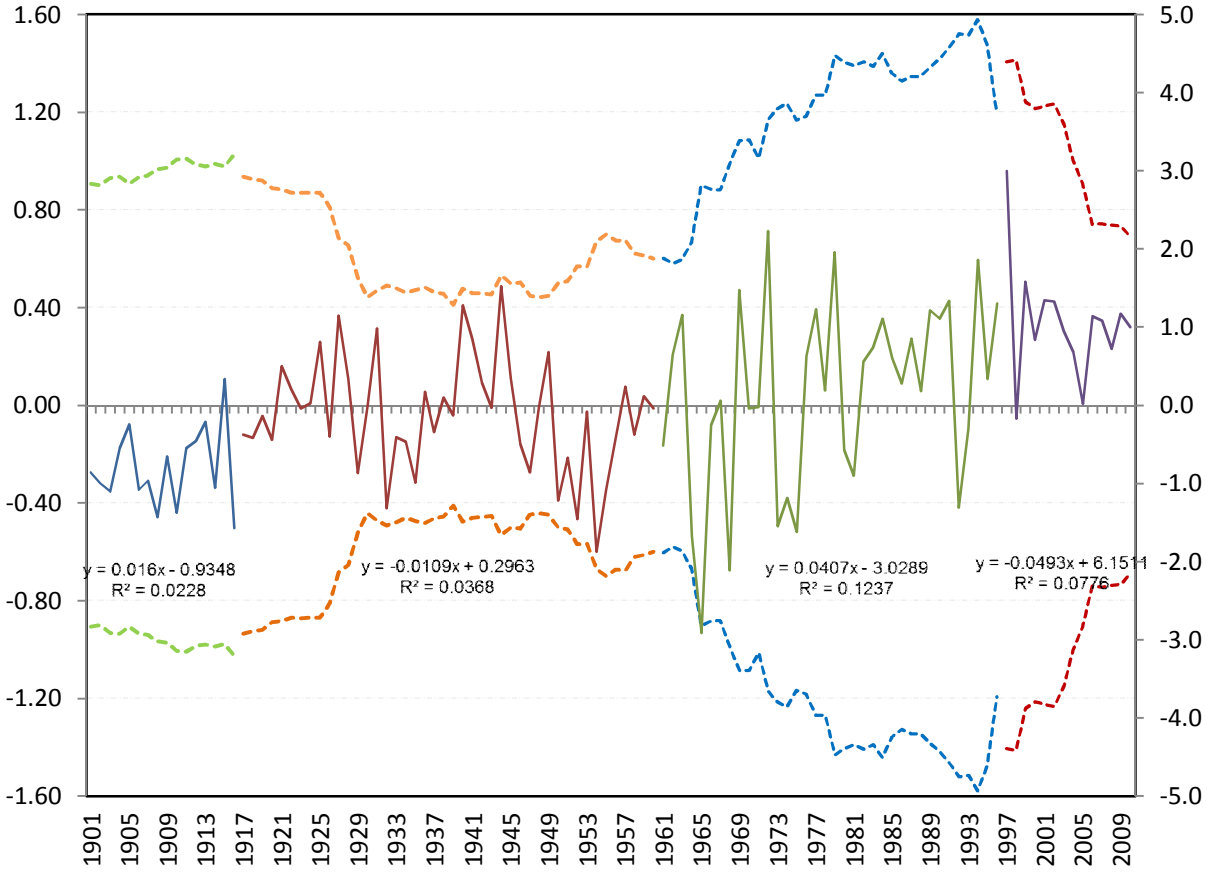

Figure 2.10: Interannual variability of the SLP anomalies in the EMH alongside its variance envelops. The variance is for 31 year overlapping segments with values at the end of the segment. Broken lines represent variance envelops from the first to the forth epoch.

To show that the MH is involved in the shifts as a system during the shift years, we present in Figure 2.11 the relative positions of the MH during year (-1) and year (0) of the three shifts to

see if there are any identifiable significant changes. Interesting characteristics of the MH as demarcated by the 1020mb isobar emerge during these years. We note that there is a general eastward displacement of the western ridge after every shift accompanied by an equatorward movement of the northern ridge (Figure 2.11) for year (0). On the other hand there is a general westward displacement of the MH during year (-1). There is also a shrinking tendency of the area covered by the 1020mb isobar after every shift. From year (-1) to year (0), the MH intensifies remarkably. These processes seem to be escalating at every shift towards the most recent one. The effect is that there is a corresponding weakening of the eastern MH ridge including the SLP over the IOD eastern pole region during the year (-1) followed by a complete reversal process in the same region during the following year. While the position of the MH during year (0) is the most eastward during a particular epoch, the reverse is not that apparent in year (-1) though there is a notable anomalous westward displacement. This links the shift related positive IOD with the eastward and northward displacement of the MH and the reverse for the related negative IOD. It then follows that the maximum contrast of south Indian Ocean pressure pattern and hence the intensity of the MH, from one year to the other is achieved during the shift years. The intensity of this process has been escalating during each of the three successive shifts.

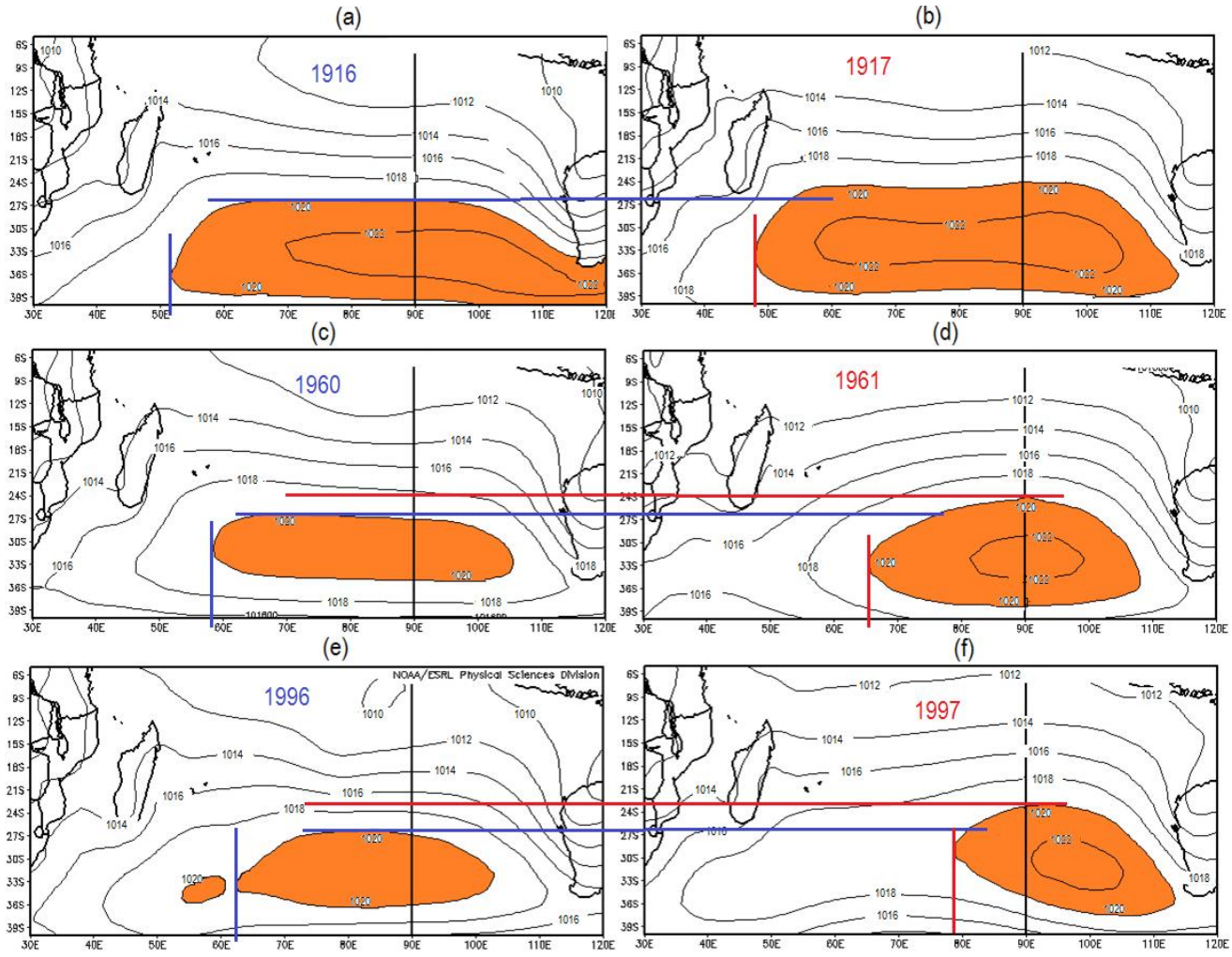

Figure 2.11: Relative positions of the MH during year (-1) (left panel) and year (0) (right panel) for the three shifts (top down panel pairs). Shaded is the pressure above 1020 hPa. The contour interval is 2 hPa.

Table 2.2 further quantifies these MH displacement observations. It is noted that during every shift, on average there is a poleward shift of the northern ridge of about 3.1 º of longitude from year (-1) to year (0). However there also appears to be an equatorward shift of the northern ridge from year (-1) to year (0) as the latitude positions have been changed from the usual 27.0 ºS and 24.0 ºS respectively in the previous two shifts to the corresponding 26.5 ºS and 23.0 ºS in the last shift. A robust progressive acceleration of the western ridge towards the east is also noted after every shift. We note that year (-1) and year (0) had respective western ridge displacement

positions from 52.0 ºE to 58.0 ºE giving a difference of 6 º of longitude in the first shift. These respective positions are then moved from 58.0 ºE to 65.0 ºE, hence covering an extended distance of 8 º of longitude in the second shift. Finally, the last epoch records the greatest eastward movement of 16 º of longitude with respect to year (-1) and year (0) from the positions of the western ridge that literary migrates from 63.0 ºE to 79.0 ºE. Since these displacements are quite robust, it can therefore be reasoned that shifts in the MH mean state position could have pitched the IOD characteristics to new intensity levels after every major shift. This implies that a unique low frequency basinwide process with an epochal escalating tendency could be manifesting itself in the SIO during the shift period.

Table 2.2 *Averaged October to December latitude (ºS) and longitude (ºE) location of the northern ridge (N Ridge) and western ridge (W Ridge) respectively using the 1020mb isoline for year (-1) and year (0) of the three shift years. Progressive differences between year (-1) and year (0) in latitude (longitude) of the northern (western) ridges are also shown.*

Year	**N Ridge**	**Yr(-1)-Yr(0)**	**W Ridge**	**Yr(-1)-Yr(0)**
1917	27.0 ºS		52.0 ºE	
1918	24.0 ºS	3 º lat	58.0 ºE	6 º lon
1960	27.2 ºS		58.0 ºE	
1961	24. ºS	3.2 º lat	65.0 ºE	7 º lon
1996	26.5 ºS		63.0 ºE	
1997	23.0 ºS	3.5 º lat	79.0 ºE	16 º lon

Therefore the variability of the EMH effectively preconditions the equatorial east IO for the development of IOD events. Thus by making this region more susceptible to the windï thermocline feedback, leads to frequent occurrences of positive events, as has been observed in the recent decades. In fact it has long been speculated that the signal related to equator ward extended trades and stronger southeast winds along Sumatraôs coast, are conducive for a mature positive IOD development (Saji et al., 1999). It is therefore more likely that the emergence of more intense and more frequent positive dipole events in recent decades may be speculated to

have a reasonable connection to the trend of the EMH. What is varying is not only the intensity of this anomalous pressure system but the strength and position of the anomalous MHôs eastern ridge relative to the eastern pole of the IOD system. It appears the number of the events per epoch is determined to some degree by the variations in the relative position of the MH. It is more likely that the abrupt and reversed changes in the MH extremes during the shift process is a prerequisite for the shift to occur as no shift has been observed to occur outside this described three year process.

2.4 **Summary and Conclusions**

The focus of this study is to characterize the discontinuities in the IOD system and document the possible role of the MH during the shifts using data sets whose period exceeds a century. The results are explicit in the demonstration of IOD epoch dependent decadal amplitude and phase variations that are separated by three major climate shifts in the Indian Ocean occurring around 1918, 1961 and 1997. Each shift is preceded by a three year sequence of IOD events that are unique in the entire time series. The order is such that a relatively moderate negative SST anomaly gradient intensifies to an extreme negative IOD event which then reverses in the shift year to an extreme positive event. The last two extreme IOD events reach record breaking magnitudes during each shift implying intensification of the shift process with time. During the 1880ï1917 epoch, negative IOD events dominate. In the subsequent epochs, the negative events gradually diminish in number at the expense the positive events at each succeeding epoch until eventually the frequency of the positive events dominate in the last epoch from 1998 to 2010. This systematic but abrupt change in the mean frequency of the positive and negative IOD events has been established through sudden change in skewness and variance of the DMI at each shift

point. On the other hand, the MH seems to also participate in the shift process. During the year before the shift, the MH is anomalously displaced poleward and westward, and it intensifies while moving equatorward during the shift years. At the same time, the pre shift year coincides with the negative IOD year while the shift year occurs during a positive IOD event. It then follows that the maximum contrast of the south Indian Ocean pressure pattern and hence the intensity of the MH, from one year to the other is achieved during the shift years. The intensity of this process has been escalating during each of the three successive shifts.

It is therefore hoped that the prediction of the multi-decadal change of IOD can be achieved upon fully understanding the processes by which the background state inþuences IOD. Further study of the interaction between interdecadal variations of the mean state and the IOD that includes the extratropical variations is required. We therefore can speculate on why prediction of IOD in the longer term has been difficult. It could be that most of the models consider the tropical IO as a standalone basin that is detached from the extra-tropics and hence prescribe a fixed mean state. However, as we have demonstrated, the tropical IO is linked to extratropical latitudes via ocean-atmosphere interactions, on both interannual and decadal timescales. In addition, most IOD prediction models excluded the intrinsic characteristics of IOD that evolved during the last century resulting from the displacement of the Mascarene high, both zonally and longitudinally. We conclude that IOD shift, despite involving to a greater extent the IOD dynamics, may primarily be an expression of the SIO basinwide dynamics rather than a direct response to internal tropical influences**.** After establishing the basinwide shifts in the IO basin, in chapter three we then move on to show how these basinwide shifts, in associated with the Mascarene High alterations could have influenced the rainfall of East Africa.

CHAPTER THREE

Linking the Indian Ocean basinwide shifts to rainfall variability over East Africa.

3.0 Brief Chapter Synopsis

Chapter four is based on the combined results published in two papers referenced as:

1. **Manatsa D**. and SK Behera (2013). On the epochal strengthening in the relationship between rainfall of East Africa and IOD. *Journal of Climate*, Doi 10.1175/JCLI-D-12-00568.1.

In this chapter I establish the strong linkages between the IOD and the OND rainfall of east Africa based on the basinwide shifts alluded to in the previous chapter.

3.1 Introduction

Changes in rainfall patterns have severe consequences for the already hard pressed and impoverished national economies of Africa, adding an immense environmental stress to a region with a reduced capacity to adapt to the mounting adverse effects of global warming. East Africa, in particular, has in recent years experienced increased frequencies in both extreme flooding and severe droughts. In this region which is characterized by sparse water resources, this change is wreaking serious impacts on millions of people and posing unparalleled threat to the community and its environment (Shongwe et al. 2011). Perhaps that is why East Africaôs climate appears to be the most extensively studied part of the African continent. Even though, many issues related to the rainfallôs modulation remain largely unresolved.

The regionôs seasonal rainfall regime is composed of two distinct seasons which are locally known as the ñlong rainsò occurring from March to May (MAM) and the ñshort rainsò taking place from October to December (OND). While the ñlong rainsò is associated with the relatively slow northward movement of the ITCZ, the ñshort rainsôô are related to a more rapid southward migration of this phenomenon (Black et al., 2003). Thus comparatively, precipitation events during the long rains season tend to be less variable, heavier and longer in duration, with less interannual variability, and more likely associated with local factors (Mutai and Wad 2000). In contrast, precipitation events during the óshort rainsô season are less intense with shorter duration and stronger intraseasonal and interannual variability that is more coherent in space and time (Clark et al., 2003).This mirrors more of typical impacts of large-scale phenomena such as ENSO and/or the Indian Ocean Dipole (IOD) during the óshort rainsô, hence our interest on this season.

Efforts have been made in explaining the rainfall variability through two of the most important tropical climate drivers, namely ENSO (Mutai et al. 1998; Reason et al. 2000; Clark et al. 2003) and the IOD (Goddard and Graham 1999; Black et al. 2003; Clark et al. 2003; Behera et al., 2005). But the increased coupling between the tropical Pacific and Indian Oceans during the ENSO cycle since the mid-1970s resulted in frequent co-occurring IOD and ENSO events (Annamalai et al. 2005). Thus the resulting indirect effects from the Pacific via the Indian Ocean could thus have resulted in the statistical relationship between East African rainfall and ENSO described in earlier studies (e.g. Janowiak 1988; Ogallo 1988) and the coincidental physical explanations offered by other more recent authors (e.g. Mutai et al 1998; Kijazi and Reason 2005). In any case, it has now become more apparent that the relationship between the rainfall of East Africa and ENSO is actually more the result of an indirect forcing by ENSO on the Indian

Ocean. Climate model simulations (e.g., Goddard and Graham 1999; Latif et al., 1999) and observation studies (e.g., Black et al. 2003; Clark et al. 2003, Behera et al. 2005) demonstrate plausible evidence of the essential role of the tropical Indian Ocean in modulating rainfall variability.

The recent rainfall characteristics of East Africa are unprecedented in duration, spatial character, intensity and seasonal expression. Hence disasters from droughts and floods have increased in the recent decades (e.g. Shongwe et al. 2011). Understanding the causes becomes essential. In fact, SST patterns linked to the IOD and the associated changes in the basinwide atmospheric circulation are implicated in the rainfall extremes of the recent two decades over East Africa, manifesting as disastrous floods in 1997 (Latif et al. 1999; Webster et al. 1999); and the devastating drought of 2005 (Hastenrath et al. 2007). However, most of these studies have been limited to the decades after the 1950s except for a few (e.g. Hong et al. 2008; Abram et al., 2008; Nakamura et al. 2009, 2011). In these investigations, it is quite evident that stationarity in the relationship with the associated climate drivers has been largely assumed. This assumption may prove to be costly as far as projecting the future climate of the region is concerned, as shifts have frequently punctuated regional global climates before and may still dominate the region in the future. In this regard it becomes logical that the long term temporal impact of the IOD and East African rainfall is established and documented in view of the recently established shifts in the IOD (Nakamura et al. 2009; Manatsa et al., 2012). This may add considerable insight into the usability of the IOD as a predictor and in the climate change modeling of the related rainfall mechanisms.

The present study focuses on OND season, not only because it coincides with the peak period of IOD activity but due primarily to the fact that it has greater impact on the society. The EASR season comes after the driest period of the year (stretching from June to September), is less in amount (accounting for only 30 to 40% of the annual total, Vuille et al. 2005) and less dependable due to its greater variability. In addition it is characterized by stronger spatial coherence of rainfall anomalies across a large part of the region (e.g. Clark et al. 2003). Hence, improved understanding of its decadal to multi-decadal variability and its possible triggers may enhance the long term forecasting of this season. However, the overarching goal of the present study is to demonstrate that it is the epochal changes related more to the IOD itself (changes which are not directly related to global warming) which influenced the observed alterations in the rainfall pattern to become more extreme.

3.2 Data and Methods of investigation

The equatorial East Africa ôShort Rainsô index (EASR) for the OND rainfall is based on a large-scale standardized area-average rainfall index for the region of East Africa depicted in figure 1. The rational for selecting this region is found in Manatsa et al., 2012. The precipitation data is from GPCC V5 and is for the period 1901 to 2009 with a spatial resolution of 0.5°. More details on the data and its usage in research are found on the GPCC Homepage: http://gpcc.dwd.de/. To verify the representativeness of this derived time series we compared it to a Kenya WMO station (63619) called Moyale with continuous rainfall data from 1915 to 2011. No significant differences were noted between the two suggesting that the known shifts in rain gauge density which characterized the region during the period of study did not significantly affect the aerially averaged rainfall time series. To ascertain the normality of the EASR index, the following three

normality test were used, the Shapiro-Wilk test, the Anderson-Darling test and the dôAgostino test. These tests are considered some of the most powerful statistics for detecting most departures from normality in time series.

The atmospheric reanalysis data by the U.S. National Centers for Environmental Prediction/National Center for Atmospheric Research (NCEPï NCAR) (Kalnay et al. 1996) for the period 1948ï 2009 are also used. Although we use this synthetic data to interpret observations, the assimilated data are far from homogeneous. Caution has to be taken as they improve over time in both quality and quantity especially after the 1970s when the satellite era begins. From this reanalysis data, we use the wind data to show large-scale tropical circulation anomalies associated with interannual rainfall variability over East Africa and OLR data to approximate convection. For spatial analysis of the sea surface temperature (SST) we used the Met Office Hadley Centre's sea ice and sea surface temperature (SST) data set, HadISST1. Details of this dataset can be found on the website http://apdrc.soest.hawaii.edu/datadoc/hadisst1.php. The Global Precipitation Climatology Project monthly precipitation dataset (GPCP v2.2; http://www.esrl.noaa.gov/psd/data/gridded/data.gpcp.html) from 1979-present which combines observations and satellite precipitation data into 2.5°x2.5° global grids was used for precipitation analysis over the ocean. The Indian Ocean Dipole (IOD) index was constructed from the SST time series of the east ï west SST gradient from averages over the eastern (0° ï 10° S, 90° E ï 100° E) and the western (10° N ï 10° S, 50° E ï 70° E) of SST time series that are not normalized. The index is derived by simply calculating the SST cumulative gradient for the

individual months of the OND season. The SST data is for the period 1901 to 2009 from the HadSST1 dataset extracted from the Climate Explorer website.

Principal component analysis PCA also known as empirical orthogonal analysis (EOF) is a widely used technique in climate research. One of the major strengths inherent in the PC analysis is that it allows fields of highly correlated data to be represented adequately by a small number of orthogonal functions and corresponding orthogonal time coefficients without a prescribed or predetermined form. The mathematical details of this technique and how it is used are described in Jolliffe (1986). In our case we extracted for analysis only the dominant PC as it was able to reproduce with time, most of the important variation in original rainfall data. In this way the first PC (1) provided an alternative and much simpler description of the data than the original rainfall field. The PC1 was then used to describe the degree of spatial coherence of the rainfall variation for each epoch demarcated by pre-existing shifts so as to assist in interpreting the possible causes of the discontinuities in the spatial variability context.

Shifts were detected using the cumulative sum technique and the shift detection technique by Rodionov (2004). The former represents the running total of the deviations of the first observations from a mean based on the same interval (Ibanez et al., 1993). These are plotted over time (years) to allow one to determine the year when an abrupt change occurred. However, despite its simplicity in implementing, this approach is considered robust in detecting change points (e.g. Breaker, 2007). The latter method provides a probability level for the identified year of regime shift in the mean and/or variance, based on the Student's t-test and F -test. This technique involves sequential data processing in which the testing is done in sequence. The

current work uses a large cutï off length (31 years) and a probability level of to 0.01 to confirm significance. This technique has been widely used in physical (Matic et al. 2011; Figura et al. 2011), biological (Overland et al. 2008) and economic context (Dionne et al. 2009). The software for the detection of a regime shift is available on the website http://www.beringclimate.noaa.gov/regimes.

The standardized precipitation index (SPI) method is used to characterize the rainfall of East Africa. The main advantage is that this technique is able to return fundamental parameters of the occurrence of different drought/wet types in terms of severity, magnitude and frequency. Technically, the SPI is the number of standard deviations that the observed value deviates from the long-term mean for a normally distributed random variable. Details about the SPI computation can be found in several papers including McKee et al. (1993), and Vicente-Serrano (2004). However, the most important aspect in its calculation is that since precipitation does not show a normal distribution, data are transformed to follow a normal distribution using an appropriate transforming method. In our case no prior transformation of the rainfall data was needed since the test for normality using various methods, whose results are depicted in Table 1, yielded rainfall data that were significantly normally distributed. This means that for our OND SPIs, we basically standardized the OND anomalies for the whole period. We also refer to the resulting times series simply as equatorial East Africa ósShort Rainsô index (EASR).

Table 3.1. Results of normality test using various methods from Tanagra Data Mining software version 1.4.42

Atrribute	*µ; Sigma*	*Shapiro-Wilk (p-value)*	*Anderson-Darling (p-value)*	*d'Agostino (p-value)*
EASR	*0.0132; 1.0092*	*0.8679 (0.0000)*	*2.1925 (p<0.01)*	*59.0763 (0.0000)*

In Table 3.2 we present the SPI values, their frequency probabilities and nominal class descriptions. We adopted the Agnew (1999) SPI nominal classification that uses the 5%, 10% and 20% occurrence probability but modified it as it classifies some historical regional rainfall seasons as normal but in fact were traditionally documented as droughts/wet seasons in East Africa. Thus the 33.3% (tercile) occurrence probability is considered, which is normally employed within the African region to define drought/wet season thresholds. In this way another class of mild drought/slightly wet is added to the original Agnew's scale to produce a new scale as depicted in Table 2 (also see Manatsa et al., 2007).

Table 3.2: Seasonal Rainfall Classification by EASR SPI Value and Corresponding Event Probabilities according to Agnew (1999). Note that 21% to 33.3% occurrence probability (in italics) has been added to the Agnew classification so as to accommodate the tercile (33.3%) method used in East Africa.

SPI Value	*Occurrence (%)*	*Nominal SPI Class*
> 1.645	*>= 5*	*Extremely Wet*
1.282 to 1.644	*6-10*	*Severely Wet*
0.842 to 1.281	*11-20*	*Moderately Wet*
0.524 to 0.841	***21-33***	***Slightly Wet***
-0.523 to 0.523	*34 – 50*	*Normal*
-0.841 to -0.524	***21-33***	***Slight Drought***
-1.281 to -0.842	*11-20*	*Moderate Drought*
-1.644 to -1.282	*6-10*	*Severe Drought*
< -1.645	*<= 5*	*Extreme Drought*

3.3: Results

3.3.1 EOF analysis of Equatorial East Africa 'Short Rains' (EASR)

It is evident from figure 3.1 that the topography of East Africa is complex hence the region is exposed to coastal and prominent topographic inþuences. Thus modulation of the rainfall is complicated by interactions of the near-surface flow with the complex topography. Because of this heterogeneity, it is not surprising that Mutai et al. (1998) noted the emergence of dramatic variations in climatological mean rainfall totals with seasonal rainfall anomalies tending to have coherence that is confined to small sub-regions. Some of the spatial coherence is generated by interaction of the large scale regional atmospheric forcing with the topography. As such we expect large scale atmospheric changes associated with, for example, IOD to have a stronger signal in the entire region. Therefore in order to assess the spatio temporal extent of this large scale forcing, a PCA was applied to the rainfall anomalies of the region. This domain free technique enabled us to extract the dominant spatio temporal characteristics of EASR for specified periods in this heterogeneous region. A scree test was used to retain the first 4 PCs as significant (Figure 5).

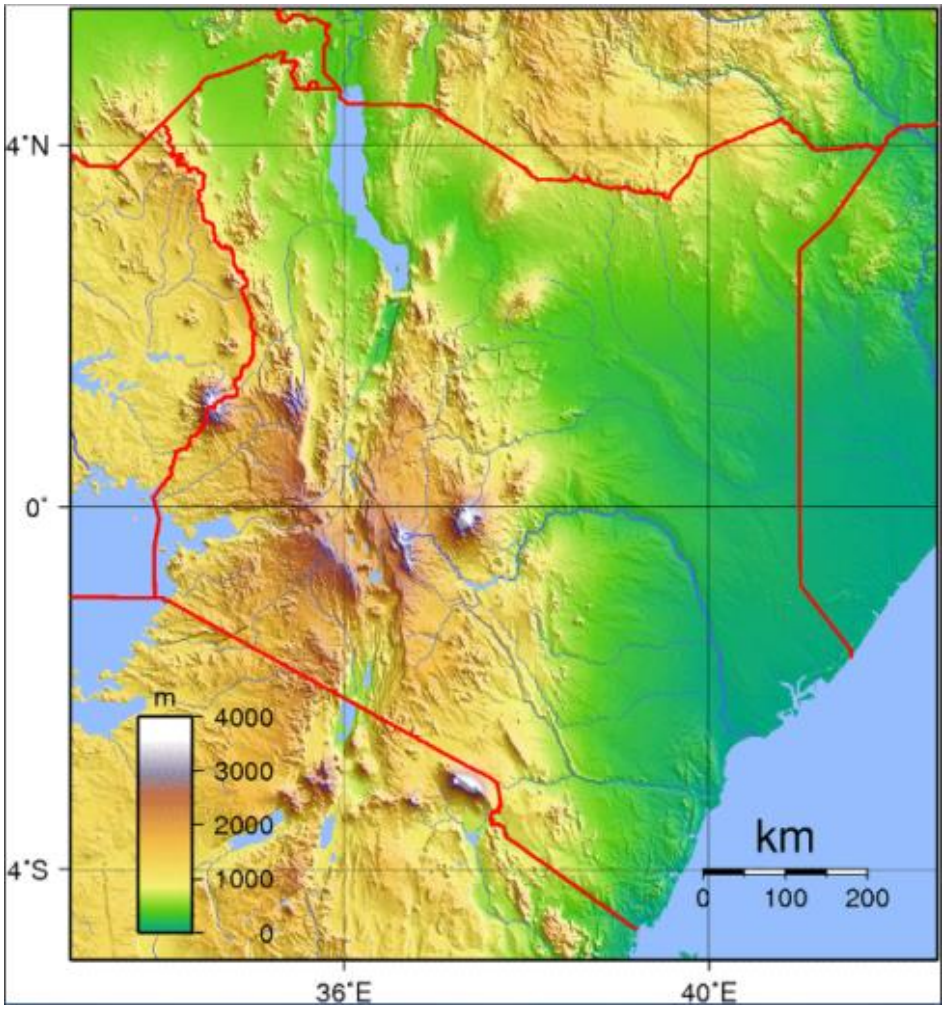

Figure3.1: Relief map for the region of equatorial East Africa from where rainfall data for EASR are extracted. Source http://mapsof.net/map/kenya-topography

PC1 explains by far the variability of EASR accounting for more than 63% of the total variance. Thus in this work we concentrate on this first mode as a guide to approximate the general spatio-temporal variability of the dominant pattern of the regional rainfall. Thus since the main strategy is to determine the changes in the regional rainfall pattern, shifts in PC1 time series will be used to estimate the location of epochal change in the rainfall system. Figure 3.2 shows the temporal manifestation of the interannual variability of PC1 time series. Epochal patterns are quite distinct which can readily be differentiated visually by the years 1918, 1961 and 1997 with the latest two

periods displaying the highest amplitudes in the data record. No significant trend is evident in this PC time mode as indicate by the regression equation inserted in the figure. In any case, a search for shifts in the variance using the regime shift detector (Rodionov 2004) revealed significant shifts during the years 1961 and 1997. However, no significant change in the variance was realized during the year 1918 despite displaying a conspicuously unique temporal variability pattern during the period prior to this year. The broken line superimposed in figure 3.2 illustrates shifts in the PC1 variance as detected by the Regime Shift Detector (Rodionov, 2004) technique using the climatological period of 30 years as the cut off length.

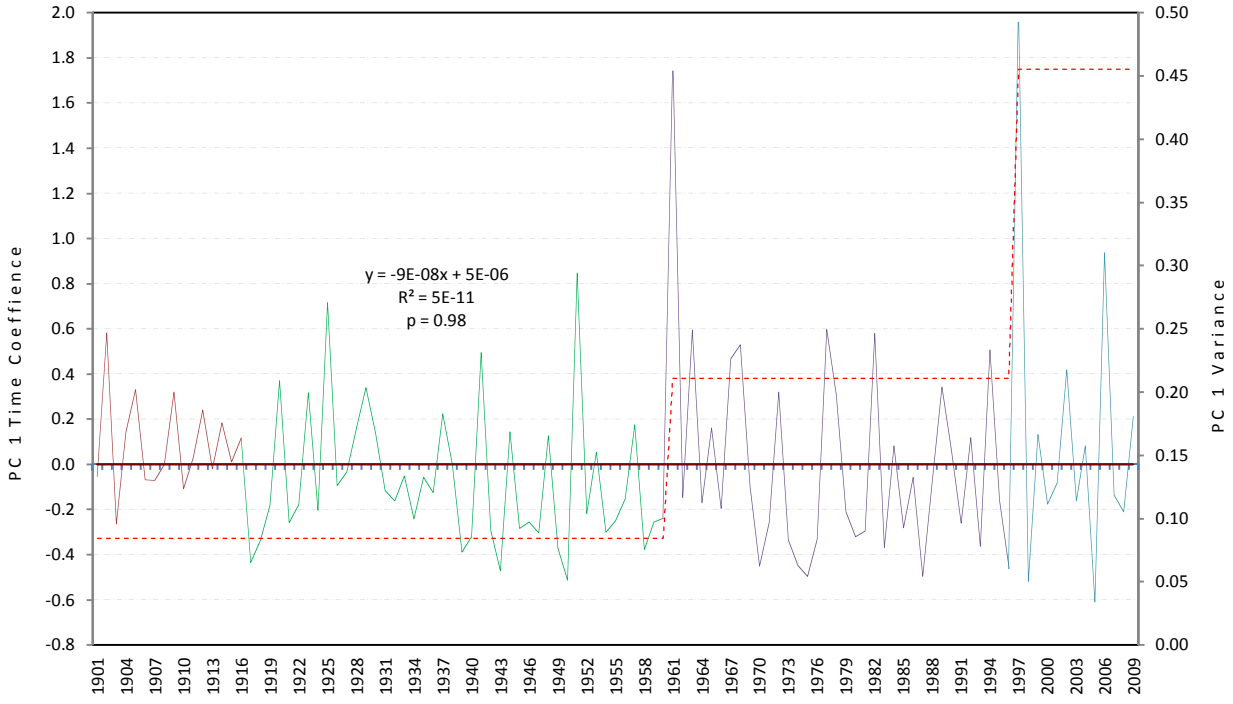

Figure 3.2: Epochal manifestation of PC1 time series and its regression line (solid horizontal line next to the x axis). In the insert is the trend line equation. The broken line represents shifts in the variance as detected by the Regime Shift Detector (Rodionov, 2004).

The statistical results of the regime shift detector test are presented in table 1. It can be noted that the first shift is more significant than the second shift with p-values of 0.002 and 0.076

respectively. This observation adds more evidence towards the physical existence of shifts of climatological significance during at least the two periods of 1961 and 1997. However, a test for the shift in the mean using the same technique did not yield any significant change in this parameter.

Table 3.3: Detected shifts in the PC1 time coefficient variance using the software designed by Rodionov (2004) when the climatological period is set as the cut off length (L = 31 years).

Shift Year	*Duration before shift*	*Variance after/before shift (Diff)*	*CSSI*	*P-Value*
1961	*60 yrs.*	*0.085/0.211 (0.126)*	*0.104*	*0.002*
1997	*36 yrs.*	*0.211/0.455 (0.244)*	*0.003*	*0.076*

In order to ascertain how these shifts could have interfered with the variance of the EASR explained by PC1 time series, we subjected the two time series to running correlation analysis. In this way the temporal changes in the representativeness of the time coefficient of the EOF1 to the actual regional rainfall variability can be deduced. In figure 3.3 we show the running correlation using the climatological period of 31-year segments. Here the correlation coefficients increase from 1948 to 1951 after a prior falling trend. The relationship then increases even more abruptly around 1961 before decreasing swiftly in 1990. An abrupt rise ensures again after 1996. It is interesting to note that the link between PC1 time series and EASR increased drastically in single year periods of, 1961 after consistently lower values in the earlier decade and 1997 also after more than half a decade of a relatively weakened relationship. In this way figure 3.3 confirms the existence of the two years as periods when significant changes took place in the relationship. Thus, we conclude that either a new (pre-existing) dominant rainfall controlling mode is triggered (enhanced) in 1961 before abruptly but temporarily subsiding in influence around 1990 and finally activated abruptly again from 1997.

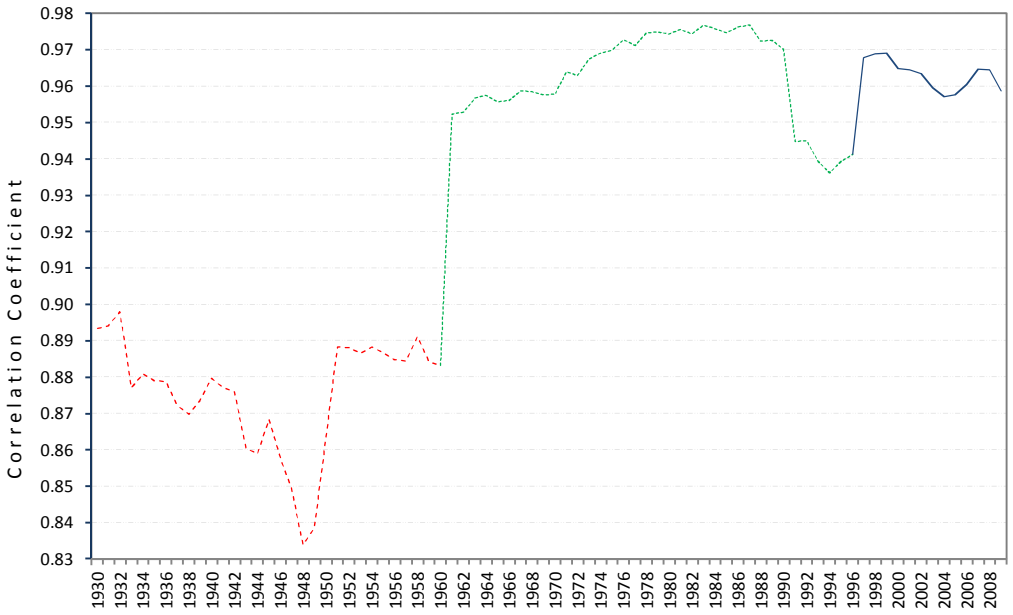

Figure 3.3: Thirty one year running correlation between EASR and its PC1. Values are at the end of the 31 year segment

The realization of the years 1918, 1961 and 1997 as important turning points within the dataset prompted us to examine the behavior of the first 4 PCs initially for the entire duration and later for the epochs as demarcated by the three turning points. In figure 4 we present the cumulative variances (%) of the 4 loading components for each epoch including the entire duration. From this figure we can see that, the first EOF component significantly varies within the demarcated epoch and contributes a minimum of 48% to the total variance in each epoch. In fact, of the 4 loading components presented, EOF1 is the mode with an interesting and unique temporal character. Moreover EOF1 modes in each epoch are well separated from the lower EOF modes in terms of explained variance suggesting that these leading EOFs are robust and stable with respect to sampling errors. This first mode has a continuously increasing trend of explained variance within the demarcated epochs. This indicates the rainfall variability over east Africa is being influenced from a source that is increasingly becoming stronger within the defined epochs. No definite systematic trends can easily be determined from the other EOF modes. This implies

that an important rainfall triggering mechanism of the rainfall of east Africa should have significantly developed or strengthened within the given epochs, principally through altering PC1 in epochs. Given that PC 1 explains a reasonably large fraction of the rainfall variance, especially in the later epochs, it becomes logical to dwell more on PC1 characteristics when making generalized statements of the changing nature of East African rainfall variability.

The increasing variance explained by PC1 in each succeeding epoch in figure 3.4 should reflect the stronger temporal control of the rainfall processes over East Africa. In other words this is a manifestation of the regionôs epochal loss of the finer-scale structure in the rainfall triggering mechanisms as the integration moves towards a more organized and coherent state. It is apparent that this may not be an artifact of direct global warming impact as the change is initiated not only swiftly but in phases also. The sudden change started with 1918 and upgraded in 1961 before further enhanced in 1997. The interpretation is that, with the phase progression in the epochs, fewer modes are correspondingly needed to represent the main features of the rainfall variability of East Africa. In such a case, it could be interesting to investigate the spatial coherence of this PC1 as determined by each epoch. This may assist in identifying the possible climatic mechanisms responsible for developing the related spatial signature over the region.

Figure 3.5a displays the spatial distribution of the PC1 for each of the four epochs including the whole period. All the spatial loadings for these dominant PC exhibit consistently positive values throughout the epochs. This predominantly monopole distribution of the spatial loadings indicates that the EASR essentially varies in a similar phase throughout the region in all the epochs. Thus during the averaged OND sub season, droughts and floods (positive and negative

rainfall anomalies) are expected to generally cut across the whole region simultaneously, though obviously intensities may differ from place to place. However, the notable differences which are conspicuous in the spatial patterns reflect the changing nature of the underlying rainfall generating processes over the region. This may become clearer as we discuss the rainfall triggering mechanisms for each epoch in later sections.

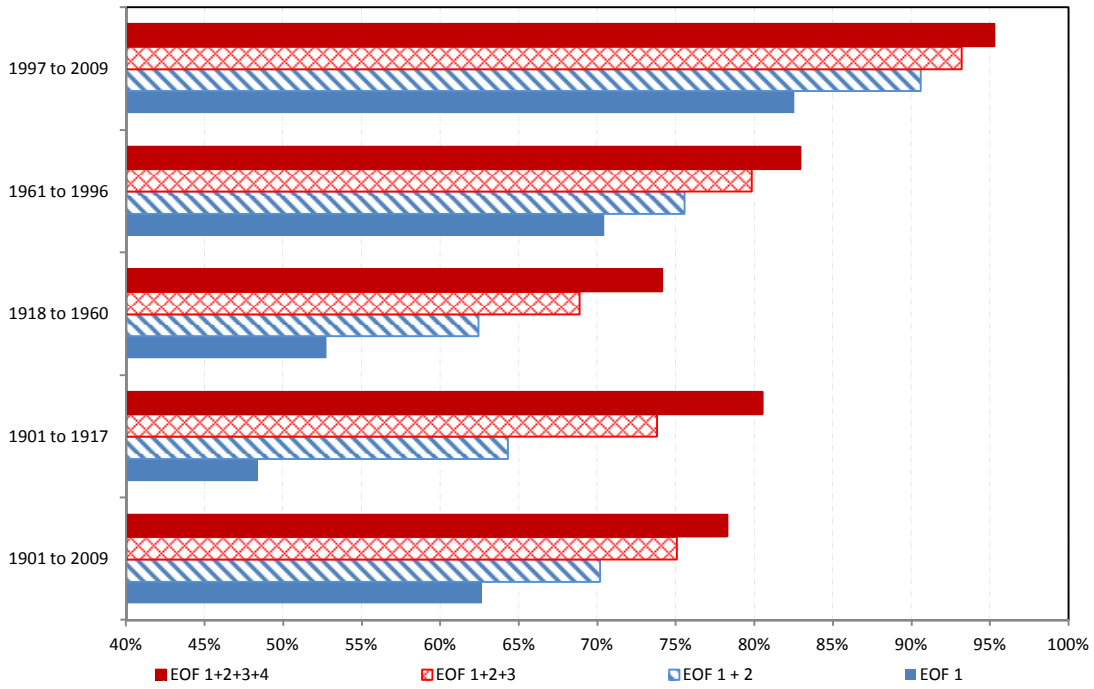

Figure 3.4: Cumulative variance of the first 4 PCs for the entire period and the four epochs.

The variation in the epochal spatial structure depicted in figure 3.5 makes sense if one considers that the rainfall mechanisms are largely a result of the combination of uplift by convection and action of relief on prevailing wind. As such PC1 for the first to the third epoch has a strong meridional orientation which principally reflects the spatial coherence of the rainfall due to uplift by the underlying land surface (e.g., topography) to surface wind with considerable meridional

component from the southern coast. This is mostly because the highlands of the region are situated in the high-value area of the first component distribution map with isolines higher than 0.9 almost reflecting the areas of high relief trend in these regions. Hence despite the intensity, these epochs are mostly representative of the rainfall variability whose cohesiveness is principally relief and meridional wind dominated.

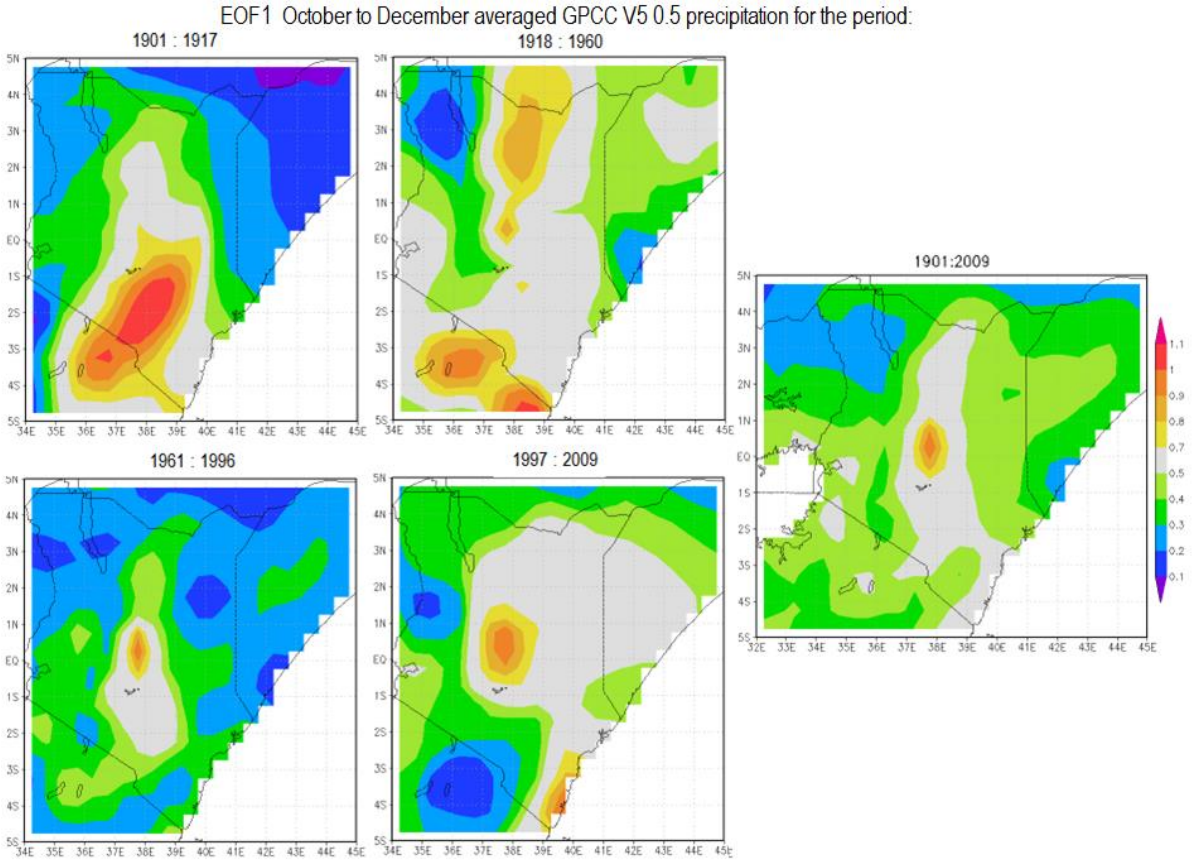

Figure 3.5. Spatial coherence of PC1 for the epochs 1901 to 1917, 1918 to 1960, 1961 to 1996, 1997 to 2009 and 1901 to 2009 for equatorial East Africa.

However, PC1 for the second epoch has more localized structures which are also scattered with no recognizable pattern over the region. Since more modes are necessary to represent the smaller-scale variations, this could explain why the cumulative variance explained by the four modes is the least relative to other epochs. In contrast, the last epoch has the greatest spatial

coherence of PC1 with limited localized features. As such the rainfall related mechanisms responsible for last epoch are so overwhelming in the region that they do not only simplify the spatial structure of the rainfall field but also increases its coherence on the spatial scale. Hence PC1 tends to explain an incredible 83% of the regionôs rainfall variation. It is interesting to note that this enhanced PC1 of the last epoch is remarkably tied to the western Indian Ocean as it displays a spatial pattern which is shaped by the 0.7 isoline that covers most of the interior and spreads to cover almost the entire coastline into the ocean. In the absence of clear cut relief dependence in the last epoch it is highly possible that this spatial structure is dominantly controlled by convection which originates from western equatorial IO. Thus we have linked epochal variations to possible rainfall triggering mechanisms.

3.3.2 The Changing Characteristics of EASR

The seasonal total that we have been analyzing may substantially conceal the finer details of the intraseasonal variability that could be responsible for general alterations in the overall rainfall pattern. We therefore investigate separately the temporal nature of the three months which constitute the EASR. Although the Mann Kendall test did not reveal any significant trend in the individual months, their 31 year moving variances displayed quite varied decadal patterns (Figure 3.6). However, these configurations bear very close resemblance to the one displayed by the DMI. A period of relatively low variability is evident before 1961 of which there is a sudden rise which levels off until the early 1990s. Thereafter the activity subsides before taking yet another abrupt upward turn in 1997. Though the moving variances for individual months convey similar patterns, magnitudes are correspondingly greatest for November and least for December. It has to be noted that while the post 1996 variance for the DMI is unprecedentedly high within

its time series, which of the rainfall are generally lower than their corresponding pre 1997 period values.

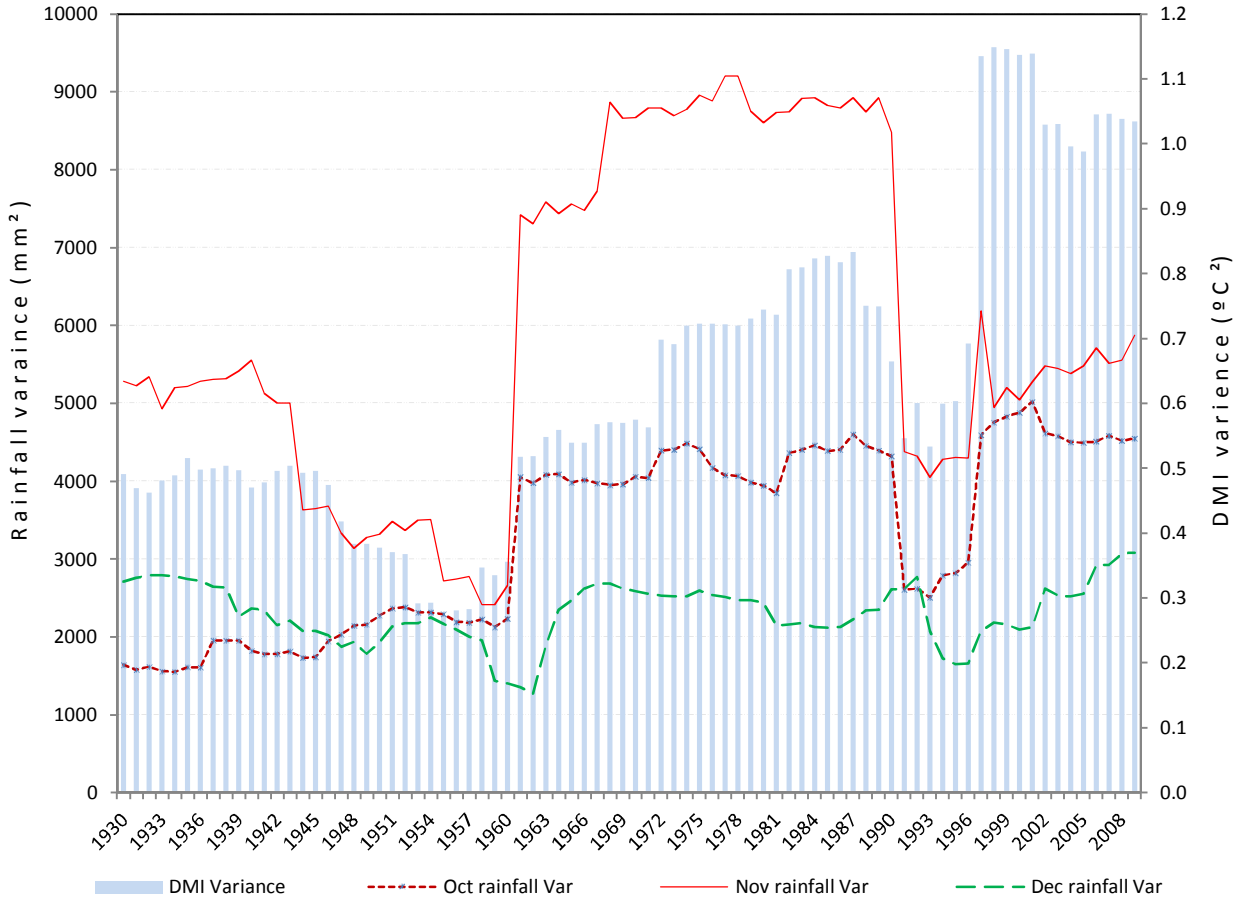

Figure 3.6: Thirty one year moving monthly rainfall variance for equatorial East Africa. Bars represent the DMI variance. Values are at the end of the 31 year segment. Rainfall data is from GPCC V5 precipitation dataset

In figure 3.7 we demonstrate that the relationship among the monthly rainfall show strong decadal variability. In this figure the two pairs of relationship which included the month of December only became significant after 1996. In fact the rise to significance was abrupt, with the correlation between October and December (November and December) shooting from 1996 values of near zero (0.1) to about 0.6 in the following year. Similar abrupt shift in correlation has been experienced at an earlier stage between October and November rainfall where the

correlation strengthened from 0.1 in 1960 to 0.6 in 1961. This demonstrates that the October rainfall became largely in phase with that of November from 1961 while December rainfall only became coupled to the variability of the other two from 1997. It has to be noted that there is a strong resemblance between this temporal correlation pattern between October and November and that between PC1 and EASR index (Figure 4). Both processes reiterate the importance of the years 1961 and 1997 with in the rainfall data set.

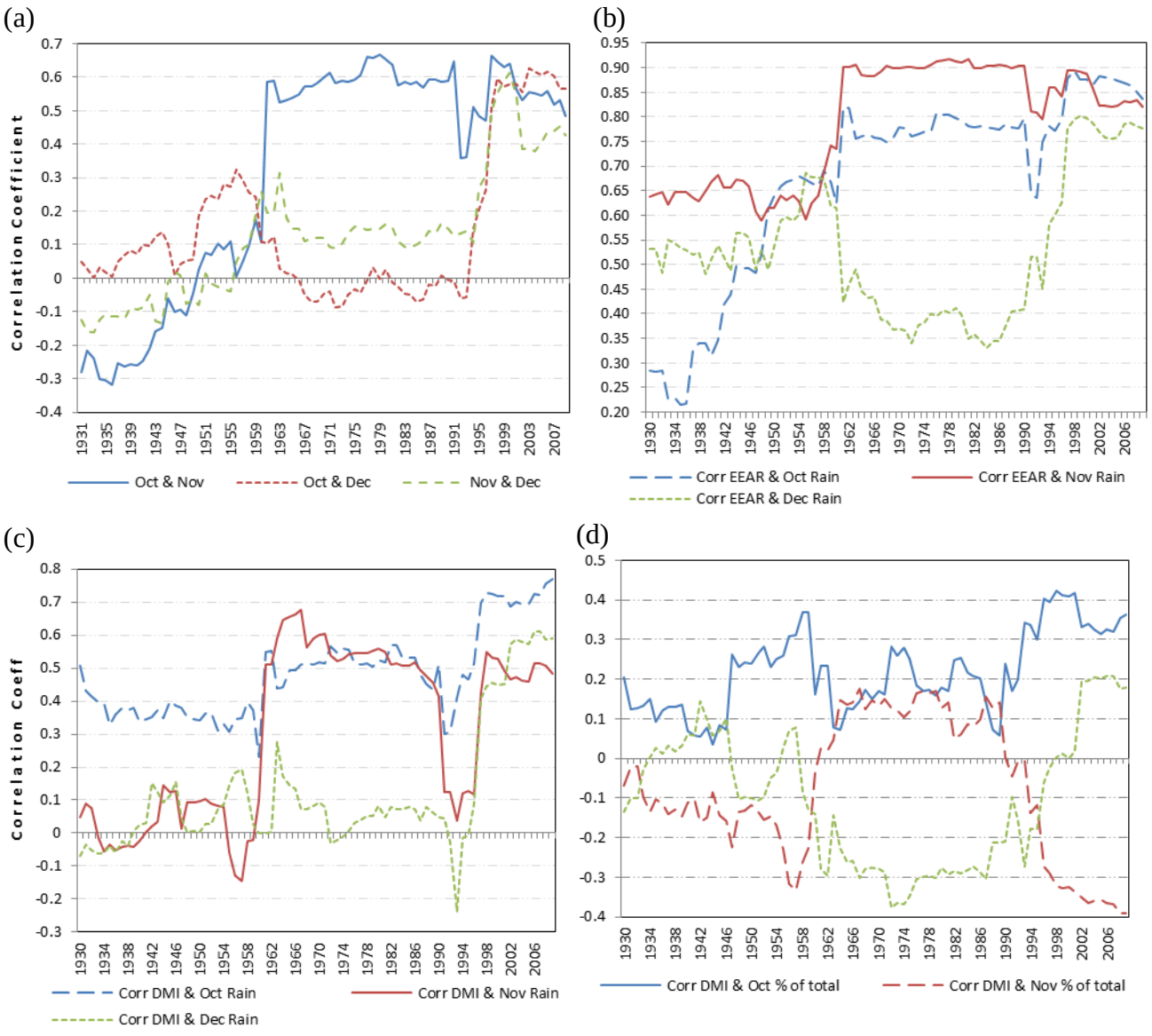

Figure 3.7: Thirty one year moving correlation between the individual months of the OND sub season. Values are at the end of the 31 year segment

This observation is further strengthened by the illustration in figure 3.7 (b) where October and November rainfall became more in phase with the seasonal rainfall index in 1961 while that of December became more strongly coupled after 1996. We also note that December rainfall became more linked to the seasonal rainfall index than the rest of the months from 1998. Thus the interannual variability of all the three months reverted to a predominantly in phase mode after 1996. It is therefore most likely that a major rainfall transforming process brought the variability of October and November rainfall largely in phase in 1961 before all the months were concentrated by becoming strongly in phase from 1997.

The close similarities between the correlation patterns of the three monthly rainfall with DMI presented in figure 3.7 (c) suggest that the IOD is the most likely climate mode responsible for the noted variations in the rainfall variability. However we note that despite the DMI becoming more significantly related to the rainfall index from 1961 the October rainfall was already consistently significantly correlated to the DMI prior to that period. Another interesting aspect is that after 1960, November rainfall had the strongest correlation average which was significant while December rainfall had the least which was insignificant. But after 1998, October rainfall had the strongest correlation of 0.7, followed by that of December with 0.6 and November occupied the least position of 0.5. This demonstrates that significant changes have occurred at monthly time scales in as far as the influence of IOD on the rainfall season is concerned.

To shed more light on these alterations which occurred at monthly timescales, in figure 3.7 d we present the correlation between the proportions of the monthly rainfall to the annual total with the DMI. Interestingly for the three decades after 1960, there was significant negative correlation between proportion of December rainfall to the total and DMI. This suggests that during lower

(higher) values of DMI, the proportion of December rainfall total was higher (lower). However, after 1996 it is the proportion of the October and December rainfall which became more significant with positive and negative correlation values respectively. Since higher (lower) values of DMI are related to surplus (deficit) rainfall, the implication in the post 1996 period is that the month of November may have a relatively bigger (smaller) proportion of the seasonal rainfall total during droughts (rainfall surpluses) compared to other years. On the other hand October may comparatively have reduced (increased) percentage of the seasonal total during droughts (floods).

We explained this observation by first selecting extreme rainfall years using the EASR SPI values of ± 0.84 as the threshold level (see table 3.2). These years are presented in figure 3.8 together with the monthly contribution to the seasonal total. The rainfall events correspond to the ten worst droughts (floods) in ascending (descending order) since 1901 with the most intense at the bottom (top). Although the events have been selected from the period from the beginning of the twentieth century, they all fall within the period from 1961. In this figure we refer to the positive years as ófloodsô and negative years as ódroughtsô. In the ódroughtsô composite October percentage is relatively low (averaging 14%) while that of November is relatively high (averaging 71%). On the other hand, in the ófloodsô composite October has a mean percentage of 27%, which is almost twice as much and November has 50% which is a reduction of about a third of its ófloodsô composite value. This interesting pattern is reflected more vividly in the worst drought of 1987 where November contributed the largest percentage to the seasonal total while October had the least during the study period. On the other hand, in the scenario of the worst floods of 1997, November and October contributions to the total were amongst the least

and largest respectively. However, December does not show much variation within these composites as it has an average of 15% for ódroughtsô and 20% for the ófloodsô composite.

These observations from figure 3.8 demonstrate that although November is the core of the rainfall season with the greatest percentage, its rainfall amount counts more during the droughts where its proportion of the seasonal total is greatest. During surplus rainfall, the other months cut into the proportion of the November total hence making the distribution relatively less skewed. The implication is that during droughts, rainfall conservation measures should be maximized during the period of November as this month may still have rainfall amounts which may not deviated significantly from the norm. At the same time, early cessation and late onset of the season is more likely. Since the described pattern has been observed to be more pronounced in the post 1996 period, it bears testimony to the changing intraseasonal rainfall variability of the short rains on monthly time scales. The significant correlation with DMI during this period signifies the importance of the IOD events not only to increased extreme events, but to the modulation of the rainfall on monthly time scales as well.

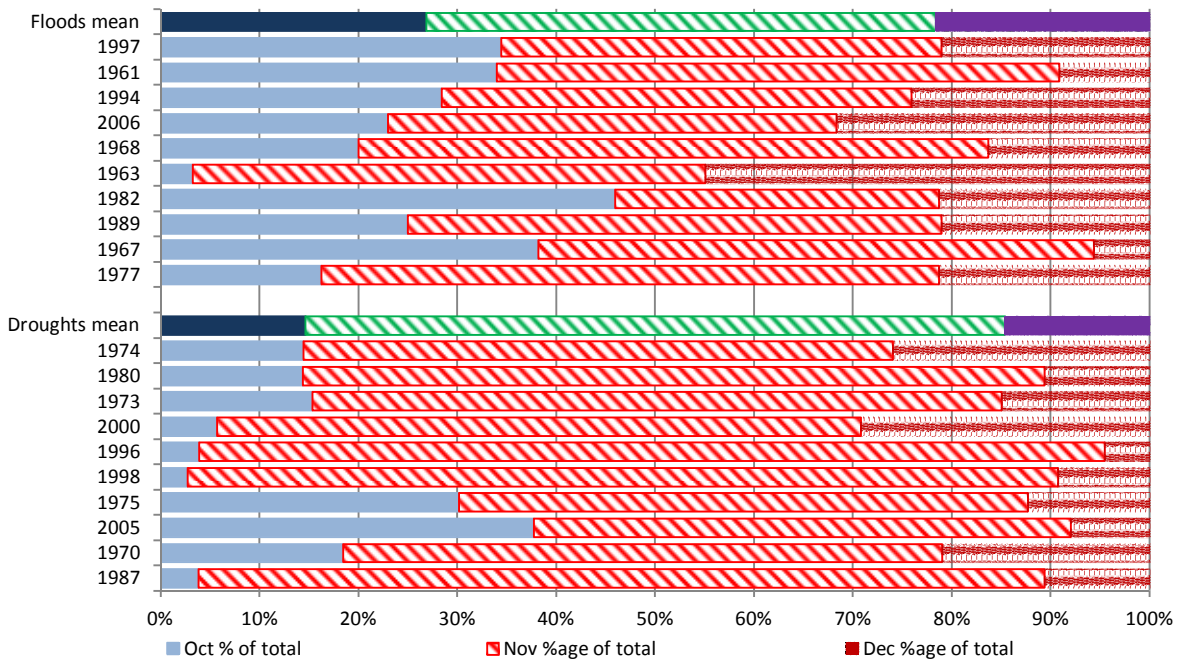

Figure 3.8: The distribution of monthly total rainfall as a percentage of the seasonal total for the 'droughts' (below) and 'floods' (above) composites and their constituent events. The years correspond to the ten worst droughts (floods) in ascending (descending order) since 1901 with the most intense events at the bottom (top).

In any case, in the absence of a clear tendency in both the monthly and seasonal rainfall time series, but with dry and wet episodes in the region becoming longer and more intense, it should then follow that the rainfall amount and intensity in the wet season may have increasing trends. We therefore adopt for use the SPI technique. This method allows for a more detailed monitoring of dry and wet periods over a wide spectrum of temporal scales (Edwards and McKee 1997) since it is able to return fundamental parameters in the analysis of the occurrence of different wet/drought types in terms of severity, magnitude, and frequency. In the SPI analysis we adopted the seasonal scale of the corresponding three months. Figure 3.9 displays the cumulative distribution of the EASR SPI classes of moderate intensity or more. It can be noted that more than 65% of the wet events of moderate class or more occurred after the 1950s while similarly about 59% of the dry events occurred after 1969. There were prolonged periods during the earlier

decades of the century when there was either no drought or wet episodes. For example no drought event of moderate class or more occurred during the two decades from 1950 to 1970 and only two such events occurred in the first three decades of the century. Although such a scenario is less pronounced in the wet events, we also note that only one event of moderately wet class or more occurred within the first two and a half decades of the 20th century. This is a clear indication of more extreme events being located within the later decades of the study period. In fact, the relative frequencies of these wet and dry episodes changed significantly as from 1961. During this year, the frequency of occurrence of wet incidences became predominantly higher than that of the dry occurrences with the moderately wet or worse classes assuming unprecedentedly greater and consistent nature of occurrence than their opposite counterparts.

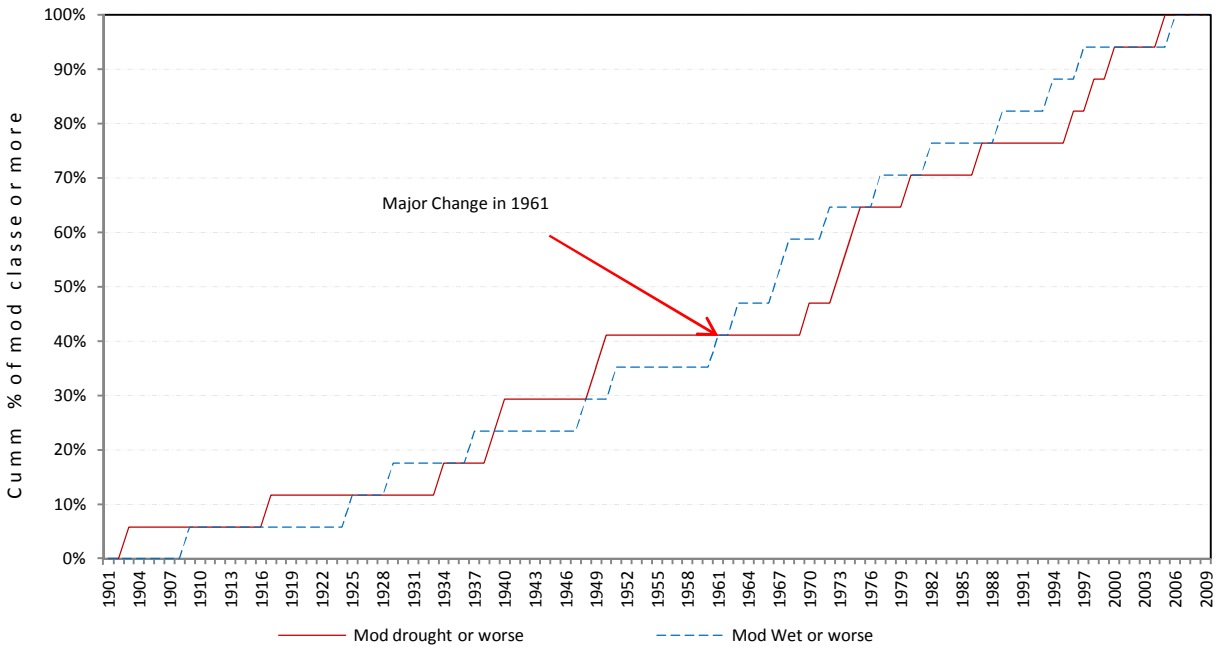

Figure 3.9: Cumulative distribution of EASR SPI with moderate or more intense classes

In order to derive a more detailed illustration of how more extreme EASR SPI classes are distributed, we present a similar graph in figure 3.10 that better illustrates more intense events of severe class or more. It is noted that the distribution of the severely wet/dry conditions is even more skewed to the left with more extremes of this nature located within the second half of the study period. Two extended periods of the severely wet conditions or worse classes occurring almost in succession are apparent in the post 1949 period. It is in this era that 86% of these excessive rainfall events are located with an equal distribution of 43% each within the two periods, 1960 to 1968 and 1993 to 2006. These two epochs are unique in the sense that they do not only display exceptionally prolonged phases of very wet conditions during the study period but they also have the wettest rainfall events occurring in 1961 and 1997. Coincidentally, these two events were years when the IOD had its greatest east west SST gradient since the late 1890s. This provides more rooted evidence that it is the behavior of the IOD which should explain better the development of these extreme wet events. However, dry episodes of similarly high intensities are however, relatively less skewed to the left with 60% of the severe droughts or worse occurring after 1968. It is the severely wet conditions or worse which are more sensitive to the 1961 period than the SPI classes of severe deficits or worse. This means that the triggering mechanisms for more intense events impacted more on the rainfall surpluses than on the deficits especially in the decades from the 1960s and mid-1990s.

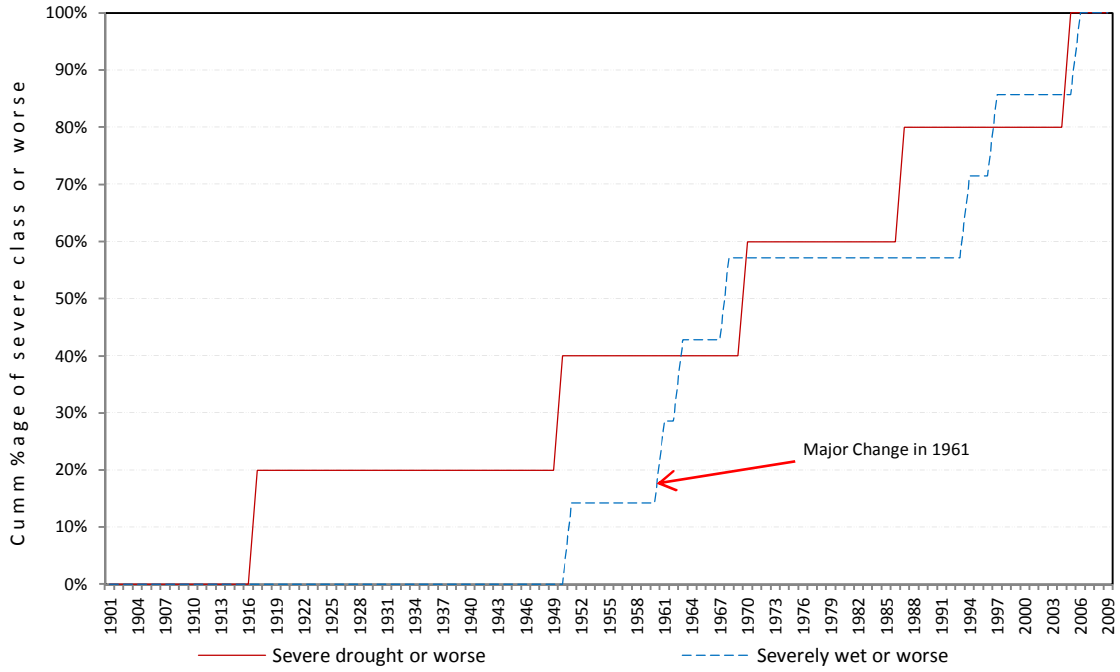

Figure 3.10: Temporal distribution of the rainfall events which are severe or more.

3.3.3 Impacts of shifts in IOD on EASR SPI

A simple correlation analysis performed between EASR SPI and the dipole mode index (DMI) time series yields an overall negative value of -0.53 which is significant above the 99% confidence level. But when the relationship is subjected to 31 year segments of the study period, epochs emerge where the correlation is insignificant for the period up to the early 1960s while is notably altered in the mid to late 1990s. In fact, when separately correlated to the SST anomalies of the eastern and western IOD poles, different patterns immerge in figure 3.11. It is noted that the most consistently significant correlation is between the SSTs of the eastern pole and the EASR whilst the least reliable link is between the EASR and the SST anomalies of the western pole.

Figure 3.11: Temporal manifestation of the 31 year running correlation coefficients among EASR, DMI and W SST.

The temporal manifestation of the 31 year running variances of the three time series also show the close relationship between the pattern depicted by EASR SPI and DMI (Figure 3.12). Although all running correlations are sensitive to the 1997 shift, only that of the DMI and EASR SPI shows a swift transition in 1961. The observation gives us a clue that it may not have been the rising temperatures in the western pole which brought about the observed changes in the regional rainfall extremes as postulated by Nakamura et al. (2009). Rather it is the DMIôs association with the EASR though the temporal coupling between the two sub systems that clearly brings about the identified shift points of 1961 and 1997. Therefore it is most likely that the latter two shift points in the rainfall variability are more related to the IOD process in its entirety than to its individual east and west SST anomaly components.

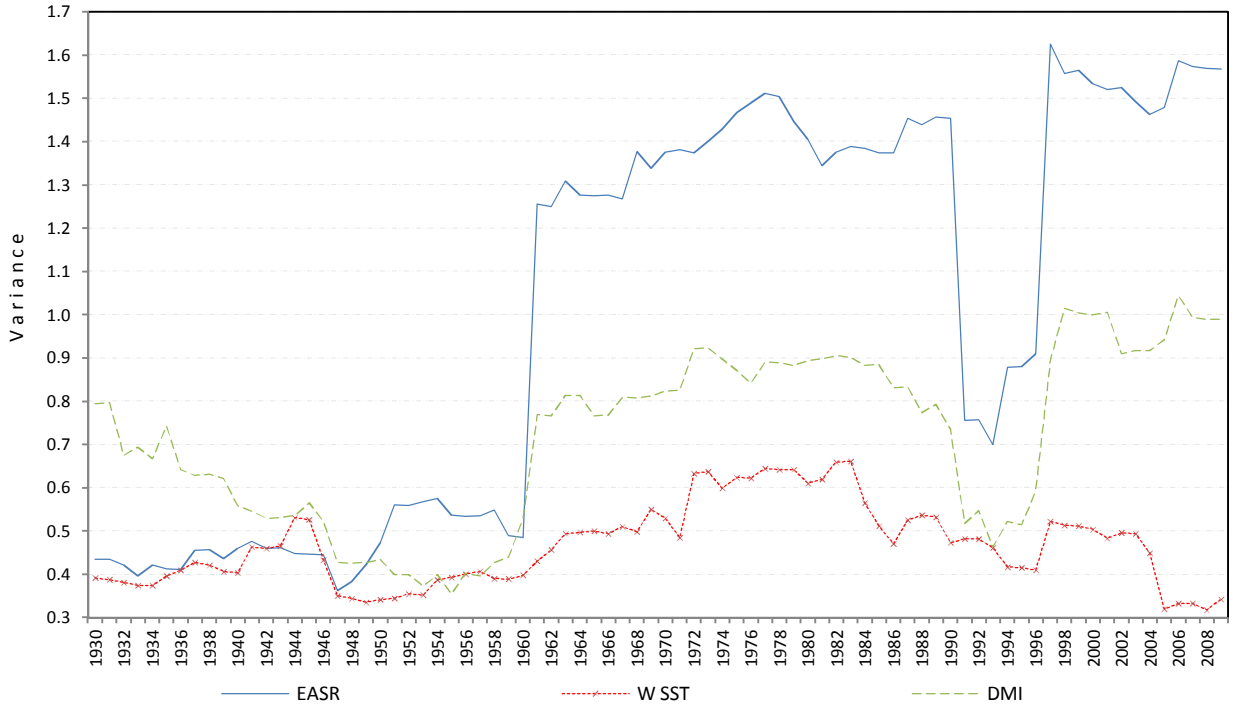

Figure 3.12: Thirty one year running variances for EASR SPI, W_SST and DMI time series. Values are at the end of the 31 year segment.

Given that the IOD has been known to be characterized by epochs demarcated by the shift points of 1918, 1961 and 1997 (Manatsa et al., 2012), we therefore hypothesise that it is these turning points which shape the noted changing characteristics of the EASR SPI classes since the turn of the 20th century. The scatter diagram (Figure 3.13) illustrates better the changing nature of the epochal relationships between DMI and EASR SPI as demarcated by the mentioned three shifts. Here it is noted that the linear relationships have only became significant in the third epoch and even stronger in the last epoch. This hypothesis can be strengthened by using the Chi Square (χ^2) test for testing the independence of the two attributes, the IOD epochs and the EASR SPI classes. This is examined in the following section.

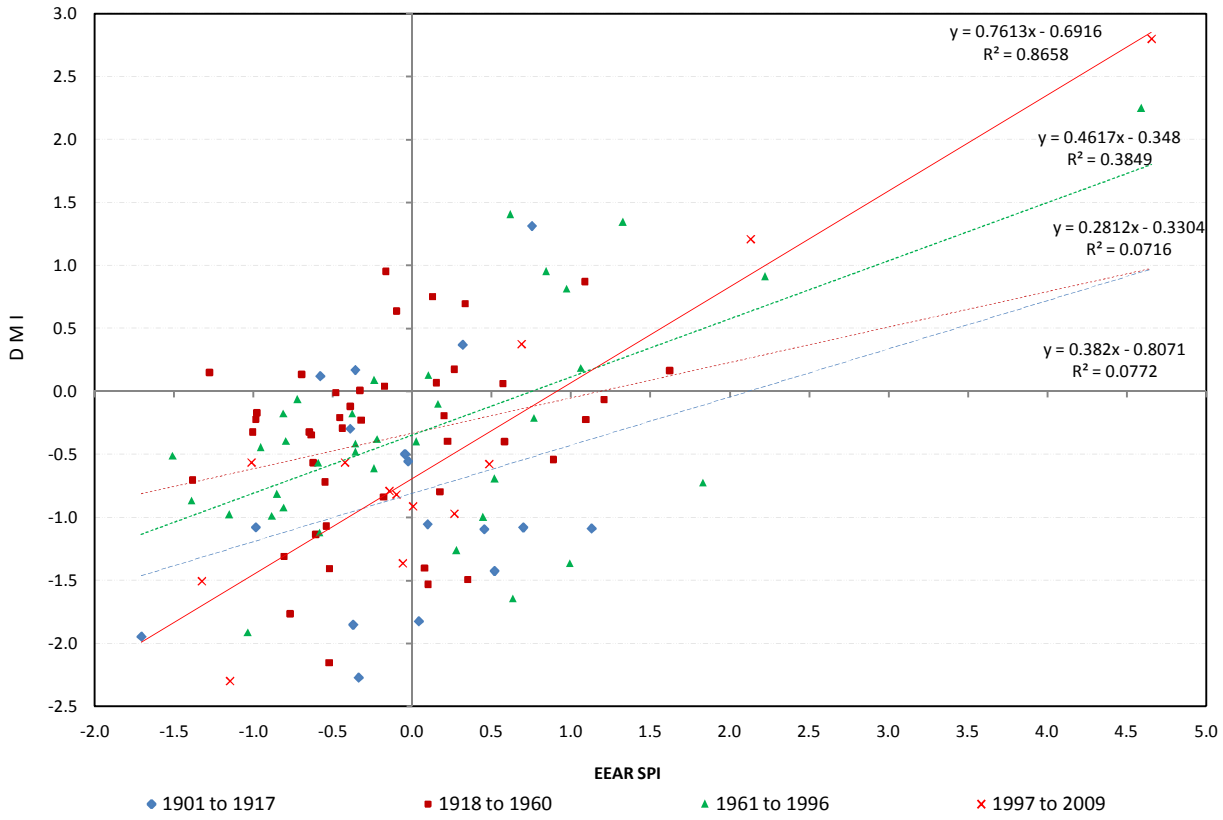

Figure 3.13: Scatterplot of EASR SPI against the DMI relative to the IOD epochs. In the insert are regression lines and corresponding regression equations for each epoch in ascending order.

3.3.4. Chi square (χ^2) test of significance between EASR SPI and IOD epochs

Since the χ^2 uses the data that has been expressed in frequencies, it was necessary to first put the frequency of the EASR SPI classes into the four DMI categories. Based on these categories, a contingency table for the observed frequencies was prepared as shown in Table 3.4. From these observed frequencies, expected frequencies and the χ^2 value were computed by the usual procedure. In the contingency table provided in Table 3.4, the null hypothesis was that there is no relationship between the two variables, i.e. the expected values in the rows and columns are independent. An analysis of the table shows that the χ^2 for the rainfall frequencies is 26.38, with a p-value of 0.0017. In this way, the null hypothesis of no relationship has to be rejected in favor of the existence of a strong dependence of the SPI classes on the epochs. This implies that on

more than 99.9% of the occasions, there is the likelihood that the frequency of the EASR SPI classes is determined by the epoch in which they occur. Thus, the demarcation of EASR based on the four epochs are realistic in both a physical and statistical sense, and are not direct consequences of the application of the statistical techniques.

Table 3.4: Contingency table for observed frequencies of EASR SPI classes and IOD epochs

IOD Epoch	*Ext Wet*	*Sev Wet*	*Mod Wet*	*Slt Wet*	*Norm*	*Slt Dry*	*Mod Dry*	*Sev Dry*	*Ext Dry*	***Total***
1900 – 1917	*0(0.95)*	*0(0.16)*	*1(1.40)*	*2(1.25)*	*11(7.80)*	*1(2.81)*	*1(1.87)*	*0(0.62)*	*1 (0.16)*	*17*
1918 – 1960	*1(2.37)*	*0(0.39)*	*4(3.55)*	*2(3.16)*	*20(19.73)*	*11(7.10)*	*4(4.73)*	*1(1.58)*	*0(0.39)*	*43*
1961 – 1996	*3(1.98)*	*1(0.33)*	*4(2.97)*	*3(2.64)*	*12(16.51)*	*6(5.95)*	*5(3.96)*	*2(1.32)*	*0(0.33)*	*36*
1997 – 2009	*2(0.72)*	*0(0.12)*	*0(1.07)*	*1(0.95)*	*7(5.96)*	*0(2.15)*	*2(1.43)*	*1(0.48)*	*0(0.12)*	*13*
Total	*6*	*1*	*9*	*8*	*50*	*18*	*12*	*4*	*1*	*109*
Df = 24		*χ^2 = 25.481*			*P-value < 0.0001*					

Having established the statistical significance of the relationship between the SPI classes and the IOD epochs, we go further to illustrate clearer in figure 3.14 how the EASR SPI classes are distributed within the epochs. The general trend from this figure is that the percentage of normal rainfall in each epoch is generally decreasing on each progressive epoch at the expense of increasing rainfall extremes. The SPI classes were more in the normal categories but became reduced toward the third epoch where the graph flattens as more extreme events classes become more prevalent. We may not conclusively explain events over the last epoch because it is still of in-determinant length. However the epoch has already recorded a fair share of extreme rainfall events at the expense of normal rainfall events. Thus although there were no long-term trends of the ósh ort rainfallô anomalies, rainfall variability in east Africa may have experienced significant

IOD induced modulations, especially in recent decades. In particular because of the recently established high spatial cohesiveness of the regional rainfall, droughts and floods have not only become more intense but also widespread.

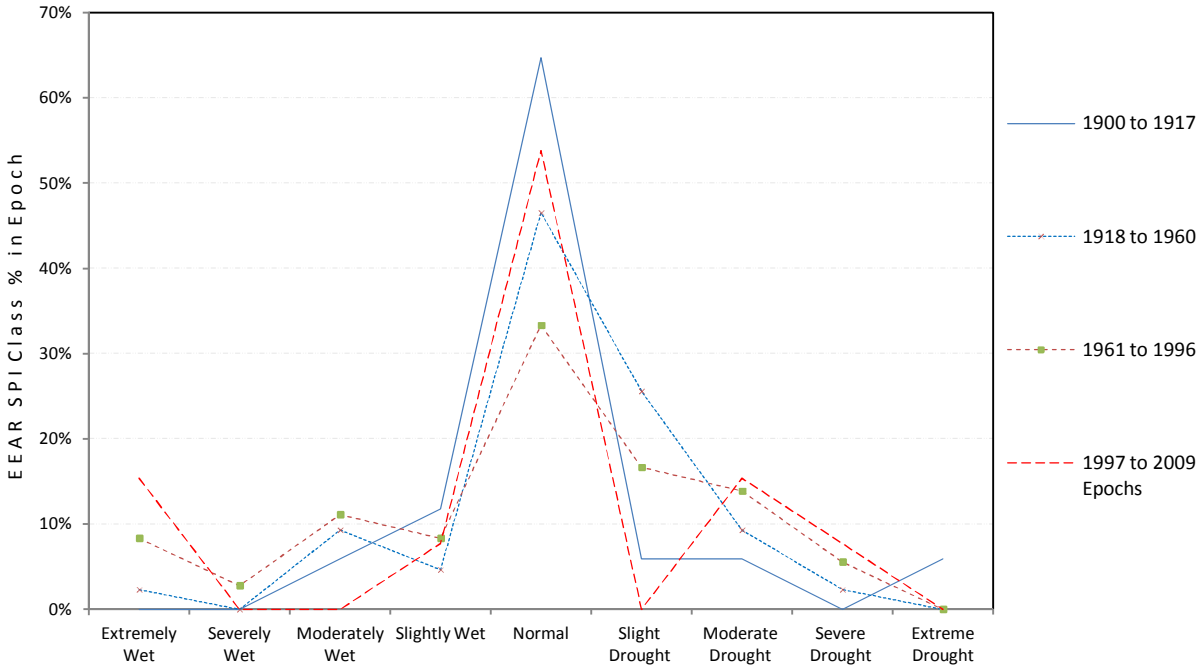

Figure 3.14: Distribution of EASR SPI classes according to the four IOD epochs.

3.3.5 The nature of the relationship between the IOD events and EASR SPI

It is expected that the discontinuities in the DMI, which define the epoch demarcations in the IOD, should also be visible in the surface zonal wind of the tropical SIO. In the light of this realization in figure 3.15 we present the interannual zonal wind stress anomalies extracted from the western IOD pole but south of the equator, alongside their cumulative temporal pattern. It can be appreciated that the wind stress anomaly values decrease from the first to the second epoch before reversing to negative. An increase in magnitude is then witnessed from the third to the fourth epoch. However, the most intriguing aspect of this analysis is demonstrated in the cumulative graph. Here we note that the cumulative pattern of the wind stress anomalies does not

only reverse gradient in 1961 but surprisingly change sign from negative to positive in 1997. For this reason, we can conclude that the circulation pattern over the western pole also carries with it information about the major turning points in the IOD system through the wind stress.

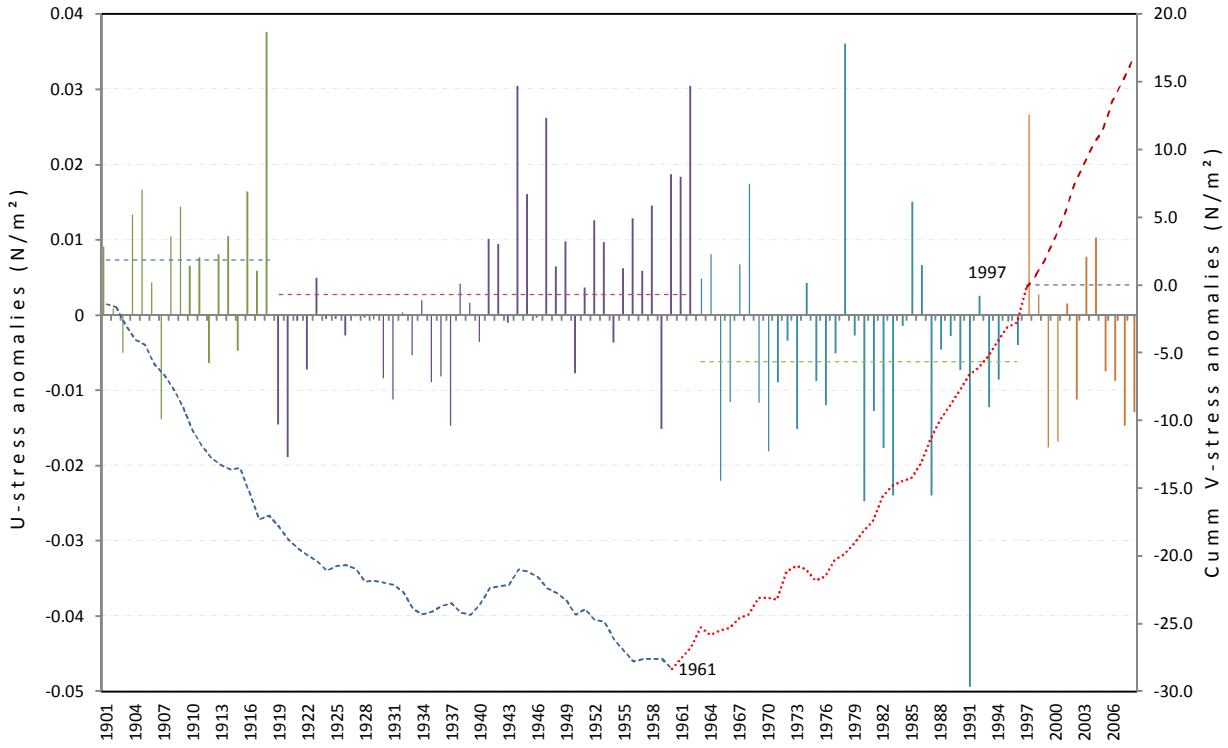

Figure 3.15: Temporal manifestation of the eastern pole's zonal wind stress anomalies (N/m²) alongside its cumulative values. In the insert are the years depicting the turning point of the cumulative graph and broken lines indicating the average wind stress values for each epoch.

Furthermore a striking temporal correlation pattern emerges in figure 3.16 where we correlated EASR SPI with the u-wind stress using 31 year running segments. Although initially insignificant, the correlation coefficient values reversed from being negative to positive around 1961. Once the positive values were initiated, they continued with a significant increasing trend until 1997 where the values began to fall gradually with a significant negative trend. It is therefore more likely that the zonal wind variability played a significant role in the changes

identified in the EASR SPI classes. It is when the zonal winds started to have a strong enough easterly anomaly that the IOD began to have a significant impact on EASR and this coincided with the IOD shift of 1961. Easterly anomalies in surface winds have been known to reduce the normal moisture transport away from East Africa (e.g. Mapande and Reason 2005) hence creating conditions conducive for rainfall development.

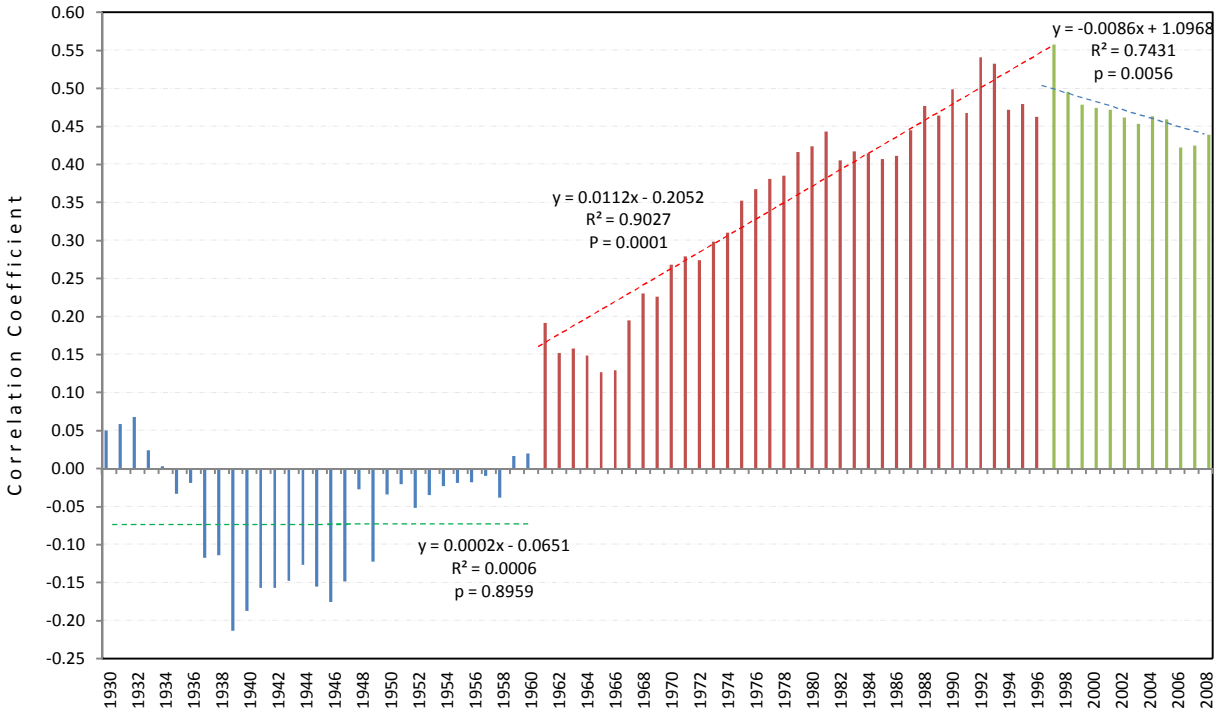

Figure 3.16: Temporal patterns of the 31-year moving correlation coefficients between EASR SPI and u-wind stress for the western pole of the IOD. In the insert are the regression lines together with their corresponding equations for the correlation values.

3.3.6 Impacts of IOD on EASR SPI

Having established the strong coupling between EASR SPI and zonal wind component over the western pole and the less significant role of the underlying SST anomalies, we move on to investigate how the IOD is actually linked to the regional rainfall. An investigation to characterize the correlation of the EASR with the Indian Ocean SST field reveals a dipole configuration that is reminiscent of the IOD mode to be captured only in the third and fourth

epochs of figure 3.17. It is therefore evident from this figure that interannual fluctuations in East African short rains became more closely tied to the large-scale atmospheric circulation through the anomalously warm and cold SSTs in the western and eastern part of the Indian Ocean domain as from 1961. While it appears in the third epoch that the EASR was linked solely to SST anomalies of the two poles, there is an additional dimension of the region with a NE-SW diagonal orientation towards East Africa in the IO during the last epoch. This attaches an equally important simultaneous influence of the south east trade winds variability to the IOD impacts on EASR in the last epoch. This is in contrast to the first epoch where the region of significant correlation is linked to the diagonal orientation but not to the IOD pattern. The second epoch has the significant region of association restricted mainly to the north of the equator with neither an exclusively defined IOD pattern nor an NE-SW orientation. It shows that despite demonstrating that the IOD SST pattern became significantly linked to EASR after 1960, there was an additional trade wind variability influence after 1996.

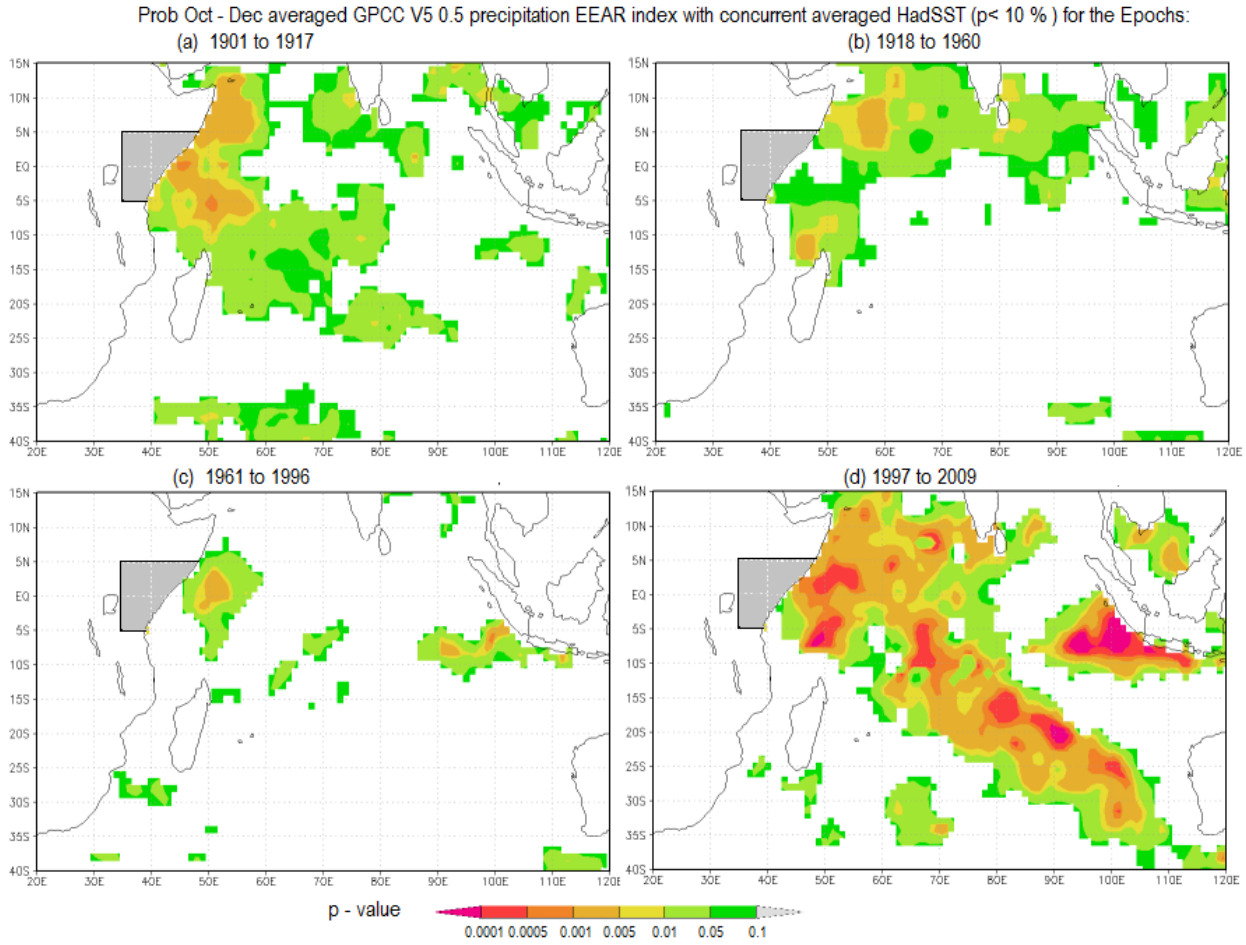

Figure 3.17: P values for the epochal correlation fields between EASR and SSTs for the Indian Ocean for (a) 1901 to 1917 (b) 1918 to 1960 (c) 1961 to 1996 (d) 1997 to 2009. Shaded region over East Africa is the area for the averaged EASR index

Further investigations on the impact of DMI on the whole region of east Africa is presented in figure 3.18. This figure reveals that the influence was insignificant in the first epoch, confined mainly to the horn of East Africa in the second epoch, widespread to most of the region west of 30 ºE in the third epoch and became mostly restricted to the central coastal regions in the last epoch. This observation demonstrate the epochal nature of the IOD influence over East Africa by indicating that the impact became established over equatorial East Africa only after 1960 before being more focused on the equatorial coastal regions in the last epoch. Thus IOD influence on the East African region varies not only in space but with time as dictated by the epochs.

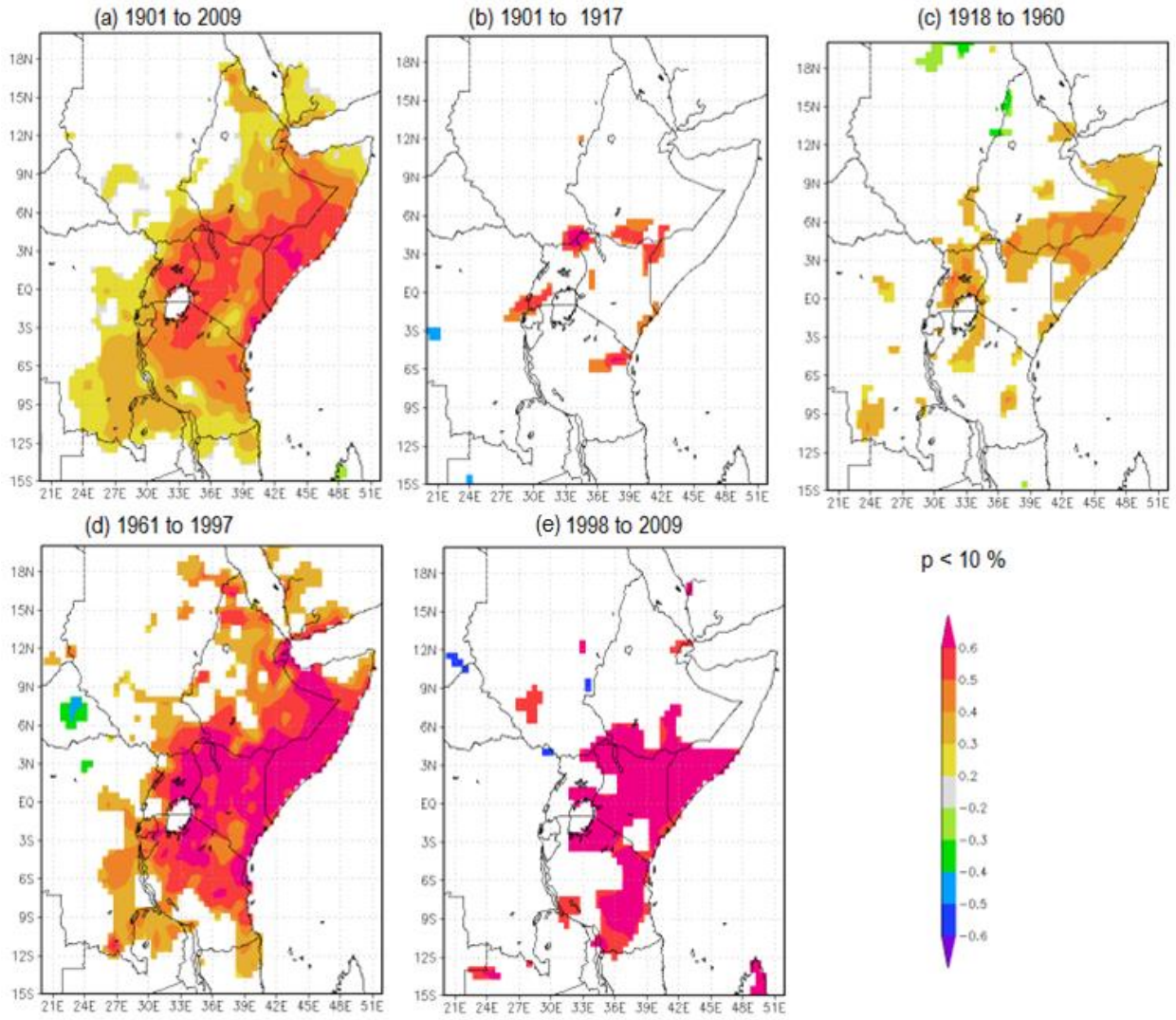

Figure 3.18: Correlation field of the DMI with the GPCC precipitation field (p < 10%) over the north eastern region of Africa for the period (a) 1901 to 2009 (b) 1901 to 1917 (c) 1918 to 1960 (d) 1961 to 1996 (e) 1997 to 2009

3.4. Summary and Conclusions

The present chapter investigates the interannual to decadal variability of the seasonally stratiýed (OND) IOD index, and the apparent impacts of the accompanying shifts on concurrent rainfall of equatorial East Africa. Unlike the previous studies that assumed linear impacts of the IOD on the region we note that the impacts are epoch dependent. This is mainly due to the observation that

the coupling strength between the IOD and EEAR climate modes does not only portray an increasing trend, but seems to be heavily involved in the definition of the shifts.

We noted through the temporal distribution of the EASR event classes determined by the SPI technique, that the EASR has intensified significantly from the turn of the twentieth century with more floods and droughts occurring in the recent decades. This increase towards more extreme rainfall events has not been gradual but is strongly characterized by epochs which were dictated by shifts in the Indian Ocean Dipole (IOD) mode. These shifts occurred during 1961 and 1997. The shifts were also quite prominent in the NCEP-NCAR wind data from the western pole of the IOD mode. The periods around 1961 and 1997 have already been confirmed as real shifts to have occurred in the IO using the IOD time series (Manatsa et al., 2012), coral records (Nakamura et al., 2009) and stable isotopes (Vuille et al., 2005).

It is intriguing to note that before 1961 no significant connection could be derived between the IOD and the EASR. However, a relatively strong coupling between the two occurred almost instantly in 1961 and thereafter, until 1997 when another abrupt shift in correlation occurred to even stronger coupling. The PC1 extracted from the EASR spatial domain initially explained just about 50% of the rainfall variability before 1961, and then catapulted to about 73% between 1961 and 1997, before eventually shifting to exceed 82 % after 1997. The PC1 for each successive epoch also displayed loadings with notably improved spatial coherence. This systematic pattern of increase was accompanied by both a sharp increase in the frequency of rainfall extremes and spatial coherence of the rainfall events over the region. Thus the epochal shifts may also explain why rainfall extremes undertook an upsurge turn after every shift with

the corresponding increased coupling between IOD and the rainfall. Hence it is most likely that the 1961 and 1997 IOD shifts are responsible for the epochal modulation of the EASR both in the spatial and temporal domain.

But the observed epochal changes in IOD attributes such as its variance and its relationship with EASR appears in this work to be a system-wide phenomenon that is yet to be comprehensively understood. Furthermore, it is evident that such nonlinearities are difficult to reconcile with the suggested smooth evolution of anthropogenic forcing (e.g. Hansen et al., 2005). Hence we are more inclined to believe that the internal reorganization of the Indian Ocean climate system may underline such discontinuities. We take cognizance of the reported recent south Indian Ocean Subtropical High (Mascarene high) buildup (Allan et al., 1995) and its epochal eastward translation (Manatsa et al 2011). This process should have correspondingly developed a background mean state in the south Indian Ocean for each eastward epoch of more strengthened relatively cool and dry southeasterly winds that affect East Africa. The resulting background epochal state would in turn generate conditions more favourable for the formation of more extreme droughts at the expense of the development of floods.

However, this epochal variation or apparent nonstationary nature in the IOD ï EASR relationship is novel and has rarely been considered by recent researchers. Yet epochal shifts if not recognized timely, can undermine statistical prediction schemes that are based on stationarity relationships in historical data. This study revealed that EASR variability was relatively constrained in the earlier decades when the IO SSTs were cooler but increased significantly in the recent decades as the SSTs warmed considerably. These findings support the notion of

greater climate variability tending to develop in warmer climate states. This inference fits the growing consensus that the current global warming will eventually increase the frequency of extreme rainfall events. Hence climate change impacts will bring further environmental stress to the region of East Africa which already has a reduced capacity to adapt to the mounting adverse effects of the current smaller scale climate variability.

Given the promising nature of our results, it is imperative that the earthôs climate system research community embraces this nonlinear paradigm if we are to move forward in the assessment of regional climate modulations under the global warming stress. In this regard, the current work has two important consequences for the region. First, the abrupt changes in the OND climate system of East Africa appear to depend on the coupling strength between the IO and the rainfall. Although the coupling strength has been improving in the past century, the shifts in the whole system seem to be triggered by a sudden development of exceptionally high coupling strength that is related to the transition in IOD variance. This may lead to the conclusion that the impact of the IO on East Africa rainfall is not linear, as previously thought, but occurs in regimes of defined levels of epochal influence. Secondly, epochal variations in fisheries in the region could have been highly probable as shifts in both the polarity and strength of the IO basinôs oscillation may correspond to shifts in fish production in the tropical Indian Ocean. Having established the significant link between the IO basinwide shifts to the rainfall over East Africa, in the following chapter we examine how this link is established through the involvement of the Mascarene High displacements.

CHAPTER FOUR

Epochal Mascarene High Displacements and Impact on Rainfall of East Africa

4.0 **Brief Chapter Synopsis**

This chapter is published as:

Manatsa D, Y Morioka, SK Behera, CH Matarira, T Yamagata (2013a) Impact of Mascarene High variability on the East African ‘short rains’. *Climate Dynamics* DOI: 10.1007/s00382-013-1848-z.

The chapter investigates how the Mascarene High (MH) epochal displacements could be linked to the rainfall of East Africa through the involvement of the wind alterations by both the meridional and zonal persistent movements.

4.1 Introduction

The East African short rains (EASR) represent one of the most complex rainfall systems over the African continent (Nicholson 1996). The dominant control of the rainfall is the intertropical convergence zone (ITCZ) which is superimposed upon regional factors associated with local impacts from the lakes, topography and maritime influence (Mutai et al. 1998). Although the EASR is linked with the regional factors, its interannual variability is considered to be related to the tropical climate modes such as El Nino/Southern Oscillation (ENSO) and the Indian Ocean Dipole (IOD, Saji et al. 1999). Some studies (Mutai et al. 1998; Indeje et al. 2000, Hastenrath 2004) discussed the paramount role of ENSO on the rainfall variability, while other studies attributed it mostly to the IOD influence (Black et al. 2003; Clark et al. 2003; Behera et al. 2005; Marchant et al. 2006, Manatsa et al. 2010). However, these studies are in agreement on the

importance of the zonal flow in the equatorial Indian Ocean on the rainfall variability, especially in inducing floods while providing limited explanation for drought development.

Recently, Shongwe et al. (2011) noted the escalation of drought occurrence in the recent decade that is not adequately resolved in seasonal forecasts. This observation suggests a weak connection of the conventional predictors like ENSO and IOD for the development of the recent droughts. Although the ITCZ plays a crucial role in rainfall variability over East Africa, especially for the ósh ort rainsô (Black et al. 2003) its connection with rainfall deficits has been largely ignored in recent literature. The ITCZ can intensify/weaken in response to changes in the southeasterly trade winds associated with the Mascarene High (MH, Anyamba and Ogallo 1985) variability. The MH is the subtropical anticyclone located in the south Indian Ocean. The intensity of the southeast (SE) trade winds provide the mechanisms for rapidly advecting subtropical influences equatorward hence their characteristics can provide a more logical explanation to drought development in the region. The fact that the EASR is strongly linked to the southward migration of the ITCZ (Black et al. 2003) entails that the variability in the strength and temperature of this relatively cool and drier low level SE airflow may interfere with the intensity and location of convergence mechanisms of the ITCZ. As one of the factors defining the ITCZ activity, the SE trades through the control from the MH, may play an important role in the EASR variability. This explains why Hastenrath et al. (2007, 2010) and Mutai et al. (2012) found a reasonably strong relationship between the EASR and the strength of the downstream SE trade winds.

However, the mentioned previous studies on EASR took for granted the subtropical influences which could be introduced by an anomalous MH variability. In fact the MH has been known to have increased in intensity during the recent decade (Xue et al., 2003). This could have caused steeper meridional pressure gradients which may have enhanced the capacity of the SE trade winds to advect the relatively cool and less moist low level airflow to the western equatorial Indian Ocean. It is due to the direction of the SE trade winds that the wettest locations on the equatorial East African highlands are prevalent on the southeast facing slopes (Thompson, 1966). This provides a clue for the assumption that the predominant rainfall is strongly related to the southeasterly trade winds emanating from the south Indian Ocean (SIO).

In this paper, we investigate the interannual variability of the EASR and its link with the MH variability. The MH variability is measured through its intensity and zonal migration of its eastern ridge. This paper is organized as follows: the data and methodologies are presented in Section 2. In Section 3, the interannual variability of the MH intensity and the zonal displacement of its eastern ridge are established to describe how they are related to the variability of the SE trade winds reaching equatorial East Africa and hence the EASR variability. In Section 4, we discuss a possible link of our result with other factors such as ENSO and the IOD. Conclusion is given in Section 5.

4.2 Data and Methods

4.2.1 Data

For pressure analysis, we used the NECP/NCAR reanalysis data during 1950-2011 (Kalnay et al. 1996). The NCEP/NCAR dataset is one of the widely used reanalysis products with relatively

long periods (>60 years) and has shown consistency with previous observation to study decadal variability over the Indian Ocean (Hastenrath et al. 2007, Ummenhofer et al. 2008). Major results obtained from NCEP/NCAR reanalysis data were verified using ERA-interim reanalysis data (Uppala et al. 2005), though the latter data was only from 1979. To verify the reanalysis data, we use the observed sea level pressure data from the UK Met Office Hadley Centre (HadSLP1; Basnett and Parker 1997). However, because the NCEP/NCAR data underestimates precipitation (Ma et al. 2009), alternative rainfall data were obtained from Global Precipitation Climatology Centre monthly *precipitation* gridded dataset (GPCC) with 0.5º x 0.5º horizontal resolution. The core source of the GPCC analysis is the observed rainfall data from networks operated by the national meteorological services worldwide (Rudolf et al. 2010). GPCC precipitation data has also been used in the simulation of rainfall of east Africa by Kaspar and Cubasch (2008). More details on the data and its usage in research are found on the GPCC Homepage: http://gpcc.dwd.de/.

The equatorial East Africa óshort rainsô index (EASR) is developed from the GPCC dataset during the period 1950 to 2011 for the averaged months of October to December (OND). This rainfall index is based on a large-scale standardized area-average rainfall for the region of East Africa depicted in Figure 1. The rationale for selecting this particular region is found in Manatsa et al., 2012. Since GPCC data is land only, GPCP precipitation data (Adler et al. 2003) were used for the purpose of extending the spatial coverage into the ocean though covering a limited period which starts from 1979.

The sea surface temperature (SST), is analyzed using observed data from the Hadley Centre Sea Ice and SST (HadISST; Rayner et al. 2003). We calculated the Indian Ocean Dipole Mode Index (DMI, Saji et al. 1999) by the SST anomaly difference between the tropical western Indian Ocean (50°E-70°E, 10°S-10°N) and the tropical eastern Indian Ocean (90°E-110°E, 10°S-0ºS). Also, we use the Niño3.4 region defined by the SST anomaly averaged in the eastern Pacific (120°W-170°W, 5°S-5°N) to determine the ENSO index.

4.2.2. Methods

Sea level pressure (SLP) was used to examine the MH intensity. We extracted the SLP using the HadSLP and NCEP/NCAR reanalysis datasets from 1950 to 2011 and ECMWF Reanalysis (ERA-interim) data set from 1979 to 2011. For the characterization of its zonal movement, the 850-hPa geopotential height was used instead of SLP to avoid underlying topographic effects on the eastern edge of the MH, especially near the western Australian coast. The cautious approach may not significantly affect our conclusions about the MH variability because the high pressure system has a predominantly barotropic structure below 600 hPa.

We define the MH intensity as the mean SLP over the region of 25ºS-35ºS and 40ºE-105ºE (Figure 1). The latitude of the area is based on the northern and southern limits reached by the 1018 hPa isobar of the climatological MSLP. Similarly, the longitudes are also based on the east and west boundaries of the same isobar. This definition differs slightly from that given by Xue et al. (2003), who used the averaged region (25ºS-35ºS and 40ºE-90ºE) to define the MH intensity. Since the 105ºE longitude for the MH eastern edge is the last isobar defining the MH intensity, the definition by Xue et al. (2003) may underestimate the actual intensity of the MH.

We demarcated the MH center as the location where the geopotential height at 850 hPa has the highest values in the selected area (25ºSï 35ºS, 40ºEï 105ºE; Figure 1). It should be noted that the comparison between the MH intensities based on the domain-averaged SLP and the geopotential height at 850hPa showed similar results. Here, we use the 1540 gpm line to represent the eastern boundary of the MH. This is because this isoline, even in the extreme case of the eastern migration in 1997, does not cross the western coast of Australia. Thus, the eastern ridge is subsequently identified as the point where the 1540 gpm intersects the 30ºS of the MH. A similar methodology was used by Li et al. (2011) to quantify the zonal movement of the eastern ridge of the North Atlantic subtropical high.

A composite analysis for the extreme westward and eastward displacements of the MH eastern ridge is conducted to examine the relation between the EASR and the derived MH parameters. We took precautions to limit the effect of spurious SLP trends reported in the Southern Hemisphere especially in the pre satellite period (Hines et al 2000, Marshall & Harangozo 2000, Renwick 2004), from affecting our results. For time series analysis, where we are interested in trends over relatively large averaged regions, we use the data with the longer period from 1950. But for the spatial analysis, we use the more accurate post satellite observed data with the shorter period from 1970. However, the pre 1970 data are still reasonable and has been used in both spatial and temporal regional analysis (e.g. Ummenhofer et al. 2009b; Huang and Shukla 2008).

4.3 Results

4.3.1 Interannual variability of the Mascarene High (MH)

The temporal manifestation of the time series derived from different data sources for the mean SLP averaged over the MH location depicted in Figure 4.1 demonstrate closely related features.

As such the correlation between the HadSLP1 and the NCEP/NCAR reanalysis data is quite strong with a significant coefficient value of 0.92, while that between NCEP/NCAR and the ERA-interim reanalysis data has a higher value of 0.97.

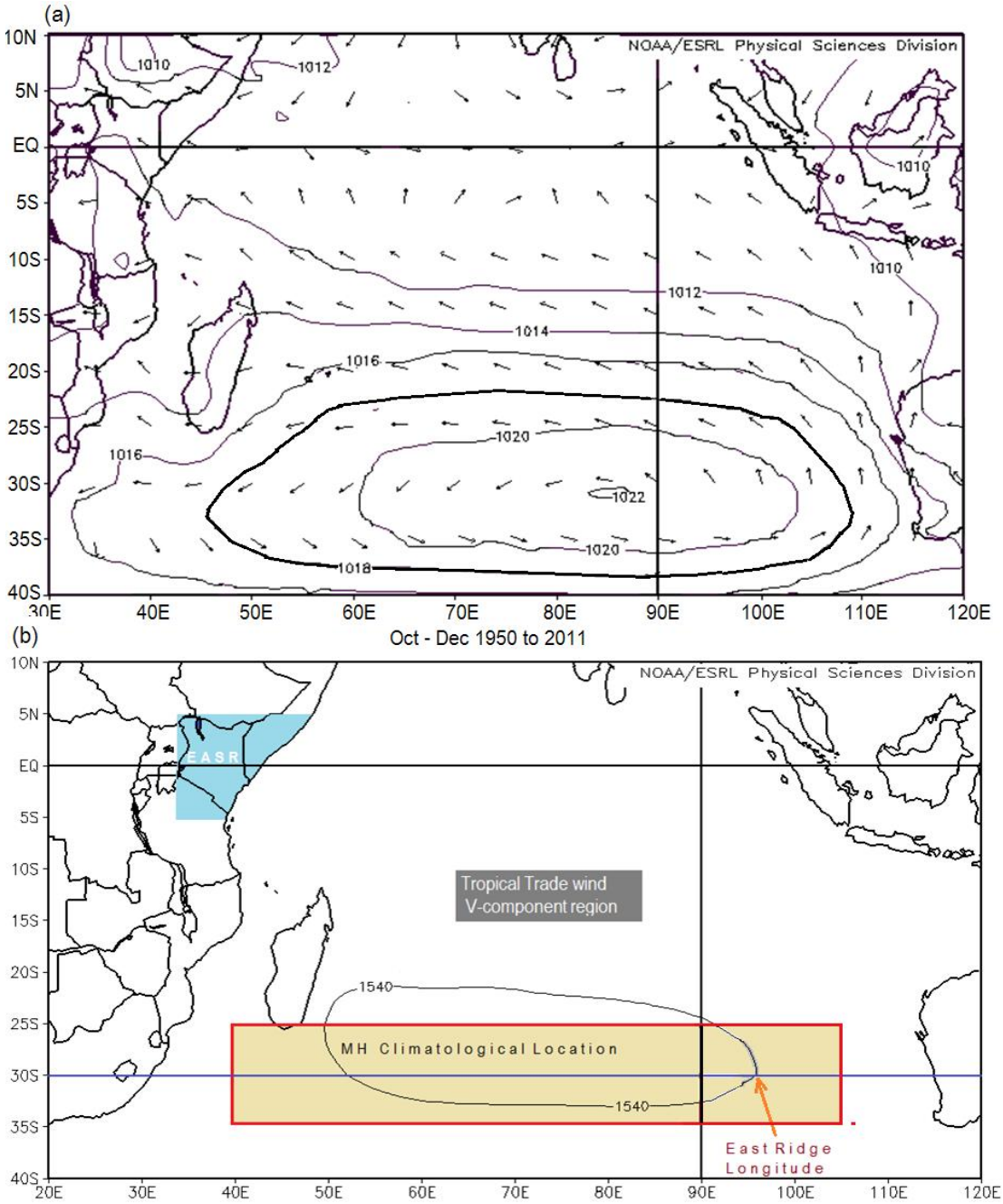

Figure 4.1: (a) Sea level pressure pattern defining the MH for the averaged 1950 to 2011 period and the related surface vector winds. (b) Regions used for the calculation of the average EASR index, trade wind meridional component, east ridge longitude and the MH averaged sea level pressure intensity.

Figure 4.2 illustrates time series of the mean SLP averaged in the region (25ºSï 35ºS and 40ºEï 105ºE) for NCEP/NCAR (solid line) alongside that of the ERA-interim (broken line). In this figure, while the NCEP/NCAR reanalysis data seem to be slightly higher than that of ERA-interim reanalysis data, all the peaks essentially coincide. However, both SLP graphs show a significant positive trend before 1997 which reverses to a negative trend thereafter. This implies that the MH has changed in its intensity with a marked shift in 1997. Since the isolines describing the spatial pressure patterns are more robust at the 850hPa level than at the surface, in the subsequent sections, we resort to define the MH parameters using the 850hPa geopotential height. We also selected for subsequent analysis the NCEP/NCAR reanalysis data, not only because they are accompanied by other model derived parameters of importance in the study but also have longer time series.

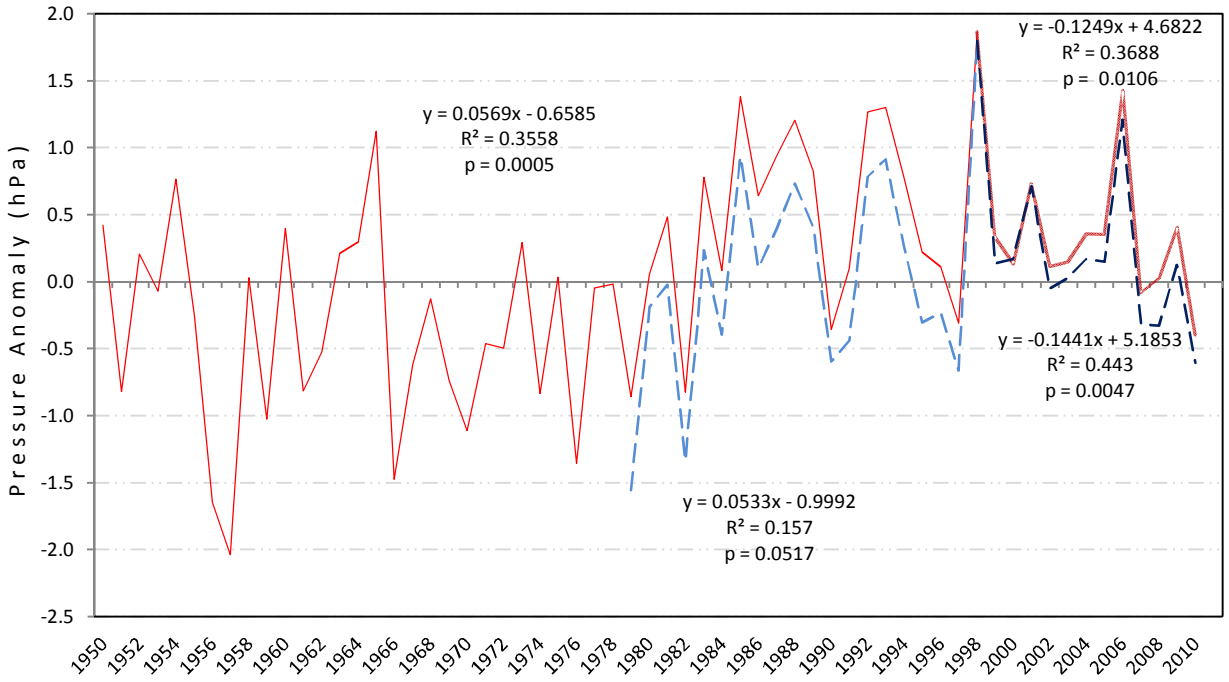

Figure 4.2: Time series of OND SLP anomaly (in hPa) averaged in the MH region (Figure 1) from the NCEP/NCAR (red line) and ERA-interim (blue dashed line) reanalysis data. The linear trend, regression coefficient, and p-value before and after the shift in 1997 are shown above (below) the line of the NCEP/NCAR (ERA-interim) reanalysis data. A value on the top left corner is correlation coefficient between the two time series.

Figure 4.3 shows the intensity of the MH center alongside its longitude location at the 850 hPa level. We omitted the highôs latitude location since this variability was found to be considerably less. The MH center latitude seemed to be perpetually located along either 30.5ºS or 27.5ºS except for 2010 when the center appear to be positioned furthest south along 32.5ºS. It is noted that the MH center has the tendency of swinging to the east and west of its normal position while changing in intensity. On the other hand, the zonal swing in the MH center is more significant than the changes in the corresponding intensity. Figure 3 also indicates that the center longitude significantly decreased during the pre-shift period while reversed to increase significantly during post-shift era. On the other hand the MH intensity has been increasing throughout, but the rise only became significant during the post-shift epoch.

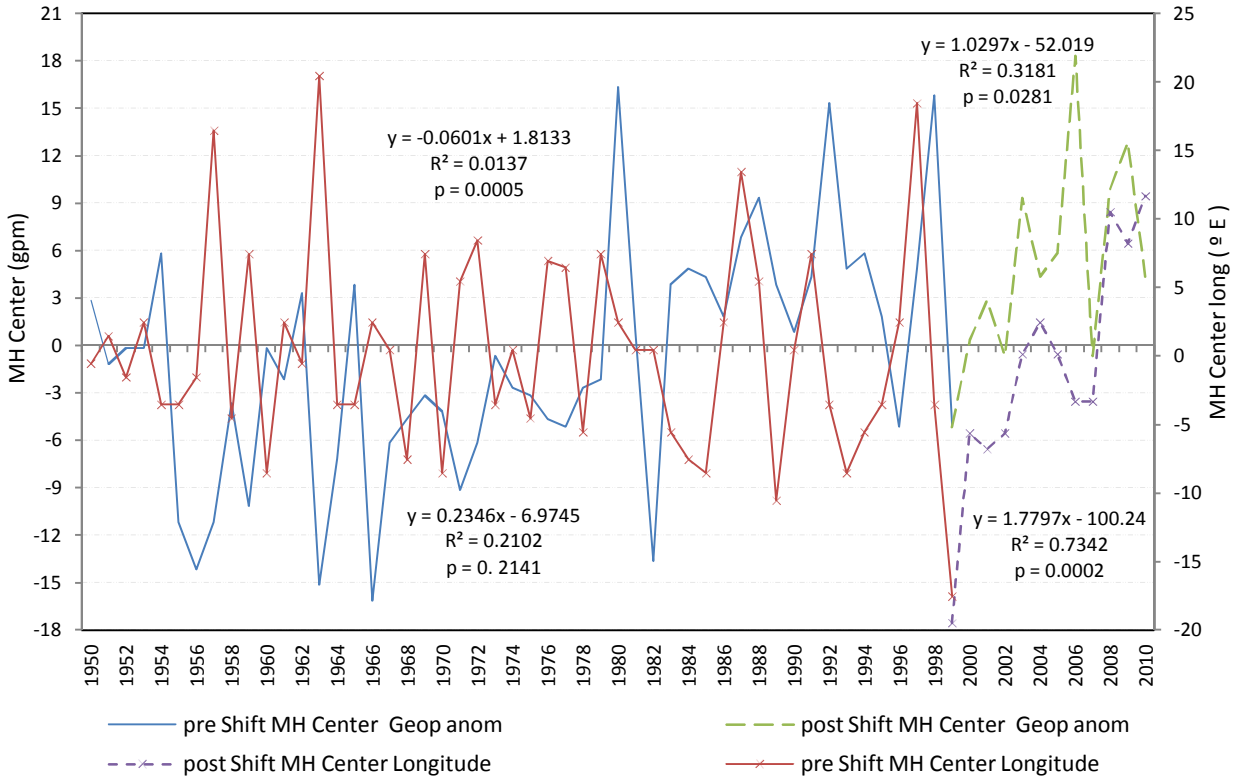

Figure 4.3: Time series of the MH OND center intensity (in gpm) at 850 hPa and its longitude anomalies (in degrees). The linear trend, regression coefficient, and p-value before and after the shift in 1997 are shown above (below) the line of the intensity (longitude) anomaly.

This implies that other external factors are at play and responsible for the loss of the expected synchronization between the MH center intensity and its zonal displacement. In this post 1997 era, the center of the MH was not only displaced eastwards but intensified more rapidly. This indicates that both the MH center and its zonal displacement have been significantly transformed and their processes were more harmonized in the latter period. This is a manifestation of novel MH characteristics in the SIO which should significantly alter the basinôs atmospheric circulation.

To look at details of the zonal movement of the MH, the zonal displacement of the MH eastern ridge along 30ºS is presented in Figure 4.4. This shows a significant eastward trend of the MH eastern ridge since the 1950s. The most westward displacement occurred in 1955 when the ridge was along 91ºE, while the easternmost location was reached in 1997 at 113ºE. The latter event coincides with a strong El Nino and the positive IOD, whilst the former event coincides with La Nina but with no anomalous SST in the tropical Indian Ocean. This relationship may suggest a rather weak connection between the zonal movement of the MH ridge and the two tropical climate modes especially the IOD. Further analysis of the ridgeôs time series shown in Figure 4.4 revealed that the average rate of the MH eastward displacement for the whole period was about 0.9° per decade. But as expected, the time series suggests a decadal shift of the MH eastern ridge movement as it shows a remarkable difference in the position of the MH eastern ridge during 1998-2011 compared to the prior period. The post-1997 era shows a relatively larger displacement trend with a rate of 3.8º per decade.

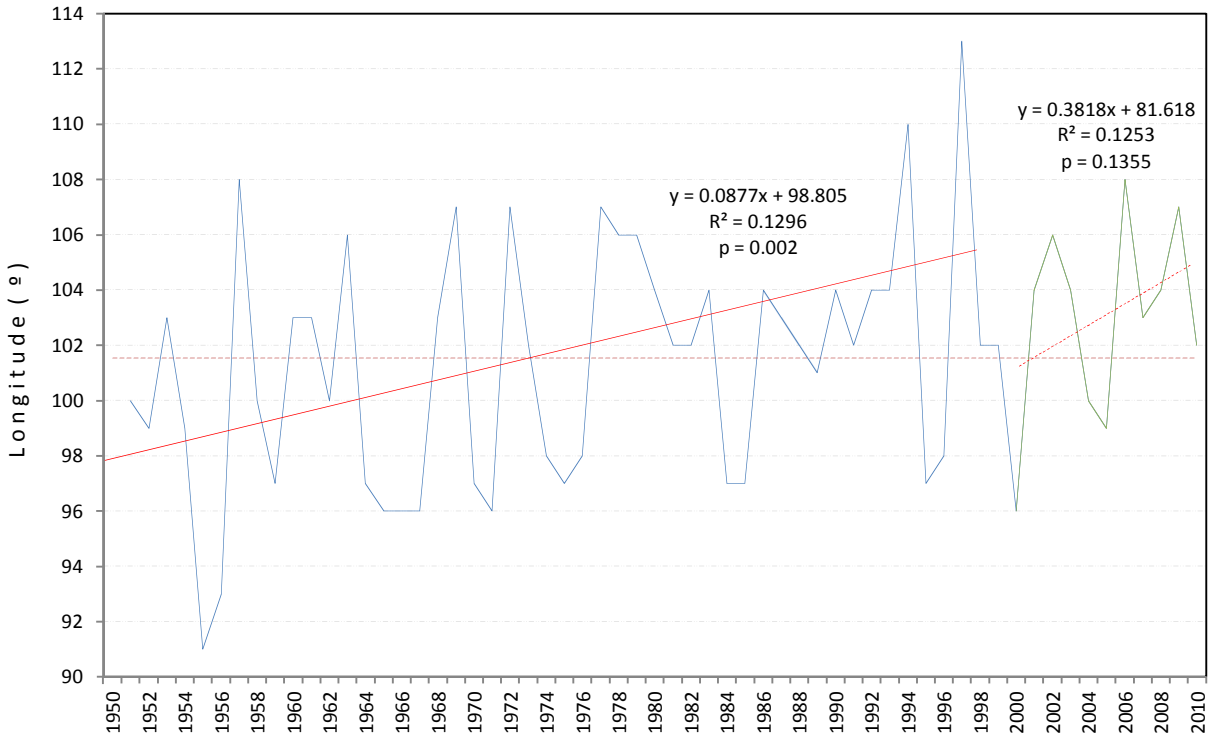

Figure 4.4: Times series of the MH OND eastern ridge longitude (in degrees). The linear trend, regression coefficient, and p-value before and after the shift in 1997 are shown above the line. The broken horizontal line represents the mean position of the MH eastern ridge.

Since the period around 1997 is coming out as a prominent point of change, it is necessary that a shift is confirmed within the MH eastern ridge longitude displacement. To this break point analysis is applied to the ridgeôs time series and the related temporal manifestation is depicted in Figure 4.5. In this figure, a shift in the time series amplitudes becomes visible for the period before and after 1995. There is a reversal in the trends for the two periods. The F- test for first trend is significant at p value of 0.022 while that of the second trend displays an insignificant trend with a p value of 0.954. However all data gives a significant p value 0.024. Since 1995 and 1997 are very close, chances are that both years could be approximating the same shift. Although we were able to demonstrate a shift in the trend between the two periods we could not identify a corresponding significant shift in the mean of the ridgeôs time series. However, changes in the

trend of climatic parameters may have similar or even greater impact on marine ecosystems than changes in the mean (e.g. Rodionov et al. 2004).

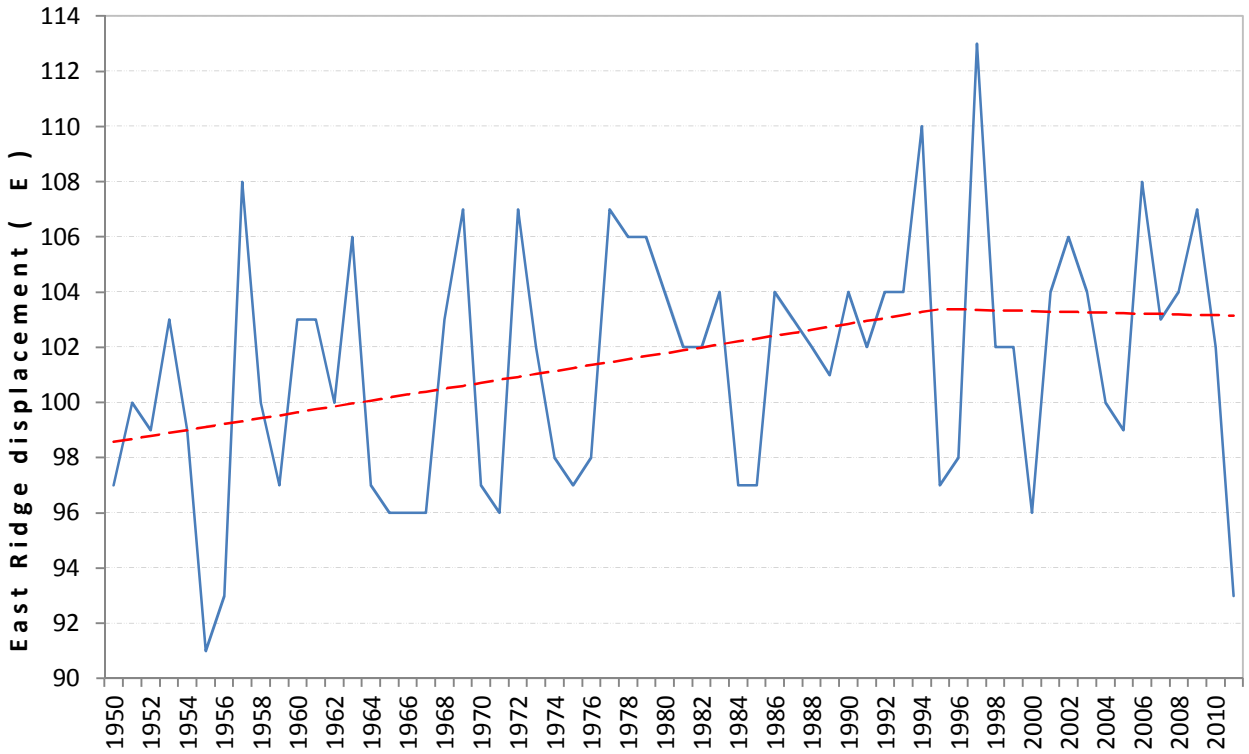

Figure 4.5: Temporal manifestation of the time series of the MH East Ridge displacement. Note the turning point in the trends (red line) imposed by the breakpoint analysis method.

Significant zonal displacement in subtropical highs is not a unique phenomenon in the Indian Ocean. Similar displacement trend is reported for the subtropical highs over the western Pacific (Zhou et al. 2009) and North Atlantic (Li et al. 2011, 2012) where significant westward trends since the 1970s were noted in their respective western ridges. However it is the shift in the displacement around 1997 which is unique to the MH and has not been reported for subtropical anticyclones of other oceans.

It could be interesting to investigate the links among the three derived MH parameters, i.e., the intensity of the MH center, its longitude and the longitude of the MH eastern ridge. The cross

correlations among the three variables is presented in table 4.1. The correlation coefficient between the MH center intensity and the eastern ridge longitude is -0.26. This suggests that the variation of the MH center intensity appears to have an inverse link with the zonal variation of the MH eastern ridge. In other words, the stronger the MH center pressure, the more westward is its corresponding eastern ridge. This suggests that the MH which is displaced to the west is generally stronger and hence is associated with stronger equatorward pressure gradients confined to the western parts of the Indian Ocean basin. The variability of the MH center pressure intensity and its latitudinal position are also significantly connected but with stronger values of 0.49. This suggests that the MH center pressure intensifies as it moves poleward but weakens as it is displaced equatorward. However, it is interesting to note that the variability of the central pressure of the MH seems not to be related to the variability of its eastern ridgeôs zonal location. The correlation coefficient is insignificant with a value of 0.02. This implies that the central pressure of the high pressure system is independent of its eastern ridgeôs zonal displacements. On the other hand, the displacements of the MH central pressure either zonally or meridionally, and its center pressure intensity are significantly connected. Thus the pressure buildup of the MH central pressure does not necessarily translate into a corresponding displacement of its eastern ridge. Hence the displacement of the eastern ridge is actually a result of the physical displacement of the MH as a system rather than changes in its intensity.

Table 4.1. Cross correlation among the central pressure of the MH, its eastern ridge longitude and latitude for the period 1950 to 2011. Coefficients which are significant at 90% level are indicated in bold.

	MH central P (mb)	MH E Ridge Lon	MH E Ridge Lat
MH central P (mb)	1	**-0.26**	**0.49**
MH central P Lon		1	0.02
MH E Ridge Lat			1

To determine which of three MH parameters has the largest impact on the East African rainfall variability, we calculate the correlation between the land only GPCC data and each of the three MH parameters. It is revealed in Figure 4.6 that the MH impact on the rainfall is predominantly restricted to the zonal migration of its eastern ridge. However, the southeast -northwest orientation of the regions with maximum correlation emanating from the ocean is quite conspicuous in the Figure 4.6a. This could be illustrating the spatial manifestation of the impact of the MH eastern ridge driven southeasterly winds on the regionôs rainfall. Also, in Figures 4.6b it is clear that the MH central pressure longitude has a limited area to the north where the correlation is marginally significantly related to the rainfall variability at 10% confidence level. However, it is noted that the significant correlation between the rainfall and the actual MH center pressure variability is none existent at 10% confidence level (Figure not shown). This provides the confidence to expound further on the link between the zonal displacement of the MH eastern ridge and the East African rainfall variability.

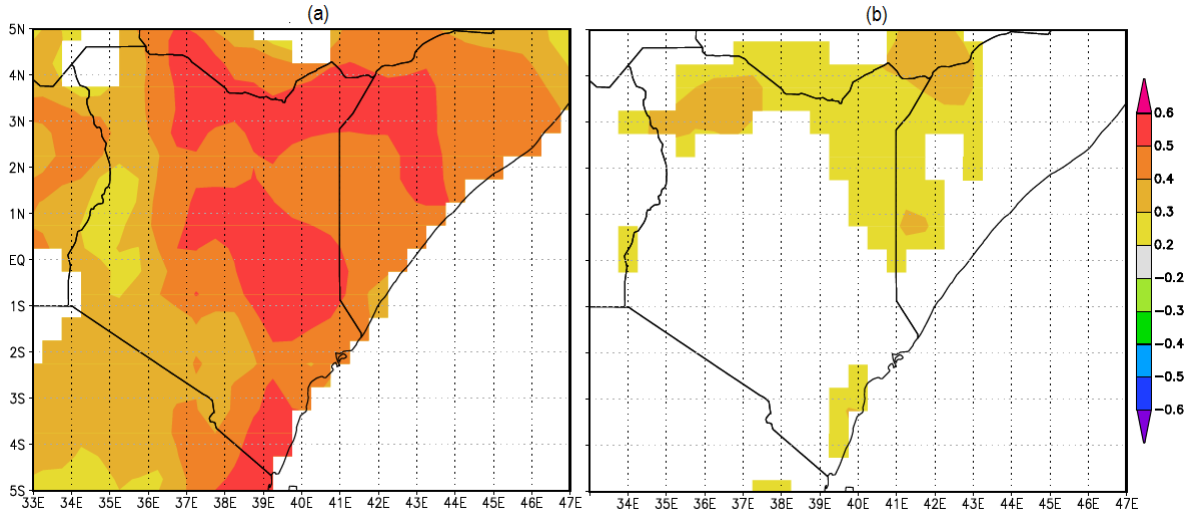

Figure 4.6: (a) The correlation between the OND MH eastern ridge longitude and the EASR during 1950-2010. (b) Same as in (a), but for the OND MH center longitude. Shown are correlation values with p < 10%.

4.3.2 Impact of the MH eastern ridge longitude on the EASR

In this section, we extracted all the years from 1950 with the EASR exceeding one standard deviation together with their corresponding MH eastern ridge longitude (Table 4.2). Here, we define west (east) displacements of the MH eastern ridge as years when the ridge movement is anomalously to the west (east) by more than 2º. The rest of the years are defined as neutral displacements (see Table 3.??4). We also refer to the EASR index values greater than 1 as floods and those less than 1 as droughts. It is found that 75% of the droughts occur when the MH ridge shows the west displacements (Table 4.2b). On the other hand, the link of the eastern ridge to the floods is not that robust as only 50% of the floods occur when the MH ridge shows the east displacements (Table 4.2b). Another 50% of the floods occur during the neutral displacements. This indicates that the anomalous displacement of the MH eastern ridge can explain droughts to a greater extent than floods implying that the relationship is not symmetric. It should be noted that there are no coincidences of floods (droughts) with the west (east) displacements.

Table 4.2: (a) Anomalies of the EASR index and the OND MH eastern ridge longitude (in degree) for drought and flood years. (b) Occurrence frequency (in %) of the droughts and floods for the west, neutral, and east displacements of the OND MH eastern ridge.

(a)	**Droughts**		**Floods**		
Year	EASR	E_Ridge lon(º)	Year	EASR	E_Ridge lon(º)
1987	-1.51	1.61	1997	4.65	11.61
1970	-1.39	-4.39	1982	1.06	0.61
1950	-1.38	-4.39	1963	1.32	4.61
2005	-1.33	-2.39	1951	1.62	-1.39
1975	-1.16	-4.39	1968	1.83	1.61
1998	-1.15	0.61	2006	2.13	6.61
1996	-1.04	-3.39	1994	2.22	8.61
2000	-1.01	-5.39	1961	4.59	1.61
Mean	-1.23	-2.53		2.21	3.81

(b)	**Droughts**	**Floods**
Number of events	8	8
West displacements	75.00 %	00.00 %
Neutral displacements	25.00 %	50.00 %
East displacement	0.00 %	50.00 %

To examine how the zonal movements of the MH eastern ridge are linked to the EASR, we plot the ridge longitude against the EASR in Figure 4.7. We note that when the ridge is displaced by more than 4º to the east of the mean position, a strong linear relationship with the rainfall emerges. It is possible in this case to estimate the intensity of a surplus rainfall event through the extent of the eastward displacement of the MH eastern ridge. When the ridge displacement is within 4º on either side of the mean position, there is no distinct linear association. However, the ridge seems to have two preferred locations along 0.6 º and 2.6 º east of the mean position on 40% (20% each) of the occasions. The two favored locations seem to indicate asymmetric variations in the E-W displacement of the eastern ridge of the MH and appear not to have any identifiable bearing on either deficits or surplus rainfall. On the other hand, in the westward displacements of more than 4º, the linear relationship with the EASR is weak and not significant with pï value of 0.3817. However, there are ten below-normal rainfall events and only one slightly above-normal rainfall event when the eastern ridge is displaced by more than 2 º to west. This suggests that this westward displacement of the ridge does not necessarily explain the magnitude of the below-normal rainfall event but may provide information about the occurrence of below-normal rainfall.

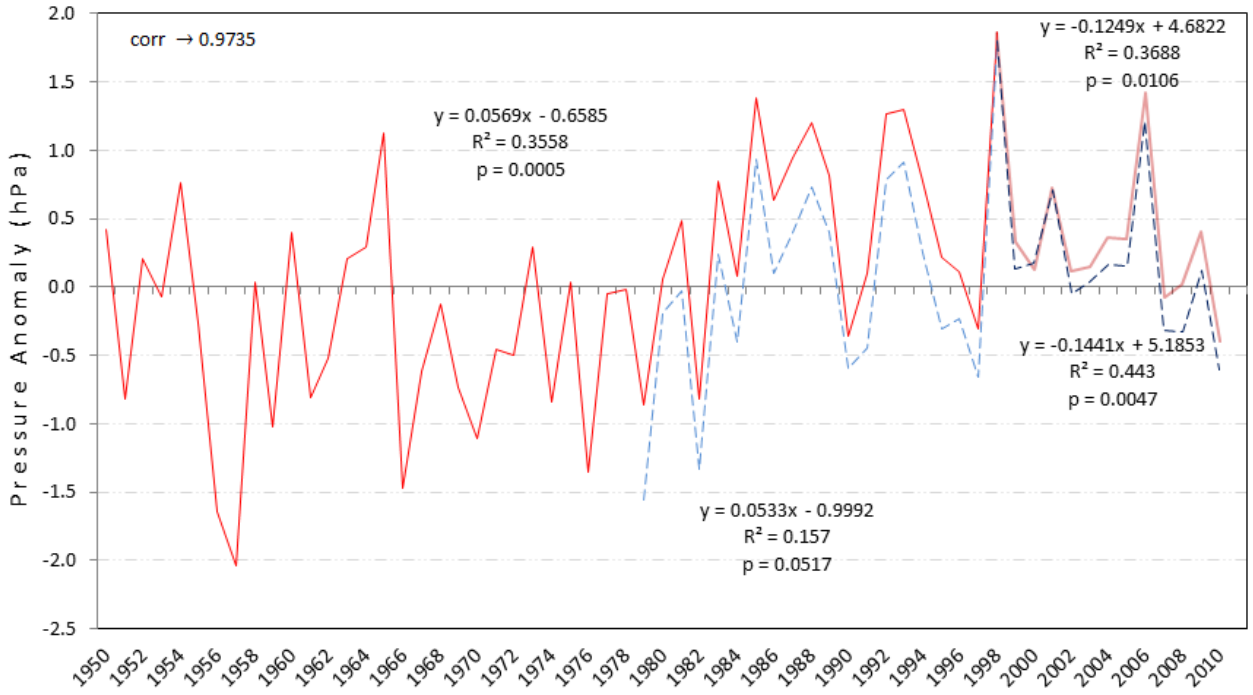

Figure 4.7: Scatterplot of the OND MH eastern ridge longitude (in degrees) anomaly against the EASR index for the west, neutral, and east displacements of the OND MH eastern ridge. The linear trend, regression coefficient, and p-value are shown above each line.

Figure 4.8 shows composite rainfall anomaly for the westward / eastward displacements, the relief map, and the spatial correlation between the rainfall and the meridional wind averaged in the SIO (65ºE-85ºE, 10ºS-15ºS, also shown Figure 4.1b). In Figures 4.8a and b, both rainfall anomaly patterns are broadly coherent. Extreme rainfall amounts are generally restricted to the highland areas (depicted in Figure 4.8c) where the rainfall range exceeds 105mm/day while the lowland regions have a relatively moderate range of rainfall amounts which do not exceed 55mm/day. However these highlands, especially the windward side to the SE trade winds show the strongest deficits in excess of 40mm/day while the relatively lower maximum positive anomalies of 45mm/day have a meridional orientation which may not be really connected to the SE trade winds. Thus the SE trade winds could be responsible for the excessive dryness which characterizes the windward slopes. This result is further supported by the map of the spatial

variance of the rainfall (not shown), which shows higher variability of the rainfall over the mountains, in particular, over the Mount Kenya. Infact Manatsa et al. (2012), noted that the dominant mode of rainfall variability of EASR extracted through the first emprical orthogonal function (EOF1) displayed the peak spatial loadings over Mount Kenya. This signifies that the most important component of the rainfall variability over east Africa varies largely in tandem with the rainfall variability over this mountain.

The emphasis on the essential role played by orography in the rainfall variability suggests that the wind direction and speed is an important component shaping the rainfall anomalies over East Africa. Figure 4.8d demonstrates that the meridional wind component of the southeasterly trade winds are important for the East African rainfall variability. All correlation coefficients in this figure are significnat above the 90% cofidence level. However, the correlations are more pronounced over the highlands where the wind explains more than 36% of the rainfall variability. On the other hand, convection seems to play a role in the rainfall over low lying coastal areas where the rainfall variability is less dependent on both relief and the meridional wind component. It appears that the rainfall anomaly composite of the westward displacements (Figure 4.8a) illustrates a more coherent pattern with strong north-south orientation. This can also be seen in Figure 4.8d and suggests that the north-south alignment is related to the meridional component of the southeasterly trade winds and hence plays a more active role in the development of droughts.

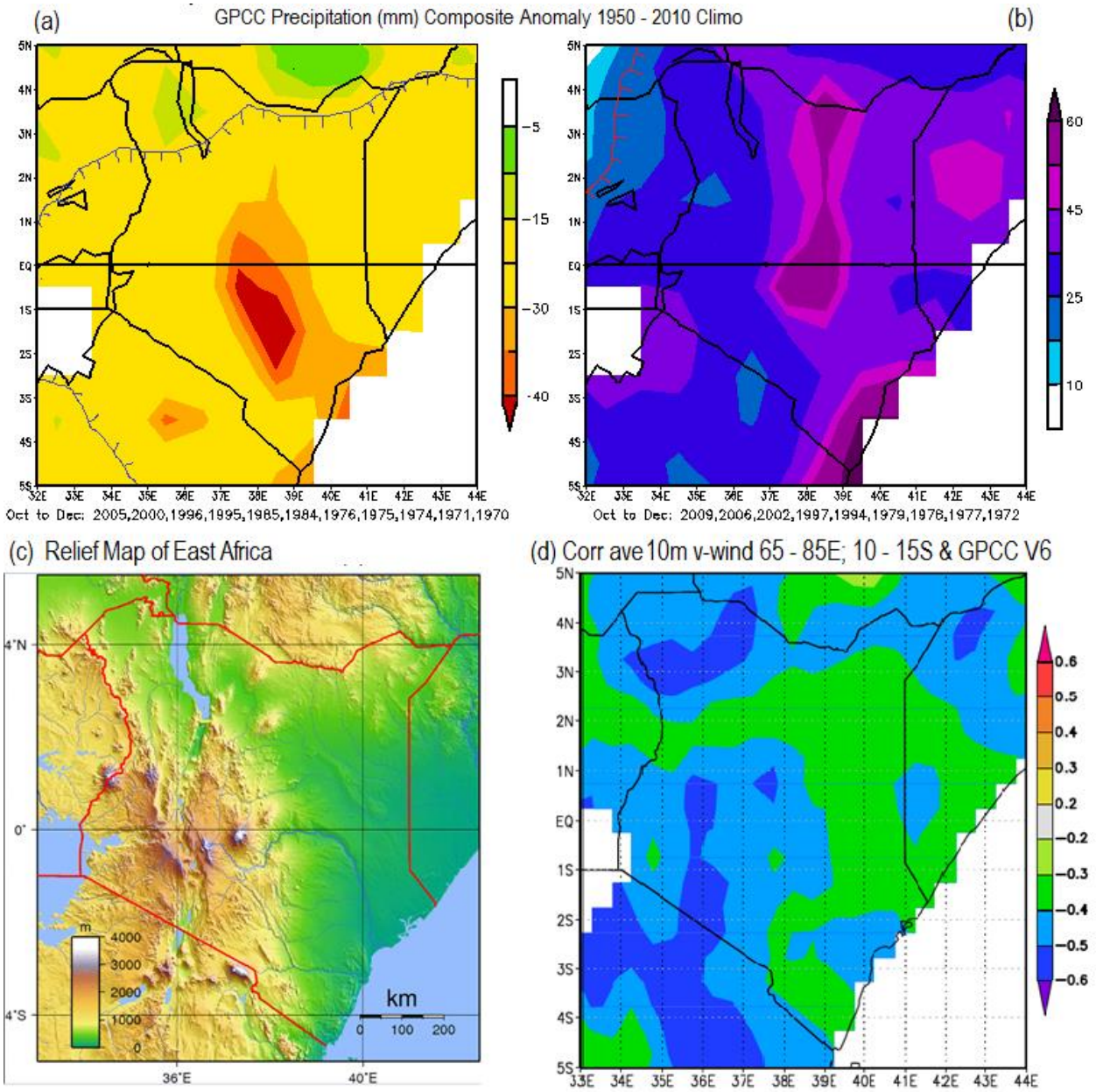

Figure 4.8: (a) Composite rainfall anomaly (mm/day) for the west displacement of the OND MH eastern ridge. (b) Same as in (a), but for the east displacement. Inserted blue/red lines show rainfall anomalies significant at 10% confidence level. (c) Relief map and (d) Correlation between the rainfall and the meridional wind averaged in the SIO region (65°E-85°E, 10°S-15°S) for the period 1950 to 2011. All the correlation coefficients are significant above the 90% confidence level.

Since the rainfall is strongly related to the moisture supply by winds, we calculate the horizontal low-level wind anomalies relative to the 1950-2011 climatology together with their meridional

and zonal components during the drought and flood years (Figure 4.9). We omitted the climatology figures though we noted that the prevailing wind over the sub region is dominated by the southeasterly trade winds. In fact, equatorial East Africa is subjected to the southeasterly trade winds during the normal rainfall seasons (Thompson, 1966). However, these trade winds are enhanced during droughts (Figures 4.9a, c, and e) while they are suppressed during floods (Figures 4.9b, d and f).

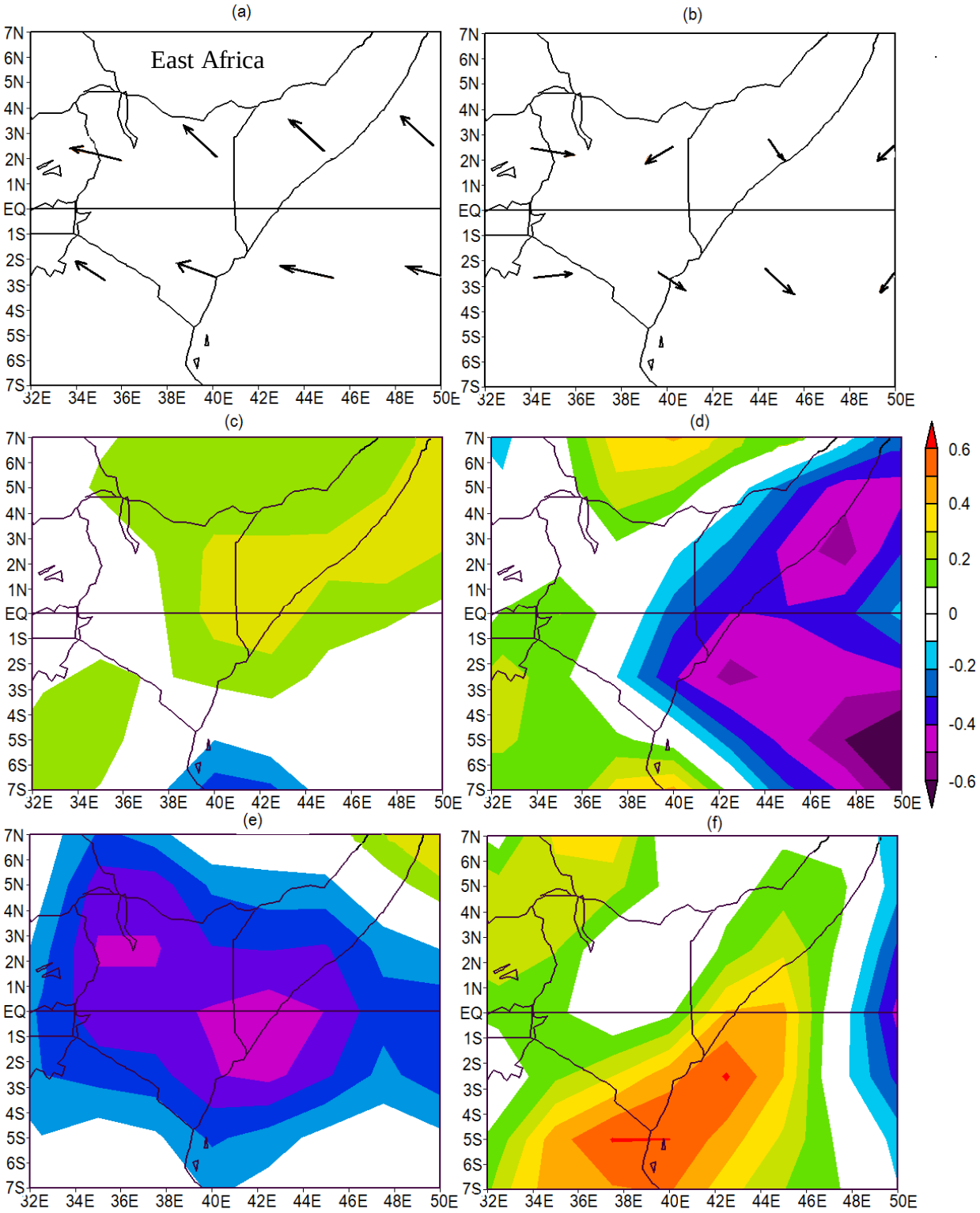

Figure 4.9: Composite wind anomalies of horizontal wind vector (a and b), meridional speed (in m/s, (c and d)) and zonal wind speed (in m/s, (e and f)) at 925 hPa during Oct-Dec. Wind anomalies are calculated relative to the period 1950 to 2011, for the drought (a, c and e) and flood (b, d, f) years. Years constituting drought and flood composites are provided in Table 4.2

Therefore the low level equatorial easterly(westerly) winds observed over central Indian Ocean and believed to advect moisture towards (away from) East Africa during floods (droughts), (e.g. Indeje et al. 2000, Black et al. 2003; Clark et al. 2003; Hastenrath 2004,2007; Behera et al. 2005; Marchant et al. 2006, Manatsa et al. 2010) actually penetrate the mainland. In fact we see that what transpires in the equatorial Indian Ocean related to the zonal wind direction is reversed over the mainland of East Africa. The low level zonal wind components have relatively strong easterly anomalies during droughts while manifesting relatively moderate westerly anomalies during floods. This plays a crucial role in the development of the rainfall deficits, because stronger winds facilitate the advection of cooler and less moist air from the SIO. As such, this particular behavior of the trade winds over east Africa is quite novel and hence warrants further scrutiny in the subsequent section.

To explain more on the relationship between the meridional wind and the rainfall, in Figure 4.10 we present the EASR index values alongside their corresponding meridional trade wind anomalies. These anomalies are sorted according to three categories identified as strongly southerly (when $v > 0.7$ m/s), neutral (when $v \leq 0.7$ m/s but ≥ -0.7 m/s) and strongly northerly (when $v < -0.7$ m/s). The figure reveals that when the meridional wind anomaly is strongly northerly the rainfall deficit occurs only in 1991 and no droughts, (when EASR is less than - 1.0) occur in this range. On the other hand, when the meridional wind anomaly is strongly southerly, the rainfall always shows deficit and similarly, no floods (when EASR is greater than 1.0) coincide with this range. As for the neutral category, no significant bias in the rainfall anomalies can be readily observed. However, we note that all the droughts and floods coincide with positive and negative wind anomalies respectively. This remarkably strong connection between

the meridional trade wind component thresholds and rainfall extremes, especially droughts is overwhelming. However it appears that other factors not related to the meridional wind anomalies, such as convection could be playing more prominent roles in enhancing rainfall during some flood years. This observation reiterates the importance of incorporating the meridional anomaly component of the trade winds in the definition of rainfall extremes, particularly droughts over East Africa.

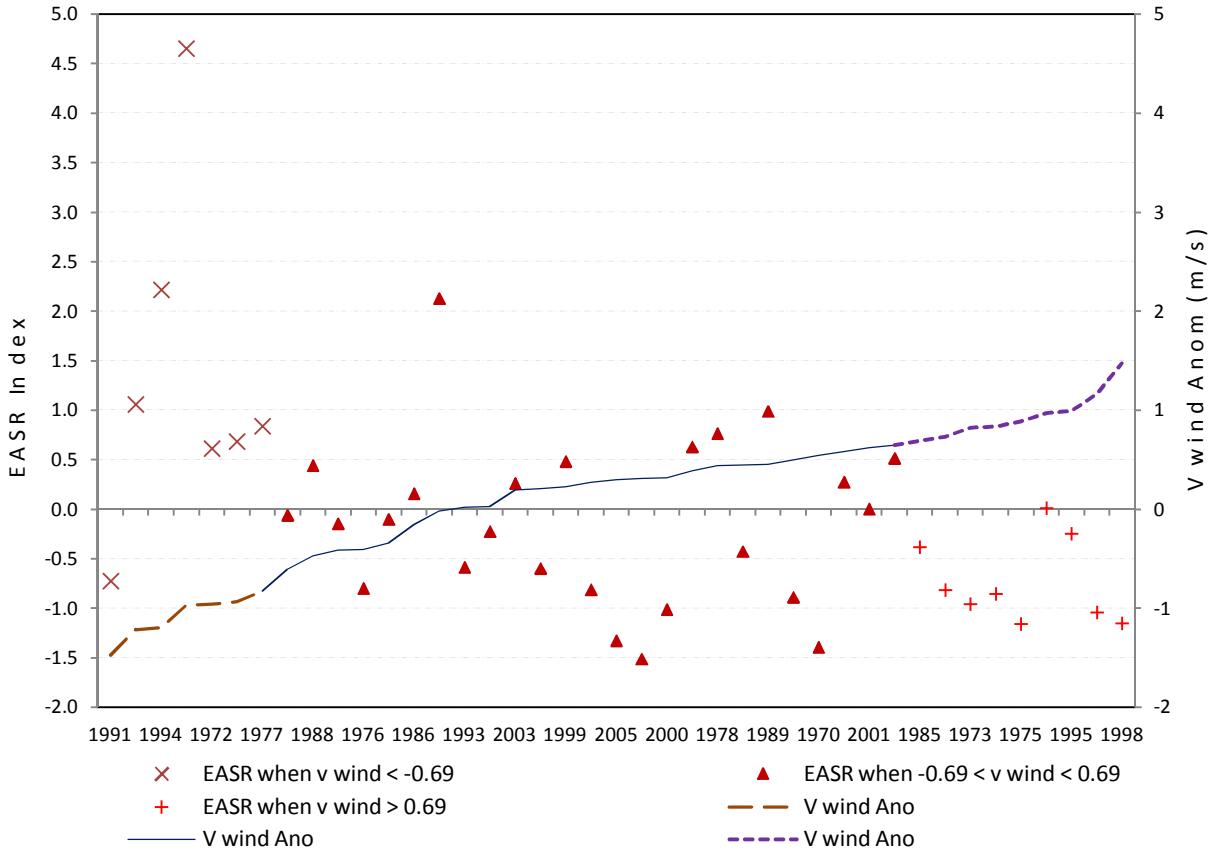

Figure 4.10: The EASR alongside the strongly northerly (left), neutral (middle) and strongly southerly (right) categories of the meridional component of the wind anomalies.

We further confirm this strong relationship between the zonal swings of the MH eastern ridge and the meridional wind anomalies by using the Chi square test. Here, we classify the frequency of the EASR into six categories in accordance with the intensity anomaly of the meridional wind.

Based on these categories, a contingency table for the observed frequencies was prepared as shown in Table 4.3 From these observed frequencies, expected frequencies (in brackets) and the χ^2 value were computed. In this case the null hypothesis was that there is no relationship between the zonal movements of the MH eastern ridge and the meridional wind values, i.e. the observed and expected values in the rows and columns in Table 4.3 are independent. It is found that the χ^2 for the rainfall frequencies is 25.48 and is significant above the 95% confidence level, suggesting the strong link between the zonal movements of the MH eastern ridge and the meridional wind strength. This result supports that the southeasterly trade wind is strongly related to the EASR variability shown in Figure 4. 8d.

Table 4.3: The observed frequencies of the OND eastern ridge displacement based on meridional wind categories. Expected frequencies are in the parenthesis, Df represents the degrees of freedom while χ^2 stands for the Chi square.

V wind strength	W Displacement	Neutral Displacement	E Displacement
< -1.0	4 (1.61)	2 (3.07)	0 (1.32)
-1.0 > - - 0.5	4 (2.68)	6 (5.12)	0 (2.20)
>-0.5 ï 0.0	2 (1.88)	3 (3.59)	2 (1.54)
>0.0 ï 0.5	0 (1.88)	7 (3.59)	0 (1.54)
>0.50 ï 1.0	1 (1.88)	2 (3.59)	4 (1.54)
> 1.0	0 (1.07)	1 (2.04)	3 (0.88)
Total	11	21	9
Df = 24	$\chi^2_{calculated}$ (25.481) > $\chi^2_{critical}$(18.31)		P-value < 0.05

To investigate how the zonal movements of the MH eastern ridge resolve the East African droughts and floods, we calculate the difference of the composite anomaly between the eastward and westward displacements (Figure 4.11). The reverse of what is depicted in Figure 4.11 can be achieved by simply subtracting the east from the west displacements. This type of composite analysis enables the identification of the salient features that are predominant in the individual composites of the two opposite extremes. In Figure 4.11a, an anomalous low pressure develops east of 70ºE over the tropics and 90ºE over the subtropics and a high pressure offshore to the

northwest of Australia. The coupling of these two opposing anomalous pressure systems may act to enhance the southeasterly trade winds. This is supported by the southeasterly wind anomaly seen right from the eastern flank of the MH to East Africa near the equator (Figure 4.11b). Interestingly, these southeasterly trade winds appear to split into two streams on encountering the coast, one continuing northwestward and the other turning eastward along the equator. These enhanced southeasterly winds coincide with most probably bring relatively less moist air from the high latitudes (Figure 4.11d), enhance evaporation. This process coincides with negative SST anomalies observed as a wide band stretching from the eastern subtropics to equatorial regions over East Africa in Figure 4.11c. Higher SST anomalies are found below over the anomalous low pressure system in the tropics of the eastern south Indian Ocean. It is important to note the spatial SST patterns depicted in this figure do not have a close correspondence to the well-known IOD system (Saji et al., 1999) but bears a close resemblance to the meridional SST dipole identified by England et al. 2006 and Ummenhofer et al. 2009a).

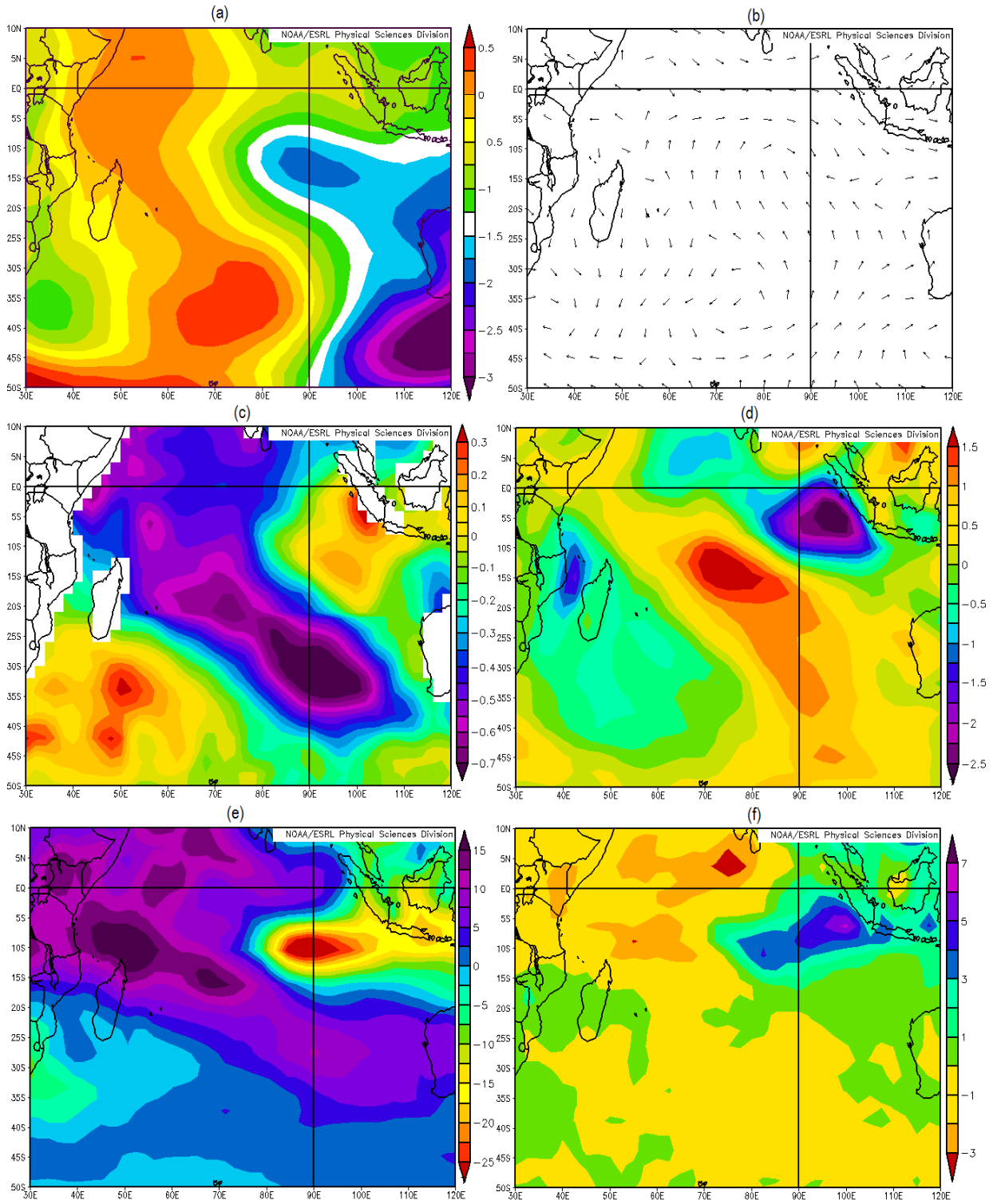

Figure 4.11: Differences in the composite anomalies between the east and west displacements of the OND MH eastern ridge for (a) SLP (in hPa), (b) surface wind vector (in m/s) (c) SST (in ºC), (d) meridional wind (m/s), (e) OLR (in W/m^2), and (f) precipitation (mm/day).Years for the east and west displacements are available in Table 4.4.

As a result, the convection is suppressed over lower SST regions (Figure 4.11e) whilst enhanced over regions of protracted positive SST anomalies especially over the low pressure region that has developed off the Sumatra-Java southwest coast. This leads to rainfall deficits over the Indian Ocean including East Africa, while surplus rainfall is experienced over the eastern India Ocean (Figure 4. 11f). Thus, the zonal migration of the MH eastern ridge is very important for the EASR variability through the change in the southeasterly trade winds.

Although it is not the prime aim of this study to prove the dependency/independency of the displacement of the MH eastern ridge from the IOD system, the temptation is overwhelming since the anomalous low (high) pressure system noted during eastern (western) displacements coincides with the exact location of the eastern pole of the IOD defined by Saji et al. (1999). At the same time the composite analysis indicates that this region could be part of the process related to the zonal displacement of the eastern ridge of the MH. Even though, as already noted, the MH zonal swings of its eastern ridge appear not to be in total conformity with the variability of the extreme IOD events. Thus it is most likely that there is a process connecting the zonal movement of the MH eastern ridge to the tropically based anomalous pressure system which is visible in Figures 4.11a and b. However we will not delve much into this aspect as it is beyond the scope of this study.

The SST correlation with the MH eastern ridge longitude and the EASR index are presented in Figures 4.12a and b respectively). It is found that the variability of the eastern ridge longitude is closely linked to the anomalous SST and the spatial pattern is very similar to the one in Figure 4.11d. Interestingly, both Figures 4.12a and b show spatial coherence save for the eastern

tropical Indian Ocean, where the signal is much weaker in the former than in the latter. This indicates that the MH eastern ridge influences the SST through the southeasterly trade winds while demonstrating that the ridge has a unique impact on the EASR.

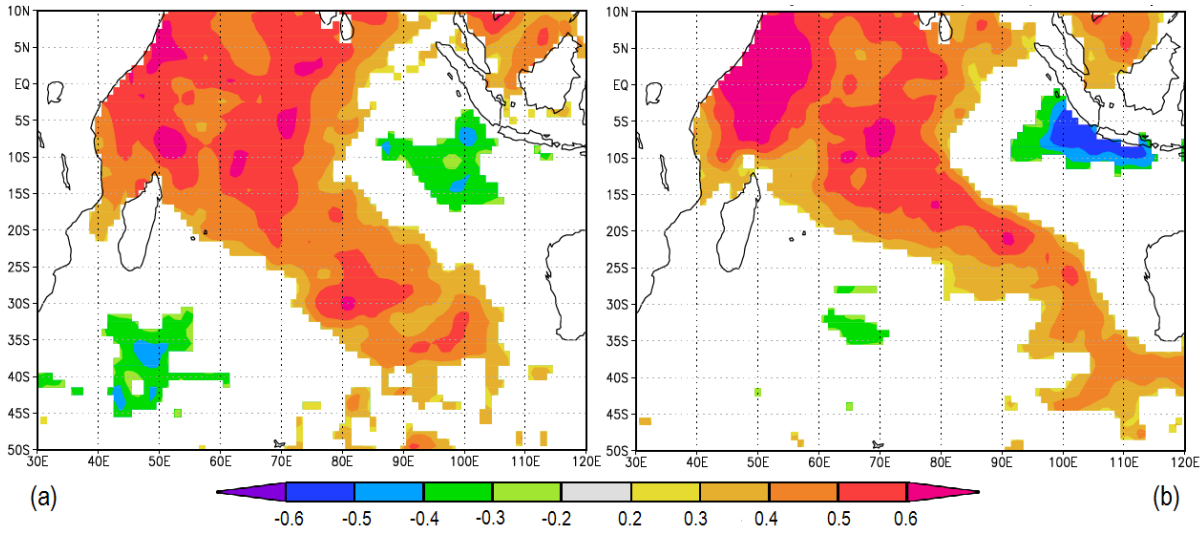

Figure 4.12: (a) Correlation coefficient (p < 10%) between the OND MH eastern ridge and the SST. (b) Same as in (a), but for the EASR index.

4.3.3 Relationship with ENSO and the IOD

Finally, we check the link between the zonal variability of the MH eastern ridge related to the meridional wind anomalies and the two tropical climate modes; ENSO and the IOD. The eleven westward displacements of the MH eastern ridge in Table 4.4 show four events (one event) co-occurring with La Nina (the negative IOD). On the other hand, six (five) of the nine eastward displacement events co-occur with El Nino (the positive IOD). This implies that the extreme western and eastern displacements of the ridge are neither strongly tied to the extreme ENSO nor IOD events though the connection is slightly stronger with ENSO. The correlation of the eastern ridge longitude with ENSO is 0.57 while that with IOD is 0.48.

Table 4.4: (a) Anomalies of the EASR index (mm/day), the MH eastern ridge longitude (R, in degrees east), the DMI index (in ºC), and the NINO3.4 index (in ºC) for the west displacement of the MH eastern ridge. (b) Same as in (a), but for the east displacement. Symbols of E, L, P, N, and no in the table indicate El Nino, La Nina, positive IOD, negative IOD, and neither ENSO nor IOD years, respectively. R_ (ºE) shown in (a) and (b) are the longitudinal anomalies (in ºE).

(a)						(b)					
Year	R_ (ºE)	EASR v (m/s)		Nino 3.4	DMI	Year	R_(ºE)	EASR v(m/s)		Nino 3.4	DMI
2005	-2.39	-1.33	0.30	-0.31(no)	-0.27(no)	2009	5.61	-0.15	-0.41	1.40(E)	0.58(no)
2000	-5.39	-1.01	0.32	-0.86(no)	-0.06(no)	2006	6.61	2.13	-0.02	1.02(E)	1.65(P)
1996	-3.39	-1.04	1.16	-0.49(no)	-1.47(N)	2002	4.61	0.69	-0.93	1.50(E)	1.32(P)
1995	-4.39	-0.24	0.99	-1.00(L)	-0.22(no)	1997	11.61	4.65	-0.97	2.63(E)	3.95(P)
1985	-4.39	-0.38	0.69	-0.47(no)	-0.33(no)	1994	8.61	2.22	-1.20	1.11(E)	1.78(P)
1984	-4.39	0.52	0.65	-1.19(L)	-0.57(no)	1979	4.61	-0.22	0.03	-1.19(L)	0.72(no)
1976	-3.39	-0.80	-0.41	0.81(no)	0.75(no)	1978	4.61	0.77	-0.44	-0.27(N)	-0.4(no)
1975	-4.39	-1.16	0.88	-1.50(L)	-0.47(no)	1977	5.61	0.84	-0.83	0.90(N)	0.34(no)
1974	-3.39	-0.85	0.21	-0.74(no)	-0.82(no)	1972	5.61	0.62	-0.96	2.06(E)	2.33(P)
1971	-5.39	-0.59	0.55	-0.89(no)	-0.08(no)						
1970	-4.39	-1.39	0.55	-1.21(L)	-0.37(no)						
Mean	-4.12	-0.75	0.54	-0.71(no)	-0.36(no)		6.39	1.28	-0.64	1.02(E)	1.36(P)

For the EASR variability, both ENSO and the IOD poorly resolve the droughts which are identified by extreme westward displacements of the MH eastern ridge and its related positive meridional trade wind anomalies. In fact, the worst drought which occurred in 1987 coincides with an El Nino rather than La Nina (not shown). No wonder why Hastenrath et al. (2004) noted that most of East African droughts have largely been unpredictable. This could be due to the predominant reliance of the drought forecasts on ENSO and the IOD states which had demonstrated immense success for predicting floods. Symmetry in the ENSO/IOD impacts on EASR was largely assumed which we have shown in this work to be largely misleading.

4. Summary and Conclusions

Using observations and reanalysis data, we have explored the interannual variability of EASR and its link with the MH variation. It is revealed that the EASR variability is strongly linked to the MH zonal displacement, in particular, the zonal movement of the MH eastern ridge. When the MH eastern ridge is anomalously displaced to the west (east) of its normal position, the SE

trade winds over the SIO anomalously strengthen (weaken). This westward (eastward) migration of the eastern ridge helps advect relatively cooler and less moist low level airflow over East Africa which in turn suppresses (enhances) both regional convection and orographic rainfall. Thus the zonal migration of the MH eastern ridge provides a novel indication for the EASR extremes which has the propensity to resolve better the droughts than the surplus rainfall. This revelation has immense social application in the region of East Africa where droughts have become more prevalent against the background of deteriorating drought forecasts which are predominantly generated from traditional indicators like ENSO and the IOD. In the next chapter we examine how the final shift of the 1990s could have altered the surface air temperature of southern Africa including the involvement of the establishment of the stratospheric ozone hole.

CHAPTER 5

Shift in Surface Air Temperature over Southern Africa

5.0 Brief Chapter Synopsis

This chapter is based on the paper which was published as:

Manatsa D, Yushi Morioka, Swadhin K. Behera, Toshi Yamagata, Caxton H. Matarira (2013). Ozone hole warming of summer temperatures over southern Africa. *Nature Geoscience Journal.* DOI: 10. 1038/NGEO1968.

In this chapter, I demonstrate that the impacts of the three shifts are not only confined to the rainfall of East Africa. The eastward displacement of the Mascarene High (MH) due to the stratospheric ozone hole influence through Southern Annular Mode (SAM)ôs shift to positive polarity in the last shift is also accounts for the abrupt increase in surface air temperature (SAT) of southern Africa from the late 1990s.

5.1 Introduction

The notable rise in surface air temperatures over southern Africa over the past two decades is thought to largely result from the human-induced increase in atmospheric greenhouse gas concentrations (Shongwe et al.2009; IPCC, 2001; Joubert and Kohler 1996). In addition, the loss of stratospheric ozone over Antarctica is thought to have had a significant impact on tropospheric circulation, and hence climate, in the southern hemisphere summer (Gillett and Thompson 2003; Thompson and Solomon 2002; Hartman et al., 2000; Arblaster et al., 2011; Shindell and Schmidt, 2004; Polvani et al., 2011), by favouring the positive phase of the Southern Annular Mode (Marshall, 2003; Saxton, 2001; Gillett and Thompson, 2003). Here, we use reanalysis data to compare the climate of southern Africa prior to and after the development of the large ozone hole, and investigate possible links between the development of the Antarctic ozone hole and summer warming in the region, defining 1970 to 1993 as the pre-ozone hole era, and 1993-2011 as the large ozone hole era. We find that the ozone-induced shift in the polarity of the

Southern Annular Mode after 1993 coincided with an intensification of the Angola Low, a continental low pressure system that normally develops in austral summer and is mostly located over Angola. I show that the deepening of this low pressure system, in turn, was associated with an increase in the flux of warm surface air from the lower latitudes to southern Africa. We suggest that the recent summer warming over southern Africa is linked to these shifts in atmospheric circulation that are probably induced by Antarctica ozone loss.

Several hints on ozone hole impacts on the tropical circulation are found in literature Thompson and Solomon 2003; Gillett and Thompson 2002; Thompson and Solomon 2002; Kang et al. 2011, Cataldo et al., 2013) Compared to greenhouse gases, there is a general consensus that the ozone hole has the paramount impact on tropospheric circulation during austral summer (Gillett and Thompson 2003; Thompson and Solomon 2002; Hartman et al., 2000; Arblaster et al., 2011; Shindell and Schmidt, 2004; Polvani et al., 2011). During this season, the ozone depletion imposes its impacts through the Southern Annular Mode (SAM, Thompson and Solomon, 2003; Gillett and Thompson, 2002; Shindell and Schmidt, 2004) but in a unidirectional way, towards SAMôs positive polarity (Saxton, 2001; Marshall, 2003). This transformation may have necessitated gradual pressure buildup of both the St Helena High (SHH) and the Mascarene High (MH, Manatsa et al., 2011; Xue et al., 2004) (Figure 5.1) which coincided with their respective westward and eastward displacement (Manatsa et al., 2011). The summertime pressure distribution over southern Africa is dominated by the Angola Low **(**AL) that plays a prominent role in the surface air temperature **(**SAT) variability through advection of warm air from the lower latitudes (Tyson and Preston-Whyte, 2000). There is also the Benguela Current which flows northwards along the coast of southwest Africa as an eastern boundary current (Garzoli and Gordon, 1996) that influences SAT in this region. The prevailing winds from the south and southeast steered by the SHH and the AL induce coastal upwelling of cold waters, hence

influencing the summer intensity of the Benguela Current. Since SHH and MH are both dynamically coupled to the AL, the apparent SAM related alterations in their pressure and zonal locations are bound to have significant impacts on the AL. In fact, there is the likelihood that an increase in the SAT ensures when AL intensifies because the AL and the SAT are significantly inversely correlated (-0.48). Therefore the ozone hole and SAM may have impacts on the regional SAT worth examining. Better understanding of SAT variability enhances adaptation measures for millions of the southern African community that are exposed to negative climate change impacts (Shongwe et al.,2009) .

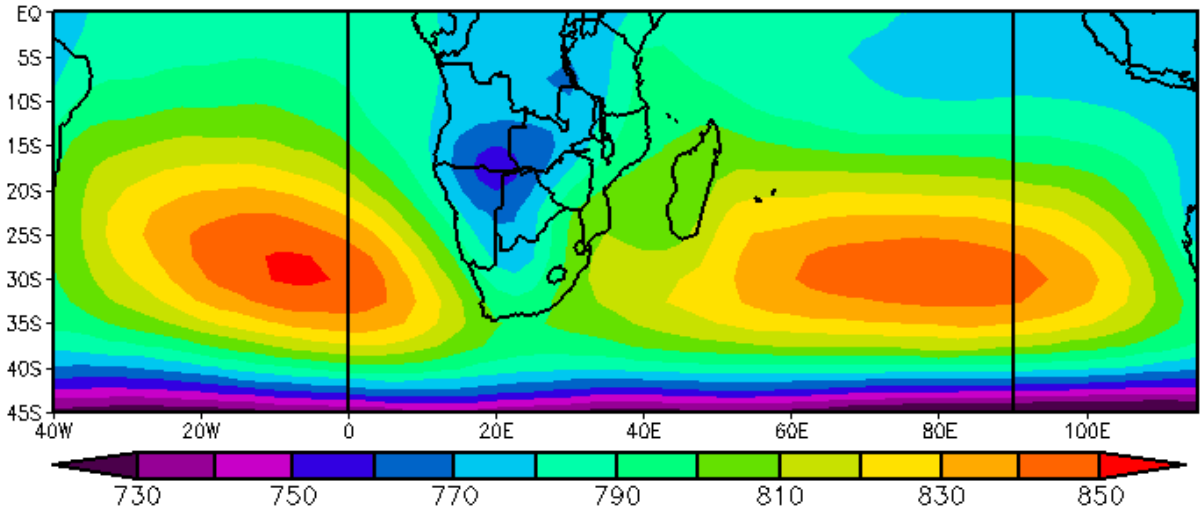

Figure 5.1: *Geopotential height (m) at 850 hPa averaged during Oct-Dec of 1979-2010. The St Helena High, Angola Low and Mascarene High are shown on the left, middle and right side respectively.*

5.2. Data and Methods

5.2.1. Data

We analyze the atmospheric observed and reanalysis data sets in the post-satellite era during 1979-2010. We focus on the Oct-Dec period, because it is associated with the maximum ozone hole and the SAM impact in the stratosphere and surface (Gillett and Thompson 2003;

Thompson et al., 2011) respectively. The total ozone column to represent the ozone hole is derived from the Nimbus-7 Total Ozone Mapping Spectrometer (TOMS version 7) from the National Aeronautics and Space Administration (NASA) Goddard Space Flight Center (GSFC). SAT over southern Africa is extracted from the Global Historical Climate Network (GHCN) data set for the same analysis period. The SAT dataset is constructed from a variety of sources for the GHCN project (Peterson et al., 1998). More details of this dataset are provided in Fan and van den Dool (2008). The data set has been successfully used to analyze surface temperature changes in East Africa (Christy et al., 2009). The NCEP/NCAR reanalysis data (Kalnay et al., 1996) are used to explain the related SAT variations.

5.2.2. Indices

The SAM is coupled to the stratospheric circulation only during a 6-8 week interval centered in November (Thompson and Wallace, 2000). Because of this shorter duration compared to the Arctic Oscillation (three months), statistics related to SAM are subjected to larger sampling variability. In order to reduce the uncertainties, we averaged the data over the Oct-Dec season. In addition, we selected for use the NOAA SAM index which is based on both station data and satellite data. NOAA index data from 1979 to present can be accessed from http://www.cpc.ncep.noaa.gov/. The characteristic of the annually measured total stratospheric ozone column translates into the ozone hole area (million km^2) from where the ozone index is created. The SAT time series and hence its index is constructed from area-averaged value in the box region (12ºE-30ºE and 10ºS-24ºS; Figure 2b).

In the analysis, we use the 850-hPa geopotential height rather than the sea level pressure to partially alleviate the ambiguities introduced by the reduction to sea level over the predominantly

high terrain of southern Africa. The atmospheric circulation analysis was also performed at 850 hPa. In order to remove the linear influence of greenhouse gas-induced global warming, we detrended the data before doing any statistical operation. We employ the empirical orthogonal function (EOF) analysis on the SAT data to identify the dominant variability and the associated spatial homogeneity. The algorithm for this EOF analysis is provided by the Climate Explorer website (http://climexp.knmi.nl/). Pearson correlation method is used to explain linear relationships between the ozone hole and atmospheric parameters. A two-sided studentôs t-significant test as $t = r\sqrt{(n-2)/(1-r^2)}$ and n=31, is used to calculate the statistical significance of the results. The climatic time series used in this study consist of 3-monthly (Oct-Dec) values per year. As expected, no robust autocorrelation on time series is found. Therefore we considered the impact of autocorrelation of the time series in significant t-test hypothesis testing as unimportant. To facilitate comparison among different variables, we normalized all the indices such that each one has unit in standard deviations, and hence are dimensionless.

5.3. Results

Figure 5.2a illustrates the mean SAT over southern Africa during October-December. Interestingly, it reveals maximum values coinciding in location with the AL. The robustness of the coincidence in geographical position is boosted by the observation that SAT and AL is derived from independent datasets (GHCN and NCEP/NCAR). South Africa experiences considerably lower SAT than the rest of the region because of the mid-latitude weather systemsô encroachment (Tyson and Preston-Whyte, 2000). Also, there exists a belt of cooler temperatures stretching along the west coast from South Africa to Namibia, a result of the influence of the cold Benguela Current. In order to characterize the dominant SAT variability, we apply the EOF

analysis to the SAT over southern Africa. The first EOF mode explains about 27.1% of the total variances and represents a spatially uniform polarity of loadings in the tropical regions, especially north of 25ºS (Figure 5.2b). Once more we note that the highest values correspond to the location of the core of the AL. Figure 5.2c shows the correlation between the time series of the principal component of this mode and the geopotential height at 850 hPa. The SAT is negatively correlated with the AL, but positively correlated with the western flank of the MH and the Antarctic region (10ºE-130ºE; 70ºS-90ºS). This provides some insight into a possible link between southern Africa and the Antarctic region.

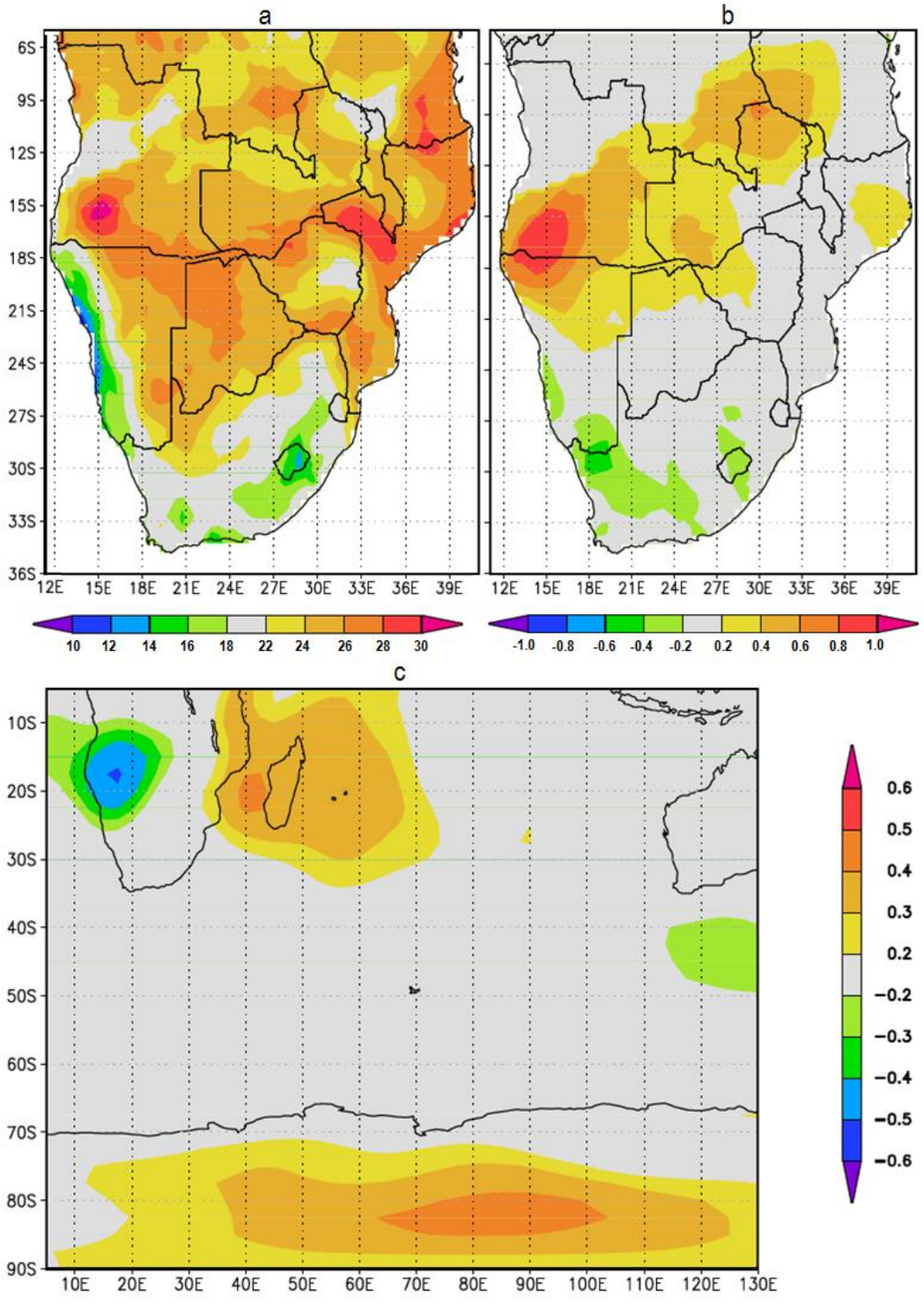

Figure 5.2: Spatial pattern maps during Oct-Dec of 1979-2010. The maps are for (a) the mean SAT (ºC), (b) SAT PC1 and (c) the correlation coefficient between the SAT PC1 and geopotential height at 850 hPa. Correlation coefficient above 0.3 is significant at 90% confidence level using a two-tailed Student's t-test. The red box indicates the region where the SAT index is calculated.

It is important to note the nature of the ozone hole over the recent decades. Although the ozone hole significantly expands from 1979, its growth rate gradually decelerates after the mid-1990s and becomes stable in the 2000s (Figure 5.3b). From 1993, the total ozone column loss exceeds 50% of its previous averaged size and its physical size expands to reach its record in 2006. Several studies discussed this significant change in the ozone hole characteristics relative to the mid-1990s (Sexton 2001; Shindell and Schmidt 2004). However, there is an isolated case in the post-1992 period when the ozone hole size suddenly decreases by almost 50% in 2002. The ozone assessment report (WMO, 2003) by the World Meteorological Organisation explained this anomaly as a result of an upward flux of planetary wave energy in the Antarctic tropospheric layer in September. This triggered a complex set of reactions, which eventually undermined the strong polar vortex, resulting in the suppressed values observed in 2002. Since the ozone hole gradually shrinks from around 1993, we will discuss the two periods before and after 1993 and refer to them as pre-large ozone hole era (pre-LOHE) and large ozone hole era (LOHE) respectively.

To characterize the dominant SAT variability over southern Africa, we define SAT index as an average SAT over the AL region (red box in Figure 5.2b). This SAT index is highly correlated with the SAT PC1 index at 0.95 (Figure 5.3a). Before the early 1990s, the SAT index mostly exhibits negative values, but reverted to positive anomalies after 1992, then become weak negative values after 2006. The difference between the two means relative to pre-LOHE and LOHE for both time series is significant ($p < 0.001$), implying that there is a noteworthy shift to a warmer state in the region during LOHE. The correlation coefficients depicted in Figures 5.3b and 5.3c are significant with values of -0.64 and 0.72 respectively. In these figures we

demonstrate how the ozone hole index anomaly amplitudes are robustly related to those of corresponding AL and SAT indices including the close similarities between their general temporal evolutions. These amplitudes were principally negative during the pre-LOHE period but become predominantly positive thereafter. Figure 5.3b reveal that as much as 80% of the corresponding amplitudes do not coincide while 84% in Figure 5.3c coincide in direction respectively. However, for stronger amplitudes of ozone hole index (> 0.4 σ), the opposite signs in Figure 5.3b improved to 86% while unidirectional amplitudes in Figure 5.3c escalated to 91%. This analysis substantiates the existence of possible coupling between ozone hole and the southern African climate, which is stronger with SAT. With stable relationships, these high figures entail that ozone hole may have the potential to be used as a predictor for not only the seasonal SAT magnitudes/anomalies but for the general seasonal strength of the AL as well. In the Northern Hemisphere, a predictive scheme with a reasonable skill was developed where similar large amplitude anomalies in the strength of the wintertime stratospheric polar vortex frequently precede correspondingly signed anomalies in the lower troposphere (Baldwin and Dunkerton, 1999).

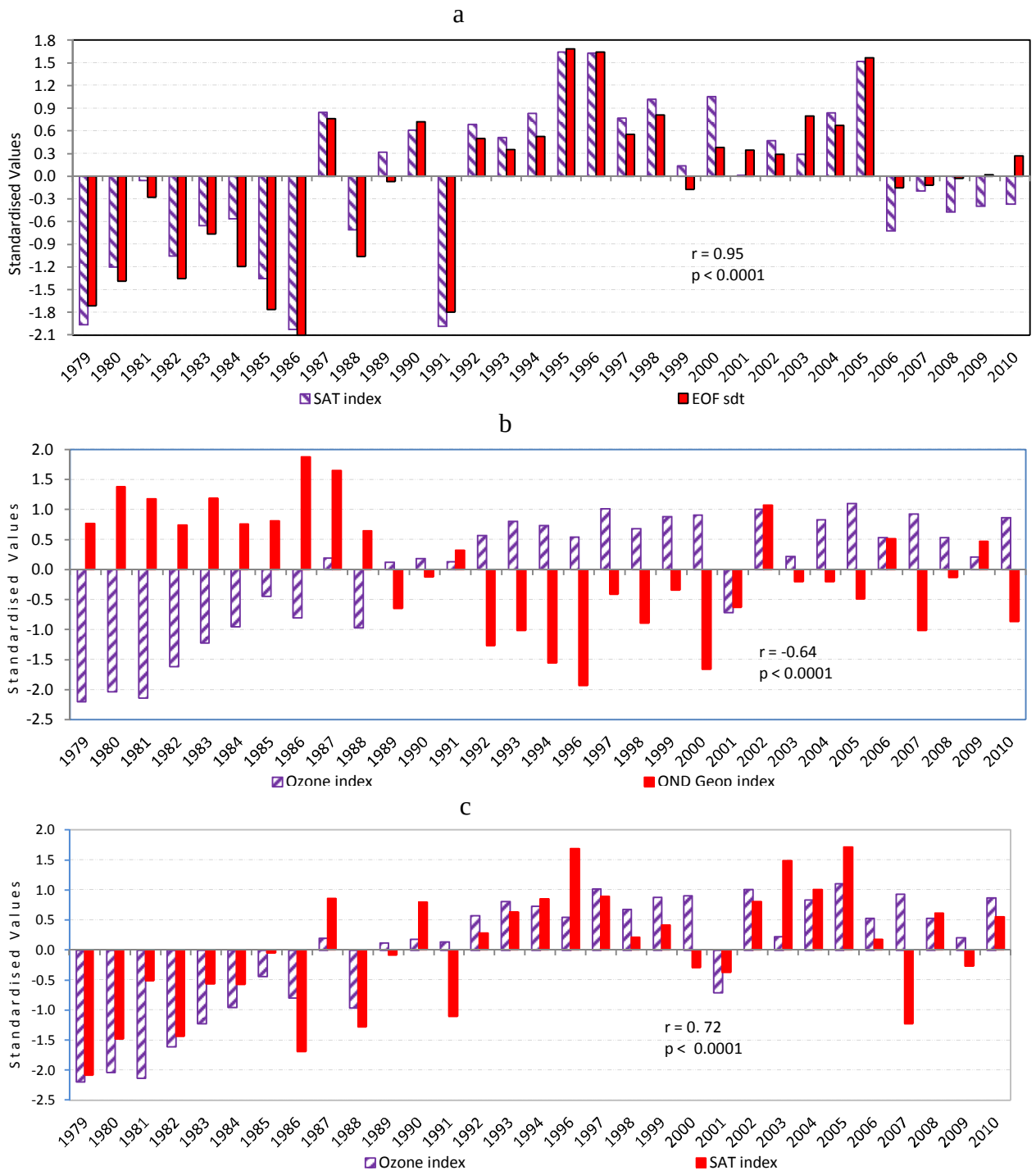

Figure 5.3: Time series during Oct-Dec of 1979-2010. The pairs of time series are for *(a) the SAT index (checked) and the SAT PC1 (solid), (b) ozone (checked) and the Angola Low (solid) indices, and (c) ozone (checked) and the SAT (solid) indices during Oct-Dec of 1979-2010. The indices are normalized with their standard deviations. Note that due to unavailability of ozone data during 1995, this year is omitted from the analysis. In the insert r and p represent the correlation coefficient and probability values respectively.*

In Figure 5.4a, we demonstrate that the ozone hole is significantly inversely connected to the AL while positively linked to an anticyclonic system to the south western part of Madagascar. Thus in accordance with the ozone hole variability, the AL deepens while the anticyclonic system intensifies and vice versa. In either case, an exchange of airflow from different meridional locations is enhanced which facilitates advection of different SAT anomalies between the two systems. The spatial distribution of the mean differences in the geopotential at 850 hPa (Figure 5.4b) reveals that the AL has substantially strengthened, coinciding with the negative geopotential anomalies extending well into the Atlantic Ocean following the west coast and spreading southwards to cover the southern part of South Africa. It is clear that this extended pattern of negative geopotential anomalies is a result of the westward displacement of the SHH. The cyclonic circulation anomalies that cover most of southern Africa resulting from the stronger AL are shown in Figure 5.4c. This figure also demonstrates that the anomaly winds from the eastern flank of the SHH veer cyclonically towards the AL in the ocean between 15ºS and 5ºS. This is coupled to the recurved warm northerly wind anomalies belonging to the offshore western flank of the AL. The result is a significant rise in the sea surface height and deepening of the thermocline shown in Figures 5.4e and f respectively, implying the weakening and warming of the northern extension of the Benguela Current during LOHE. Since this region coincides with what appears like a ǿprotruding AL tailô into the Atlantic Ocean, of significant correlation coefficients (Figure 5.4a), the ozone hole could also be connected to the northern extension of the Benguela Current. The steepened gradient created between the intensified MH and AL may have enhanced the northerly wind anomalies resulting in the significant mean difference in SAT that we see in Figure 5.4d.

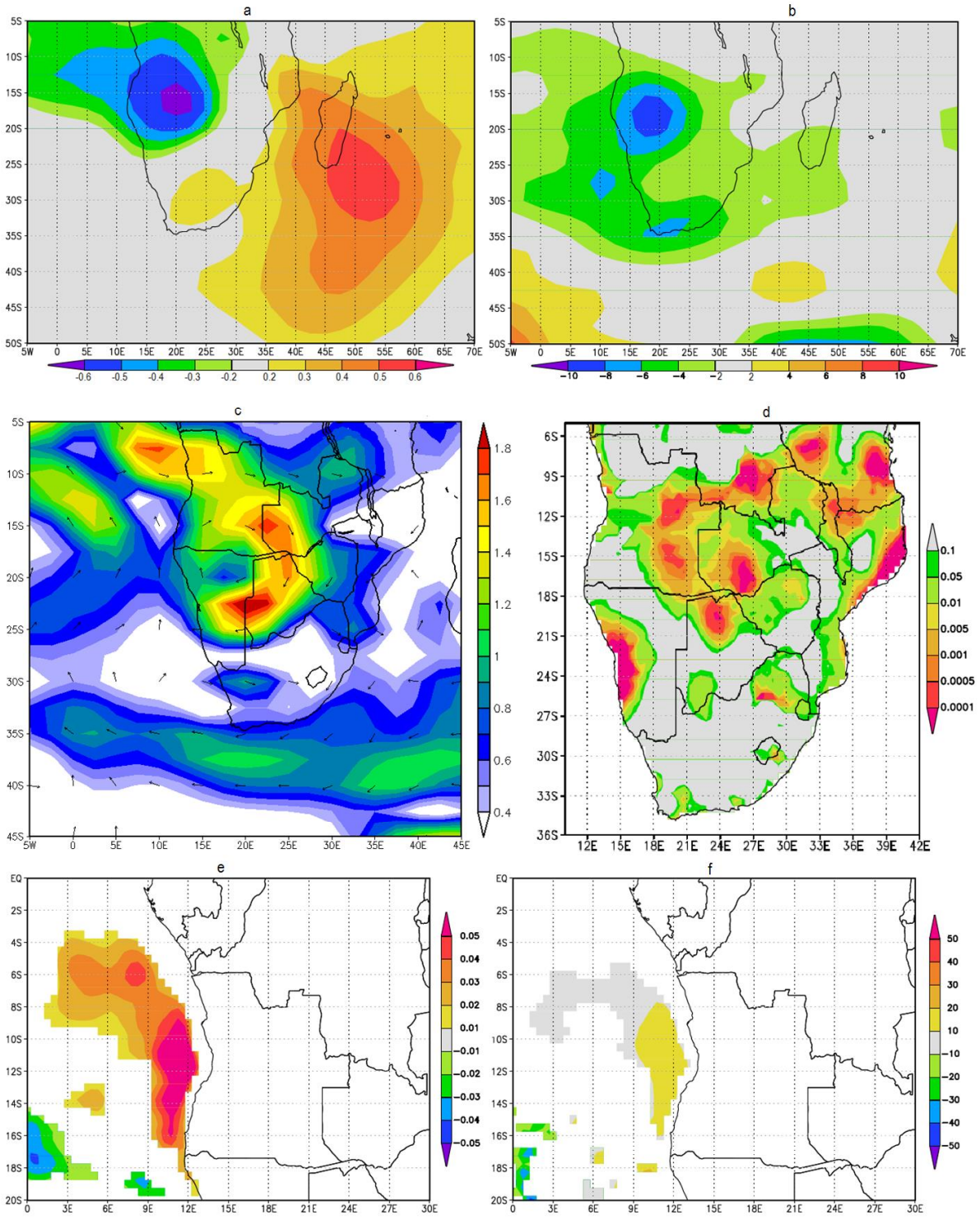

Figure 5.4: Correlation coefficient and mean difference maps. (a) Correlation coefficient between the ozone index and geopotential height at 850 hPa during Oct-Dec of 1979-2010. Differences in, (b) geopotential height (m) at 850 hPa, (c) wind vectors (m s^{-1}), at 850 hPa, (d) the SAT (ºC), (e) sea surface height (m) and (f) Z_{20} thermocline depth (m), between the LOHE and pre-LOHE. Values larger than (a) 0.3, (b) 6 m, (c) 0.8 ms^{-1} and the area shaded in (e) and (f) are significant above the 90% confidence level using a two tailed Student's t-test.

SAM and ozone hole appear separable in their impact on SAT, as no robust connections were realized when SAM was correlated to the spatial fields of SAT and the geopotential at 850hPa height. Nevertheless, it has to be noted that both SAM and SAT were driven towards positive polarity around 1993 and that a ten year running correlation applied on SAM and the ozone hole indices display significant correlation only after 1993. However, on analyzing the correlations between the SAT and SAM with regard to the pre-LOHE and LOHE the association became 0.52 ($p = 0.05$) and -0.36 ($p = 0.17$) respectively. This demonstrated that the relationship was relatively strong in the earlier epoch but became rather weak and reversed thereafter. These seemingly controversial correlation results are explained by the reversal in the regional mean meridional circulation in which warm and cold SAT are advected by northerly and southerly winds respectively (Figure 5.5a). Therefore the negative phase of SAM during pre-LOHE was associated with cooling of SAT. In a similar but opposite manner, the anomalously strong northerlies maintain the observed above-normal SAT coinciding with the migration to the high index state of SAM (Marshall 2003; Saxton 2001) during LOHE. In a similar research, Ozone/SAM related circulation patterns outside the Antarctic region, steered meridional wind anomalies that led to transportation of significant amounts of mineral dust from the lower latitudes (Cataldo et al., 2013).

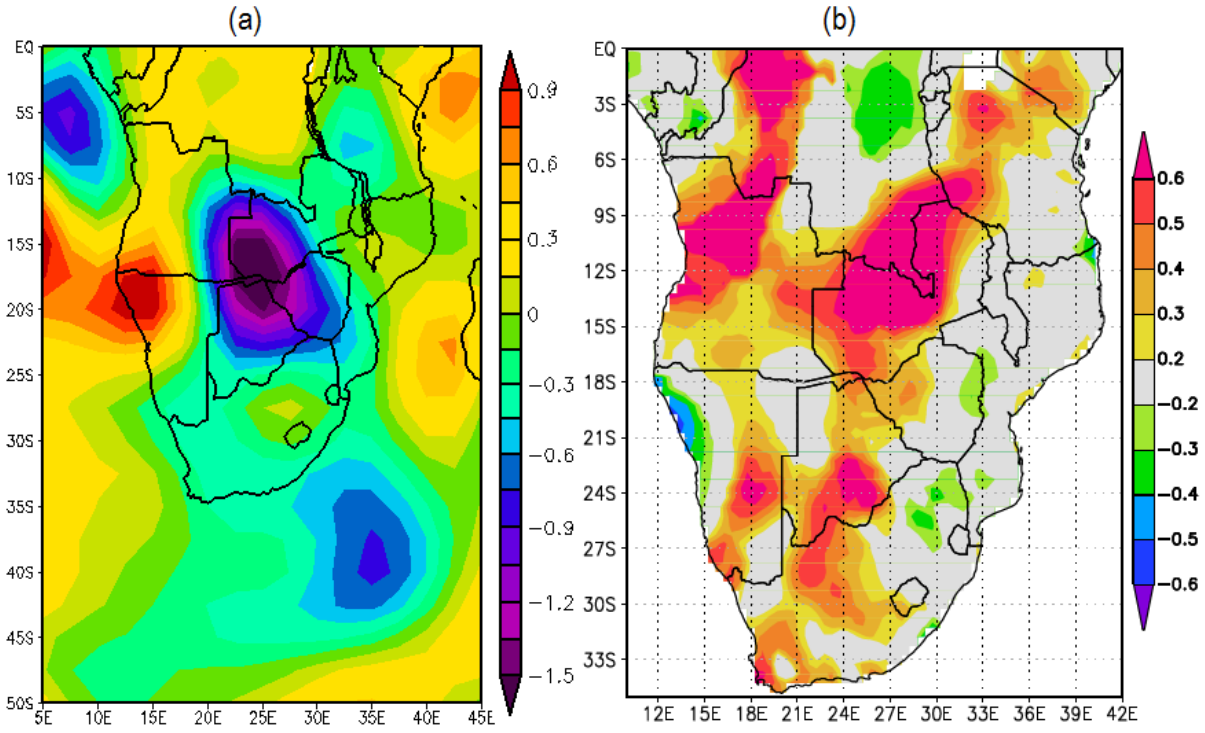

Figure 5.5: Maps for the mean difference in meridional winds and the spatial distribution of correlation coefficients. (a) Difference in the meridional winds (m s^{-1}) between the LOHE and pre-LOHE. (b) Correlation coefficient between the SAM index and the SAT during Oct-Dec of 1979-2010. Values larger than (a) 0.4 (m s^{-1}) and (b) 0.3 are significant above the 90% confidence level using a two tailed Student's t-test.

5.4. Summary and Conclusions

Although greenhouse gases and associated changes in radiative forcing are uniform over the much of southern Africa (Joubert and Kohler, 1996), the changes we have seen in SAT are related to the dynamical alterations in the atmospheric circulation most probably induced by the ozone hole. However, the significance in linear correlation that we have demonstrated does not necessarily imply that the ozone hole is driving the observed variance in the AL and SAT, but it does identify possible connections between them. Nevertheless, the robustness of the relationship between SAT and ozone revealed in this study may lead to possible SAT predictability associated with the knowledge of stratospheric ozone anomalies. In fact, if the positive SAM

trend continues into the future (Polvani et al., 2011) the relationships may have negative climate change implications for the future climate of southern Africa. Fortunately enough, several studies concur that the ozone amount over Antarctica might restore to its level of the 1980s (Newman et al., 2006; Purich and Son, 2012) and the ozone hole may disappear after 2050 ((Newman et al., 2006) since the release of ozone-depleting gases such as chlorofluorocarbons have been reduced under the Montreal Protocol. This suggests that, as the ozone hole closes up (Newman et al., 2006; Purich and Son, 2012) accompanied by a return to negative polarity during austral summer, the AL may weaken and concurrently influence the reduction of regional SAT in the near future. Modeling studies become essential in this regard. In any case, it is intriguing to note that the paramount SAT trends over southern Africa can possibly be traced to recent changes in the lower stratospheric polar vortex, which are predominantly due to photochemical ozone losses (Thompson and Solomon, 2002; Cataldo et al., 2013).

CHAPTER VI

SUMMARY AND CONCLUSIONS

Using observations and reanalysis data, we have explored the decadal shifts which occurred from the last century and how they are linked to the climate of east and southern Africa. The focus of this study is to characterize the discontinuities in the IO basinôs system and document the possible role of the MH during the shifts on the rainfall and surface air temperature of East and southern Africa respectively. The results are explicit in the demonstration of the MHôs movements and its involvement in the transformations of the IOD which resulted in the low frequency modulation of the rainfall of East Africa. The MH displacements due to SAMôs related shift to positive polarity that coincided with the stratospheric ozone holeôs development in the mid-1990s is also implicated in the abrupt warming of surface air temperature of southern Africa.

The thesis particularly demonstrated the IOD epoch dependent decadal amplitude and phase variations that are separated by three major climate shifts in the Indian Ocean occurring around 1918, 1961 and 1997. Each shift is preceded by a three year sequence of IOD events that are unique in the entire time series. The order is such that a relatively moderate negative SST anomaly gradient intensifies to an extreme negative IOD event which then reverses in the shift year to an extreme positive event. The last two extreme IOD events reach record breaking magnitudes during each shift from the beginning of the twentieth century implying intensification of the shift process with time in this period. The IOD shifts also characterize shifts in phase modulation such that during the 1880ï1917 epoch, negative IOD events dominate. In

the subsequent epochs, the negative events gradually diminish in number at the expense the positive events at each succeeding epoch until eventually the frequency of the positive events dominate in the last epoch from 1998 to 2010. This systematic but abrupt change in the mean frequency of the positive and negative IOD events has been established through sudden change in skewness and variance of the DMI at each shift point. On the other hand, the MH seems to also participate in the shift process. During the year before the shift, the MH is anomalously displaced poleward and westward but coinciding with the negative IOD event. The high intensifies while moving equatorward during the shift years thereby possibly amplifying the coinciding positive IOD event through enhancing upwelling over the eastern pole of the mode. It then follows that the maximum contrast of the south Indian Ocean pressure pattern and hence the intensity of the MH, from one year to the other is achieved during the shift years. The intensity of this process has also been escalating during each of the three successive shifts.

These three shifts are not only found in the IOD time series but are identified in the rainfall characteristics over East Africa. However the coupling between the IOD and the rainfall of East Africa seem to have become robust and rather abrupt in 1961 with a further sudden increase also from 1997. It is noted through the temporal distribution of the EAR event classes determined by the SPI technique, that the EASR has intensified significantly from the turn of the twentieth century with more floods and droughts occurring in the recent decades. This increase towards more extreme rainfall events has not been gradual but is strongly characterized by epochs which were dictated by shifts in the Indian Ocean Dipole (IOD) mode. These shifts occurred during 1961 and 1997. The shifts were also quite prominent in the NCEP-NCAR wind data from the western pole of the IOD mode. The periods around 1961 and 1997 have already been confirmed

as real shifts to have occurred in the IO using the IOD time series (Manatsa et al., 2012), coral records (Nakamura et al., 2009) and stable isotopes (Vuille et al., 2005). Thus unlike the previous studies that assumed linear impacts of the IOD on the region we note that the impacts are epoch dependent. This is mainly due to the observation that the coupling strength between the IOD and EEAR climate modes does not only portray an increasing trend, but seems to be heavily involved in the definition of the shifts.

The rainfall variability is more related to the epochal increase in variability of the eastern pole of the IOD than to the western pole implying that there is a process taking place in the eastern pole that is enhancing the variability of the rainfall. I attributed this to the epochal eastward shift of the MH which subsequently added a meridional wind anomaly component at each shift that is to take part in the upwelling of the eastern pole. This could have resulted in the observed epochal increase in positive IOD events. It is also revealed that the EAR variability is strongly linked to the MH zonal displacements, in particular the zonal movement of the MH eastern ridge. When the MH eastern ridge is anomalously displaced to the west (east) of its normal position, the SE trade winds over the SIO anomalously strengthen (weaken). This westward (eastward) migration of the eastern ridge helps advect relatively cooler and less moist low level airflow over East Africa which in turn suppresses (enhances) both regional convection and orographic rainfall. Thus the zonal migration of the MH eastern ridge provides a novel indication for the EASR extremes which has the propensity to resolve better the droughts than the surplus rainfall. This revelation has immense social application in the region of East Africa where rainfall extreme events have become more prevalent against the background of deteriorating drought forecasts

which are predominantly generated from traditional indicators like ENSO and the IOD. This is represented schematically in Figure 6.1.

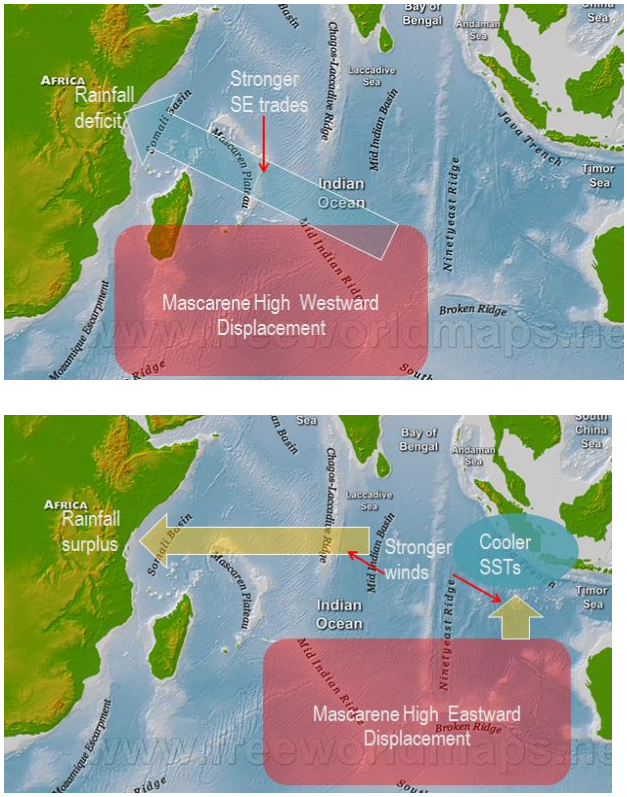

Figure 6.1: The westward (left panel) and eastward displacement (right panel) of the MH eastern ridge and the related rainfall anomalies.

But the observed epochal changes in IOD attributes such as its variance and its relationship with EASR appears in this work to be a system-wide phenomenon that is yet to be comprehensively understood. Furthermore, it is evident that such nonlinearities are difficult to reconcile with the suggested smooth evolution of anthropogenic forcing (e.g. Hansen et al., 2005). Hence we are more inclined to believe that the internal reorganization of the Indian Ocean climate system may underline such discontinuities. We take cognizance of the reported recent south Indian Ocean Subtropical High (Mascarene high) buildup (Allan et al., 1995) and its epochal eastward translation (Manatsa et al., 2011). This process should have correspondingly developed a

background mean state in the south Indian Ocean for each eastward epoch of more strengthened relatively cool and dry southeasterly winds that affect East Africa. The resulting background epochal state would in turn generate conditions more favourable for the formation of more extreme droughts at the expense of the development of floods.

With regard to the abrupt change in SAT over southern Africa, we also note that the displacement of the MH and the SHH southwards and away from the mainland also led to the deepening of the Angola Low. As a result warm air was advected from the lower latitudes towards the low, thereby warming southern Africa. This process coincided with the change to positive polarity in SAM which could have been influenced by the development of the stratospheric ozone hole in the mid-1990s. The events leading to the abrupt significant warming of SAT over southern Africa are illustrated in the schematic diagram in Figure 6.2.

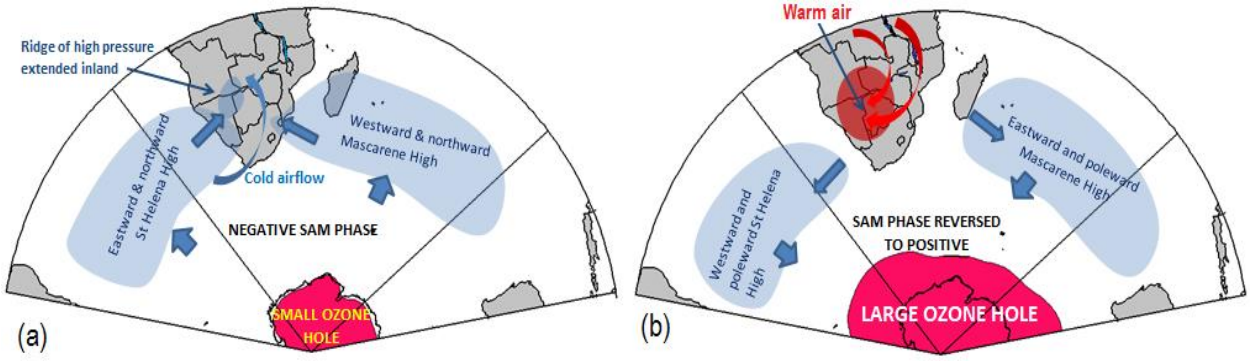

Figure 6.2: Schematic diagram showing the state before the development of the large ozone hole of 1993 (a) and (b) after

However, this epochal variation or apparent nonstationary nature in the IOD ï EAR and Ozone hole- SAT relationship is novel and has rarely been considered by recent researchers. Yet epochal shifts if not recognized timely, can undermine statistical prediction schemes that are based on stationarity relationships in historical data. This study revealed that EAR variability

was relatively constrained in the earlier decades when the IO SSTs were cooler but increased significantly in the recent decades as the SSTs warmed considerably. These findings support the notion of greater climate variability tending to develop in warmer climate states. This inference fits the growing consensus that the current global warming will eventually increase the frequency of extreme rainfall events. On the other hand the relationship of the ozone hole development and warming over southern Africa is detached from global warming that is mostly attributed to carbon dioxide emissions. It is likely that the low frequency modulations of the SAM from anthropogenic causes could be responsible for the changing climate of both East and southern Africa. In any case irrespective of the causes, climate change impacts will bring further environmental stress to the region of East and southern Africa which already has a reduced capacity to adapt to the mounting adverse effects of the current smaller scale climate variability. Given the promising nature of my results, it is imperative that the earthôs climate system research community embraces this nonlinear paradigm if we are to move forward in the assessment of regional climate modulations under the anthropogenic stress.

References

Abram N J, Gagan M K, McCulloch M T, Wahyoe J C, and Hantoro S (2003); Coral Reef Death during the 1997 Indian Ocean Dipole linked to Indonesian Wild res; *Science* 301952 doi:10.1126/science.1083841.

Abram, N.J., M.K. Gagan, J.E. Cole, W.S. Hantoro, and M. Mudelsee (2008); Recent intensification of tropical climate variability in the Indian Ocean. *Nature Geoscience*, **12**, 849-853, doi:10.1038/ngeo357.

Adler RF, Huffman GJ, Chang A, Ferraro R, Xie P, Janowiak J, Rudolf B, Schneider U, Curtis S, Bolvin D, Gruber A, Susskind J, Arkin P (2003); The Version 2 Global Precipitation Climatology Project (GPCP) Monthly Precipitation Analysis (1979-Present). J. Hydrometeor., **4,** 1147-1167.

Agnew, C.T. (1999); Using the SPI to identify drought. *Drought Network News* **12**, 6ï 12

Allan RJ, Reason CJC, Lindesay JA, Ansell TJ. (2003); Protracted ENSO episodes and their impacts in the Indian Ocean region, *Deep Sea Res., Part II*, **50**: 2331ï 2347.

Alley RB, Clark PU, Kelwin LD, Webb RS (1999); Making Sense of Millennium Scale Climate Change. *Amer. Geophys. Union Geophys Monogr* 112: 385-394.

Andrew G. Marshall; Debra Hudson; Matthew C. Wheeler; Harry H. Hendon; Oscar Alves (2011); Simulation and prediction of the Southern Annular Mode and its influence on Australian intra-seasonal climate in POAMA Simulation and prediction of the Southern Annular Mode and its influence on Australian intra-seasonal climate in POAMA. *Clim Dyn* (2012) 38:2483ï 2502 DOI 10.1007/s00382-011-1140-z

Annamalai, H., S.P. Xie, J.P. McCreary, and R. Murtugudde (2005); Impact of Indian Ocean sea surface temperature on developing El Nino. *J. Climate*, **18**, 302ï 319.

Anyamba EK, Ogallo LJ (1985); Anomalies in the wind field over East Africa during the east African rainy season of 1983/1984: proceedings of the first WMO workshop on diagnosis and prediction of monthly and seasonal atmospheric variations over the globe, Long-range forecasting research report seriesno.6 v1 WMO/TD. No. 87, pp 128-133.

Arblaster, J. M., Meehl, G. A. & Karly, D.J. (2001); Future climate change in the Southern Hemisphere: Competing effects of ozone and greenhouse gases. *Geophys. Res. Lett*. **38**, L02701.

Ashok K, Chan W, Motoi T, Yamagata T. (2004); Decadal variability of the Indian Ocean Dipole. Geophysical Research Letters 31, L19306, doi:10.1029/2004GL020842

Ashok K, Guan Z, Yamagata T. (2003); Influence of the Indian Ocean Dipole on Australian winter rainfall. *Geophysical Research Letters* 30(15): 1821, Doi: 10.1029/2003GL0179 26.

Baldwin, M. P. & Dunkerton, T. J. (1999); Propagation of the Arctic Oscillation from the stratosphere to the troposphere. *J. Geophys. Res*. **104**,30937.

Basnett T, Parker D (1997); 'Development of the Global Mean Sea Level Pressure Data Set GMSLP2', Climate Research Technical Note, 79, Hadley Centre, Met Office, FitzRoy Rd, Exeter, Devon, EX1 3PB, UK

Behera SK, Luo JJ, Masson S, Delecluse P, Gualdi S, Navarra A, Yamagata T (2005); Paramount Impact of the Indian Ocean Dipole on the East Africa Short Rains: A CGCM Study. *J. Climate,* **18**, 4514-4530.

Behera SK, Yamagata T. (2001); Subtropical SST dipole events in the southern Indian Ocean, *Geophysical Research Letters* **28**: 327ï 330.

Black E, Slingo J, Sperber KR. (2003); An observational study of the relationship between excessively strong short rains in coastal east Africa and Indian Ocean SST. *Monthly Weather Review* **131**: 74-94.

Boccaletti S, Kurths J, Osipov G, Valladares DJ, Zhou CS (2002); The synchronization of Chaotic systems. Physics Rep 366: 1-101.

Breaker L.C. (2007); A closer look at regime shifts based on coastal observations along the eastern boundary of the North Pacific. *Cont. Shelf Res.* **27**, *2250–2277.* doi:10.1016/j.csr.2007.05.018

Cai, W, Sullivan A, Cowan T (2009); Climate change contributes to more frequent consecutive positive Indian Ocean Dipole events. *Geophys Res Lett* 36, L23704, doi:10.1029/ 2009GL040163.

Cai, W, Sullivan A, Cowan T, Ribbe J, Shi G (2011); Simulation of the Indian Ocean Dipole: A relevant criterion for selecting models for climate projections, *Geophys Res Lett* 38 L03704, doi:10.1029/2010GL046242.

Cataldo. M. et al. (2013); Mineral dust variability in central West Antarctica associated with ozone depletion. *Atmos. Chem. Phys.* **13**, 2165-2175.

Christy, J.R., Norris, W.B., McNider, R.T. (2009); Surface Temperature Variations in East Africa and Possible Causes. *J. Clim*, **22,** 3342ï 3356.

Clark CO, Cole JE, Webster PJ. (2000); Indian Ocean SST and Indian summer rainfall; predictive relationships and their decadal variability. Journal of Climate **13**: 2503-2519.

Clark CO, Webster PJ, Cole JE (2003); Interdecadal variability of the relationship between the Indian Ocean zonal mode and East African coastal rainfall anomalies*, J Climate* 16: 548ï 554.

Conway, D., E. Allison, R. Felstead, M. Goulden (2005); Rainfall variability in East Africa: implications for natural resources management and livelihoods. *Phil. Trans. Roy. Soc*. A **363**, 49ï 54 doi:10.1098/rsta.2004.1475

Cook KH. (1998); On the response of the Southern Hemisphere to ENSO. *Proc. 23rd Climate Diagnostics and Prediction Workshop,* Miami, FL, American Meteorological Society 323ï 326.

DôAbreton PC, Tyson PD. (1995); Divergent and non-divergent water vapour transport over southern Africa during wet and dry conditions. *Meteorology and Atmospheric Physics* **55**:47ï 59.

Dionne, G., P. Francois, and O. Maalaoui (2009); Detecting Regime Shifts in Corporate Credit Spreads ; Cahiers du CIRPÉE;09-29; https://depot.erudit.org/id/003093dd

Edwards, D.C., and T.B. McKee (19970); Characteristics of 20th century drought in the United States at multiple timescales. Climatology Report No. 97ï 2. Colorado State University, Fort Collins

England, M., C. C. Ummenhofer, and A. Santoso (2006); Interannual rainfall extremes over southwest western Australia linked to Indian Ocean climate variability. *J. Climate*, 19, 1948ï 1969.

Fan, Y. & van den Dool, H. (2008); A global monthly land surface air temperature analysis for 1948ï present, *J. Geophys. Res*., **113**, D01103, doi:10.1029/2007JD008470.

Fauchereau N, Pohl B, Reason CJC, Rouault M, Richard Y. (2009); Recurrent daily OLR patterns in the Southern Africa/Southwest Indian Ocean region, implications for South African rainfall and teleconnections *Climate Dynamics*. **32**:575ï 591 DOI 10.1007/s00382-008-0426-2.

Figura, S., D.M. Livingstone, E. Hoehn, and R. Kipfer (2011); Regime shift in groundwater temperature triggered by the Arctic Oscillation, *Geophys. Res. Lett.*, **38**, L23401, doi:10.1029/2011GL049749.

Folland CK, Karl TR, Christy JR, Clarke RA, Gruza GV, Jouzel J, Mann ME, Oerlemans J, Salinger MJ, Wang SW. (2001); Observed Climate Variability and Change, in Climate Change: The Scientific Basis, edited by J. T. Houghton *et al.*, 99ï 181, Cambridge Univ. Press, New York.

Garzoli, S. L. & Gordon, A. L. (1996); Origins and variability of the Benguela Current. *J. Geophys. Res*. **101**, 897ï 906.

Gill AE. (1982); *Atmosphere-Ocean Dynamics.* New York: Academic Press, 662 pp.

Gillet, N.P., Kell, P.D. & Jones, P.D. (2006); Regional climate impacts of the Southern Annular Mode. *Geophys. Res. Lett*. **33**, L23704.

Gillett, N. P. & Thompson, D. W. J. (2003); Simulation of recent southern hemisphere climate changes. *Science*, **302**, 273ï 275.

Goddard, L. and N.E. Graham (1999); The importance of the Indian Ocean for GCM based climate forecasts over eastern and southern interior of Southern Africa. *J. Geophys. Res*., **104**: 19099ï 19116.

Gualdi, S, Guilyardi E, Navarra A, Masina S, Delecluse P (2003); The interannual variability in the tropical Indian Ocean as simulated by a CGCM. Climate Dyn 10: 567ï 582.

Hansen J et al. (2005); Earth's energy imbalance. Confirmation and implications *Sc* doi:10.1126/science. 1110252.

Hartmann, D.L., et al. (2000); Can ozone depletion and global warming interact to produce rapid climate change? *Proc. Natl. Acad. Sci. U.S.A*., **97,** 1412ï 1417.

Hastenrath S, Polzin D, Camberlin P (2004); Exploring the predictability of the ósho rt rainsô at the coast of East Africa. *Int. J. Climatol*., 24, 1333ï 1343.

Hastenrath S, Polzin D, Mutai C (2007); Diagnosing the 2005 drought in equatorial East Africa. *J. Climate*, 20, 4628ï 4637.

Hastenrath S, Polzin D, Mutai C (2010); Diagnosing the Droughts and Floods in Equatorial East Africa during Boreal Autumn 2005-08. *J. Climate, 23*, 813ï 817. doi:10.1175/2009 JCL3094.1

Hastenrath S, Polzin D, Mutai C (2011); Circulation Mechanisms of Kenya Rainfall Anomalies. J. Climate, **24**, 404ï 412. doi: 10.1175/2010JCLI3599.1

Hastenrath, S., (2007); Circulation mechanisms of climate anomalies in East Africa and the equatorial Indian Ocean. *Dyn. Atmos. Oceans*, **43**, 25ï 35.

Haylock MR, Jones PD, Allan RJ, Ansell TJ. (2007); Decadal changes in 1870ï 2004 Northern Hemisphere winter sea level pressure variability and its relationship with surface temperature, *Journal of Geophysical Research*, *112*, D11103, doi: 10.1029/ 2006 JD007291.

Hines KM, Bromwich DH, Marshall GJ (2000); Artificial Surface Pressure Trends in the NCEPï NCAR Reanalysis over the Southern Ocean and Antarctica. *J. Climate*, **13**, 3940ï 3952.

Hoerling, M. P., Hurrell, J. W., Xu, T., Bates, G. T., & Phillips, A. S. (2004); Twentieth century North Atlantic climate change. Part II: Understanding the effect of Indian Ocean warming. *Climate Dynamics*, *23*, 391-405.

Hong, C.C., T. Li, J.S. Lin Ho Kug (2008); Asymmetry of the Indian Ocean Dipole. Part I: observational analysis. *J. Climate,* **21,** 4834ï 4848

Huang B, Shukla J (2008); Influence of the Mascarene High and Australian High on the summer monsoon in East Asia. *Indian Journal of Marine Sciences* **37,** 13-34.

Huang B, Xue Y, Behringer DM (2008); Impacts of Argo salinity in NCEP Global Ocean Data Assimilation System: The tropical Indian Ocean. J Geophys Res 113 C08002, doi: 10.1029/2007JC004388.

Huang, H.-P., R. Seager, and Y. Kushnir (2005); The 1976/77 transition in precipitation over the Americas and the influence of tropical SST, *Clim. Dyn.,* 24, 721 ï 740.

Ibanez F., J.M. Fromentin, J. Castel (1993); Application of the cumulated function to the processing of chronological data in oceanography. *C.R. Acad. Sci. III Vie,* 316*, 745*–748.

Ihara, Chie, Yochanan Kushnir, Mark A. Cane (2008); Warming Trend of the Indian Ocean SST and Indian Ocean Dipole from 1880 to 2004. *J. Climate,* **21**, 2035ï 2046. doi: http://dx.doi.org/10.1175/2007JCLI1945.1

Indeje M, Semazzi HFM, Ogallo IJ (2000); ENSO signals in East African rainfall seasons. Int J Climatol 20: 19-46.

IPCC (2001); Climate Change 2001: Impacts, Adaptation, and Vulnerability. Contribution of Working Group II to the Third Assessment Report of the Intergovernmental Panel on Climate Change, J.J. McCarthy, O.F. Canziani, N.A. Leary, D.J. Dokken and K.S. White, Eds., (Cambridge University Press, Cambridge, 1032 pp 2001).

IPCC (2007); Climate Change 2007: The Physical Science Basis. Contribution of Working Group I to the Fourth Assessment Report of the Intergovernmental Panel on Climate Change [Solomon, S., D. Qin, M. Manning, Z. Chen, M. Marquis, K.B. Averyt, M.Tignor and H.L. Miller (eds.)]. Cambridge University Press, Cambridge, United Kingdom and New York, NY, USA.

Janowiak JE. (1988); An investigation in interannual rainfall variability in Africa. *Journal of Climate* **1**: 240-255.

Janowiak, JE, Xie P. (1999); CAMS_OPI: A Global Satellite-Rain Gauge Merged Product for Real-Time Precipitation Monitoring Applications. *Journal of Climate* **12:** 3335-3342.

Jolliffe I.T (1986); Principal Component Analysis, New York: Springer-Verlag.

Jones PD, Hulme M. (1996); Calculating regional climatic time series for temperature and precipitation: Methods and illustrations. *International Journal of Climatology* **16:** 4: 361-377.

Joubert A.M. and Kohler M.O. (1996); Projected temperature increases over southern Africa due to increasing levels of greenhouse gases. *South African Journal of Science*. **92** Issue 11/12, p524.

Kalnay E, et al. (1996); The NCEP/NCAR 40-year reanalysis project, Bull. Amer. Meteor. Soc., **77**, 437 ï 471.

Kang, S.M. et al (2011); The impact of polar ozone depletion on subtropical precipitation. *Science* **332**, 951.

Kaplan A, Cane MA, Kushnir Y, Clement A, Blumenthal M, Rajagopalan B. (1998); Analyses of global sea surface temperature 1856-1991, *Journal of Geophysical Research* **103**, 18,567-18,589.

Kaplan D, Glass L (1995); Understanding Nonliner Dynamics, Springer-Verlag, New York.

Kaspar F, Cubasch U (2008) Simulation of East African precipitation patterns. *Meteorol.* 17(4), 511-517.

Kendall M (1980); Multivariate Analysis. (Second Edition). Charles Griffin and Co London. High Wycombe, U.K .

Kijazi A.L., C.J.C. Reason (2009); Analysis of the 1998 to 2005 drought over the northeastern highlands of Tanzania. *Climate Res.,* **38**:209-223

Kripalani R.H and Kumar P (2004); Northeast monsoon rainfall variability over south peninsular India vis-à-vis the Indian Ocean dipole mode. *International Journal of Climatology*. **24:**1267ï 1282.DOI: 10.1002/joc.1071.

Kripalani, RH, Kulkarni A. (2001); Mansoon rainfall variations and teleconnections over south and east Asia *International Journal of Climatology*. **21**: 603ï 616.

Kruger AC. (1999); The influence of the decadal scale variability of summer rainfall on the impact of El Nino and La Nina events of South Africa. *International Journal of Climatology*. **19**: 59-68.

Kumar KK, Rajagopalan B, Cane MA. (1999); On the weakening relationship between the Indian Monsoon and ENSO. *Science* **284**: 2156 ï 2159 DOI: 10.1126/science. 284.5423.2156.

Latif M, D. Dommenget, M. Dima, A. Grotzner (1999); The role of Indian Ocean sea surface temperature in forcing East African rainfall anomalies during Decemberï January 1997/98. *J. Climate* **12,** 3497ï 3504.

Li W, Li L, Fu R, Deng Y, Wang H (2011); Changes to the North Atlantic Subtropical High and its role in the intensification of summer rainfall variability in the Southeastern United States. *J. Climate*, **24,** 1499-1506.

Li W, Li L, Ting M, Liu Y (2012); Intensification of Northern Hemisphere subtropical highs in a warming climate. *Nature Geoscience*, 5, 830-834.

Lindesay J A. (1988); Southern Africa rainfall, the Southern Oscillation and a Southern Hemisphere semi-annual cycle. *Journal of Climatology* **8**:17-30.

Luo, J. J., B. S. K., Y. Masumoto, and H. Sakuma (2008); Successful prediction of the consecutive IOD in 2006 and 2007, *Geophys. Res. Lett*., 35, L14S02, doi: 10.1029/2007GL032793.

Ma, L., T. Zhang, O. W. Frauenfeld, B. Ye, D. Yang, *and* D. Qin *(*2009*);* Evaluation of precipitation from the ERA-interim, NCEP-1, and NCEP-2 Reanalyses and CMAP-1, CMAP-2, and GPCP-2 with ground-based measurements in China*, J. Geophys. Res*., 114, D09105, doi*:*10.1029/2008JD011178.

Manatsa D, Chingombe H, Matarira CH. (2008).The Impact of the positive Indian Ocean Dipole on Zimbabwe Droughts. *International Journal of Climatology*. DOI: 10.1002/joc.1695.

Manatsa D, Chingombe W, Matsikwa H, Matarira CH. (2007). The Superior Influence of the Darwin Sea Level pressure anomalies over ENSO as a simple drought predictor for southern Africa. *Theoretical and Applied Climatology.* DOI 10.1007/s00704-007-0315-3.

Manatsa D, Matarira CH (2009). Changing dependence of Zimbabwe rainfall variability on ENSO and the Indian Ocean dipole/zonal mode. *Theor Appl Climatol* doi 10:1007/s00704-009 -0114-0.

Manatsa D, Matarira CH, Mukwada G (2010); Relative Impact of ENSO and Indian Ocean Dipole/zonal mode on east SADC rainfall. Int. *J. Climatol,* **31**,558-577, doi: 10.1002/joc.2086.

Manatsa D, Reason CJC, Mukwada G (2011); On the decoupling of the IODZM from southern African rainfall variability. *Int J Climatol* doi: 10.1002/joc.2306.

Manatsa D., B. Chipindu and S. K. Behera (2012); Shifts in IOD and their Impacts on Association with East Africa Rainfall. *Theor Appl Climatol, doi*: 10.1007/s00704-012-0610-5.

Manatsa D. and SK Behera (2013). On the epochal strengthening in the relationship between rainfall of East Africa and IOD. *Journal of Climate*, Doi 10.1175/JCLI-D-12-00568.1.

Manatsa D, Y Morioka, SK Behera, CH Matarira, T Yamagata (2013) Impact of Mascarene High variability on the East African ósho rt rainsô *Climate Dynamics Journal*, DOI: 10.1007/s00382-013-1848-z

Manatsa D, Yushi Morioka, Swadhin K. Behera, Toshi Yamagata, Caxton H. Matarira (2013). Link between Antarctic Ozone depletion and summer warming over southern Africa. *Nature Geoscience Journal,* DOI 10.1038/ngeo1968.

Manatsa D and SK Behera (2013). On the major shifts in the IOD during the last Century, the role of the Mascarene High displacements (2013). *International Journal of Climatology, The Royal Meteorological Society* DOI: 10.1002/joc.3820.

Mapande A.T. and C.J.C. Reason (2005); Interannual rainfall variability over western Tanzania. *Int J Climatol,* **25**,1355ï 1368

Marchant R, Mumbi C, Behera S,Yamagata T (2006); The Indian Ocean dipole ï the unsung driver of climatic variability in East Africa. *African Journal of Ecology*. **45**, 4-16.

Marshall, G. J. (2003); Trends in the Southern Annular Mode from observations and reanalyses. *Journal of Climate*, **16**: 4134-4143.

Marshall, GJ, Harangozo (2000); An appraisal of NCEP/NCAR reanalysis MSLP data viability for climate studies in the South Pacific. *Geophys. Res. Lett*., 27, 3057-3060.

Mason SJ, Jury M. (1997); Climatic variability and change over Southern Africa : a Reflection on underlying processes. *Progress in Physical Geography* **21:**23ï 50.

Mason SJ. (1995); Sea-surface temperature - South Africa rainfall associations, 1910-1989. *International Journal of Climatology* **15**:119-135.

Matarira CH. (1990); Drought over Zimbabwe in a regional and global context. *International Journal of Climatology* **10**: 609ï 625.

McHugh MJ, Rogers CJ. (2001); North Atlantic Oscillation influence on the precipitation variability around south-east African Convergence Zone. *Journal of Climate* **14***:* 3641-3642.

McKee T.B., N.J. Doesken, J. Kleist (1993); The relationship of drought frequency and duration to time scales. In: 8th conference on applied climatology, Anaheim, CA. *Amer. Meteor. Soc.*, 179ï 184

Miller, A.J., D.R. Cayan, T.P. Barnett, N.E. Graham and J.M. Oberhuber (1994); The1976-77 climate shift of the Pacific Ocean*. Oceanography* 7, 21-26.

Miller, R.L., Schmidt, G.A. & Shindell, D.T. (2005); Forced annular variation in the 20th century Intergovernmental Panel on Climate Change Fourth Assessment Report models. *J. Geophys. Res.,* **111,** D18108, doi:10:1029/2005JD006323.

Murtugudde R, McCreary JP Jr, Busalacchi AJ. (2000); Oceanic processes associated with anomalous events in the Indian Ocean with relevance to 1997ï 1998. *Journal of Geophysical Research* 105: 3295ï 3306.

Mutai C, Polzin D, Hastenrath S (2012); Diagnosing Kenya Rainfall in Boreal Autumn: Further Exploration. *J. Climate*, **25**, 4323ï 4329. doi:10.1175/JCLI-D-11-00414.1

Mutai, C. C. and M.N. Ward (2000); East African rainfall and the tropical circulation/convection on intraseasonal to interannual timescales. *J. Climate,* **13**, 3915ï 3939

Mutai, C. C., N. Ward, and A.W. Colman (1998); Towards the prediction of the East African short rains based on sea-surface temperatureï atmosphere coupling. *Int. J. Climatol.*, **18,** 975ï 997

Nakamura N, H. Kayanne, H. Iijima, T. R. McClanahan, S. K. Behera, T. Yamagata (2009); Mode shift in the Indian Ocean climate under global warming stress**.** *Geophys. Res. Lett.*, **36** (23): L23708 doi:10.1029/2009GL040590

Nakamura N, H. Kayanne, H. Iijima, T. R. McClanahan, S. K. Behera, T. Yamagata (2011); Footprints of IOD and ENSO in the Kenyan coral record. *Geophys. Res. Lett.*, **38**, L24708 doi:10.1029/2011GL049877.

Newman, P. A. et al. (2006); When will the Antarctic ozone hole recover? *Geophys. Res. Lett.*, **33,** L12814, doi: 10.1029/2005GL025232.

Nicholson S, Webster JP. (2007); A physical basis for the interannual variability of rainfall in the Sahel. *Quarterly Journal of the Royal Meteorological Society* **133**: 2065-2084.

Nicholson SE (1996); A review of climate dynamics and climate variability in Eastern Africa. In: Johnson, T.C., Odada, E.O. (Eds.), *The Limnology, Climatology and Paleoclimatology of the East African Lakes. Gordon and Breach, Amsterdam*, pp. 25-56.

Nicholson SE, Kim J. (1997); The relationship of El Niño Southern Oscillation to African rainfall. *International Journal of Climatology* **17:** 117-135.

Nicholson SE. (1997); An analysis of the ENSO signal in the tropical Atlantic and western Indian Oceans. *International Journal of Climatology* **17:** 345-375.

Nyenzi BS (1992); An analysis of interannual rainfall over eastern Africa. J African Meteorol Soc 1: 57-79.

Overland J, Rodionov S, Minobe S, Bond N (2008); North Paciýc regime shifts: Deýnitions, issues and recent transitions . *Progress in Oceanography* 77 (2008) 92ï 102

Overland JE, Percival DB, Mofjeld, HO (2006); Regime shifts and red noise in the North Pacific. Deep-Sea Res. *Oceanogr. Res.*54: 582-588.

Pecora LM, Carroll TL, Johnson GA, Mar DJ, Heagy JF (1997); Fundamentals of synchronization in chaotic systems, concepts, and applications. *Chaos* 7: 520-543.

Peter A. Stott. (2003); Attribution of regional-scale temperature changes to anthropogenic and natural causes. *Geophys. Res. Lett.,* **30, 14**, 1728, doi:10.1029/2003GL017324.

Peterson, T.C., Karl, T. R., Jameson, P. F., Knight, R. & Easterling, D. R. (1998); The first difference method: Maximizing station density for the calculation of long-term global temperature change, *J. Geophys. Res*., **103**, 25,967ï 25,974.

Poccard I, Janicot S, Camberlin P. (20000; Comparison of rainfall structures between NCEP/NCAR reanalysis and observed data over tropical Africa. *Climate Dynamics* **16:** 897-915.

Polvani, L., Waugh, D., Correa, G. & Son S.-W. (2011); Stratospheric ozone depletion: The main driver of 20th century atmospheric changes in the Southern Hemisphere. *J.* Clim. **24**, 795ï 812.

Purich, A. & Son, S.-W. (2012); Impact of Antarctic ozone depletion and recovery on Southern Hemisphere precipitation, evaporation and extreme changes *J. Climate*., **25**, 3145ï 3154, doi:http://dx.doi.org/10.1175/JCLI-D-11-00383.1.

Ramstorf S (2000); The thermohaline ocean circulationð a system with dangerous thresholds? Clim. Changes, 46: 247ï 256.

Rao SA, Behera SK, Masumoto Y, Yamagata T. (2002); Interannual variability in the subsurface tropical Indian Ocean with a special emphasis on the Indian Ocean Dipole. *Deep Sea Research*-II 49: 1549ï 1572.

Rayner NA, Horton EB, Parker DE, Folland CK, Hackett RB (1996); Version 2.2 of the Global Sea-Ice and Sea Surface Temperature Data Set., 1993-1994. *Clim Res Tech Note* 74

Rial JA, and company (2004); Nonlinearities, feedbacks and critical thresholds within the earthôs climate system. *Climate Change* 65: 11- 38.

Rayner NA, Horton EB, Parker DE, Folland CK, Hackett RB. (1996); Version 2.2 of the Global Sea-Ice and Sea Surface Temperature Data Set., 1993-1994. *Climate Research Technical Note* 74 (Hadley Center for Climate Prediction and Research, Meteorological Office, London Road, Bracknell, RG12 2SY).

Rayner NA, Parker DE,Horton EB, Folland CK, Alexander LV, Rowell D P, Kent EC, Kaplan A (2003); Global analyses of sea surface temperature, sea ice, and night marine air temperature since the late nineteenth century, *J. Geophys. Res.*, **Vol. 108**, No. D14, 4407. doi 10.1029/2002JD002670.

Reason CJC, Jagadheesha D. (2005); A model investigation of recent ENSO impacts over southern Africa. *Meteorology and Atmospheric Physics* **89**:181ï 205.

Reason CJC, Landman W, Tennant W. (2006); Seasonal to decadal prediction of southern African climate and its links with variability of the Atlantic Ocean. *Bulletin of the American Meteorological Society* **87**; 941-955.

Reason CJC, Mulenga H. (1999); Relationship between South African Rainfall and SST anomalies in the South West Indian Ocean. *International Journal of Climatology* **19**: 1651-1763.

Reason CJC, Rouault M. (2002); ENSO like decadal variability and southern African rainfall. *Geophysical Research Letters* **29***, No 0,10. 1029/2002GL014663.*

Reason CJC. (2001); Subtropical Indian Ocean SST dipole events and southern African rainfall, *Geophysical Research Letters* **28**: 2225ï 2227.

Reason CJC. Keibel A. (2004); Tropical Cyclone Eline and its unusual penetration and impacts over the southern African mainland. *Weather and Forecasting* **19:** 789-805.

Reason, C. & Rouault, M. Links between the Antarctic Oscillation and winter rainfall over western South Africa (2005); *Geophys. Res. Lett*. **32**(7): 10.1029/2005GL022419.

Reason, C.J.C., R.J. Allan, J.A. Lindesay, T.J. Ansell (2000); ENSO and climatic signals in the Indian Ocean basin in the global context: part 1, inter-annual composite patterns. *Int. J. Climatol.,* **20**:1285ï 1327

Renwick (2004); Trends in the Southern Hemisphere polar vortex in NCEP and ECMWF reanalyses. *Geophys. Res. Lett*., 31, L07209, doi:10.1029/2003GL019302.

Richard Y, Fauchereau N, Poccard I, Rouault M, Trzaska S. (2001); 20th century droughts in southern Africa: spatial and temporal variability, teleconnections with oceanic and atmospheric conditions. *International Journal of Climatology* **21**: 873-885.

Rocha A, Simmonds I. (1997); Interannual variability of south-eastern African summer rainfall. Part 1: Relationships with air-sea interaction processes. *International Journal of Climatology* **17**:235ï 265.

Ropelewski, C. F. and Halpert, M. S. (1987); ógGlobal and regional scale precipitation associated with El Niñeo/Southern Oscillationô, *Monthly Weather Review* **115:** 985ï 996.

Rodionov S (2004); A sequential algorithm for testing climate regime shifts. Geophy Res Lett 31, L09204, doi:10.1029/2004GL019448.

Rodionov SN, Overland JE (2005); Application of a sequential regime shift detection method to the Bering Sea ecosystem. ICES *J. Mar. Sci* 62: 328-332.

Rouault M, Richard Y. (2005); Intensity and spatial extent of droughts in southern Africa. *Geophysical Research Letters* **32**: L15702, doi:10.1029/2005GL022436.

Roxy M, Gualdi S, Drbohlav HKE, Navarra A (2010); Seasonality in the relationship between El Nino and Indian Ocean dipole. *Clim Dynamics*, DOI: 10.1007/s00382-010-0876-1

Rudolf B, Becker A, Schneider U, Meyer-Christoffer A, Ziese M (2011); New Full Data Reanalysis Version 5 provides high-quality gridded monthly precipitation data. *GEWEX News*, 21: 2, 4-5.

Rudolf B, Becker A, Schneider U, Meyer-Christoffer A, Ziese M (2010); GPCC *Status Report, December* 2010, 7pp.

Saji NH, Goswami BN, Vinayachandran PN, Yamagata T. (1999); A dipole mode in the tropical Indian Ocean. *Nature* **401**: 360-363.

Saji NH, Yamagata T. (2003); Possible roles of Indian Ocean dipole mode events on global climate. *Climate Research* **25**: 151ï 169.

Schott FA, Xie SP, McCreary JP. (2009); Indian Ocean circulation and climate variability *Reviews of Geophysics,* **47:** RG1002, doi:10.1029/2007RG000245.

Schreck CJ, Semazzi FHM (2004); Variability of the recent climate of eastern Africa. *Int. J. Climatol.* 24: 681 ï 701

Sexton, D. M. H. (2001); The effect of stratospheric ozone depletion on the phase of the Antarctic Oscillation. *Geophys. Res. Lett.*, **28**, 3697ï 3700.

Shindell, D. T. & Schmidt, G. A. (2004); Southern Hemisphere climate response to ozone changes and greenhouse gas increases. *Geophys. Res. Lett.,* **31**, L18209, doi:10.1029/2004GL020724.

Shongwe, M. E., van Oldenborgh, G. J., van den Hurk, B. J. J. M.. de Boer, B., Coelho, C. A. S. & van Aalst, M. K. (2009); Projected Changes in Mean and Extreme Precipitation in Africa under Global Warming. Part I: Southern Africa. *J. Climate*, **22**, 3819ï 3837.

Shongwe, M.E., van Oldenborgh, van Aalst (2011); Projected changes in mean and extreme precipitation in Africa under global warming, Part II: East Africa. *J. Climate*., **24**:3718-3731

Smith TM, Reynolds RW (2003); Extended Reconstruction of Global Sea Surface Temperatures Based on COADS Data (1854-1997). *J. Climate* 16: 1495-1510

Song Q, Vecchi GA, Rosati AJ (2007); Indian Ocean Variability in the GFDL Coupled Climate Model. **J Climate** 20:13, 2895-2916

Terray P, Dominiak S, Delecluse P. (2005); Role of the southern Indian Ocean in the transitions of the monsoon-ENSO system during recent decades. *Climate Dynamics* **24**: 169-195.

Thompson BW (1966); "The mean annual rainfall of Mount Kenya". Weather **21**: 48ï 49. doi:10.1002/j.1477-8696.1966.tb02813.x.

Thompson, D. W. J & Solomon, S. (2002); Interpretation of recent Southern Hemisphere climate change. *Science*, **296**, 895ï 899.

Thompson, D. W. J. & Wallace J. M. (2000); Annular modes in the extratropical circulation. Part I: Month-to-month variability. *J. Climate*, **13**, 1000-1016.

Thompson, D.W.J., Solomon, S., Kushner, P.J., England, M.H., Grise, K.M. & Karoly, D.J. (2011); Signatures of the Antarctic ozone hole in Southern Hemisphere surface climate change. *Nature Geoscience*. doi:10.1038/ngeo1296.

Todd MC, Washington R, Palmer PI. (2004); Water vapour transport associated with tropical-temperate trough systems over southern Africa and the southwest Indian Ocean, *International Journal of Climatology* **24:** 555ï 568.

Tozuka, T., J.-J. Luo, S. Masson, and T. Yamagata (2007); Decadal modulations of the Indian Ocean Dipole in the SINTEX-F1 coupled GCM, *J. Climate*, 20, 2881-2894.

Tsonis AA, Roebber PJ (2004); The architecture of the climate network. Physica, 333: 497-504.

Tsonis AA, Swanson KL, Roebber PJ (2006a); A new dynamical mechanisms for major climate shifts. *Geohys Res Lett.*, 34, L13705, doi: 10.1029/2007GL030288.

Tsonis AA, Swanson KL, Wang G (2006b); On the role of atmospheric teleconnections in Climate. *Geohys J Climate* 21: 2990-3001.

Tyson P, Preston-Whyte R. (2000); *The Weather and Climate of Southern Africa* (Second edition). Oxford University Press Southern Africa, Cape Town: pp 334.

Ummenhofer, CC, Gupta AS, Taschetto AS, England MH (2009a); Modulation of Australian Precipitation by Meridional Gradients Indian Ocean Sea Surface Temperature. *J. Climate*, 22, 5597ï 5610.

Ummenhofer CC, Gupta AS, England MH, Reason CJC (2009b); Contributions of Indian Ocean sea surface temperatures to enhanced East African rainfall. *J. Climate*, 22, 993-1013.

Ummenhofer, CC, Gupta AS, Pook MJ, England MH (2008); Anomalous rainfall over southwest Western Australia forced by Indian Ocean sea surface temperatures. *J. Climate*, 21, 5113ï 5134.

Uppala SM and Coauthors (2005); The ERA-interim re-analysis. *Quart. J. Roy. Meteor*. 256 Soc., **131,** 2961-3012.

Vicente-Serrano SM, J.C. Gonz´alez-Hidalgo, H. de Luis, J. Ravent´os, (2004); Drought patterns in the Mediterranean area: the alencia region (eastern Spain). *Climate Res.,* **26**:5ï 15

Vuille M, M. Werner, R. S. Bradley, R. Y. Chan, F. Keimig (2005); Stable isotopes in East African precipitation record Indian Ocean zonal mode *Geophys. Res. Lett.*, **32,** L21705, doi:10.1029/2005GL023876.

Wang F, Chang P (2008); A Linear Stability Analysis of Coupled Tropical Atlantic Variability. J Climate 21: 2421ï 2436. doi: 10.1175/2007JCLI2035.1

Washington R, Preston A. (2006); Extreme wet years over southern Africa: Role of Indian Ocean sea surface temperatures, *Journal of Geophysical Research*, *111*, D15104, doi:10.1029/ 2005JD006724.

Washington R, Todd M. (1999); Tropical-temperate links in southern African and Southwest Indian Ocean satellite-derived daily rainfall, *International Journal of Climatology* **19**: 1601ï 1616.

Webster PJ, Moore AM, Loschnigg JP, Leben RR (1999); Coupled oceanï atmosphere dynamics in the Indian Ocean during 1997ï 98. *Nature* 401: 356ï 360.

WMO (2002); World Meteorological Organization: *Scientific assessment of ozone depletion: (2002);* (Global Ozone Research and Monitoring Project-Report No. 47. Geneva, Switzerland, 2003).

WMO (1996); World Meteorological Organization: Climate Change, *WMO technical Note No 79*. WMO No. 195-TP-100, World Meteorological Organisation, Geneva, 53pp.

Xie, S.P., K. Hu, J. Hafner, Y. Du, G. Huang, and H. Tokinaga (2009); Indian Ocean capacitor effect on Indo-western Pacific climate during the summer following El Niño. *J. Climate,* **22**, 730-747.

Xu Q. (2001); Abrupt change of the mid-summer climate in central east China by the influence of atmospheric pollution. *Atmosphere and Environment* **35:** 5029ï 5040.

Xue F, Jiang D, Lang X, Wang H (2003); Influence of the Mascarene High and Australian High on the summer monsoon in East Asia: Ensemble simulation. *Adv. Atmos. Sci*., 20 799-809.

Xue. F., Wang, H. J. & He, J.H. (2004); Interannual variability of Mascarene High and Australian High and their influence on the East Asian summer monsoon. *Journal of Meteorological Society, Japan*, **80**, 4, 173-1186.

Yamagata T, Behera1 S, Luo J, Masson S, Delecluse P, Gualdi P, Navarra A (2003); Impact of the Indian Ocean Dipole on the East African Short Rains: A CGCM Study *CLIVAR Exchanges* 27**:** 43-45.

Yuan Y, Chan CLJ, Zhou W, Li CY (2008); Decadal and interannual variability of the Indian Ocean dipole. *Adv. Atmos*. Sci 25: 856-866, doi: 10.1007/s00376-008-0856-0.

Zhou T, Yu R, Zhang J, Drange H (2009); Why the western Pacific subtropical high has extended westwards since the late 1970s. *J. Climate,* 22, 2199-2215.